AD-A108 418 TORONTO UNIV DOWNSVIEW (ONTARIO) INST FOR AEROSPACE --ETC F/G 14/2
ON A DUSTY-GAS SHOCK TUBE.(U)
MAY 81 H MIURA, I I GLASS AFOSR-77-3303
UNCLASSIFIED UTIAS-250 AFOSR-TR-81-0787 NL

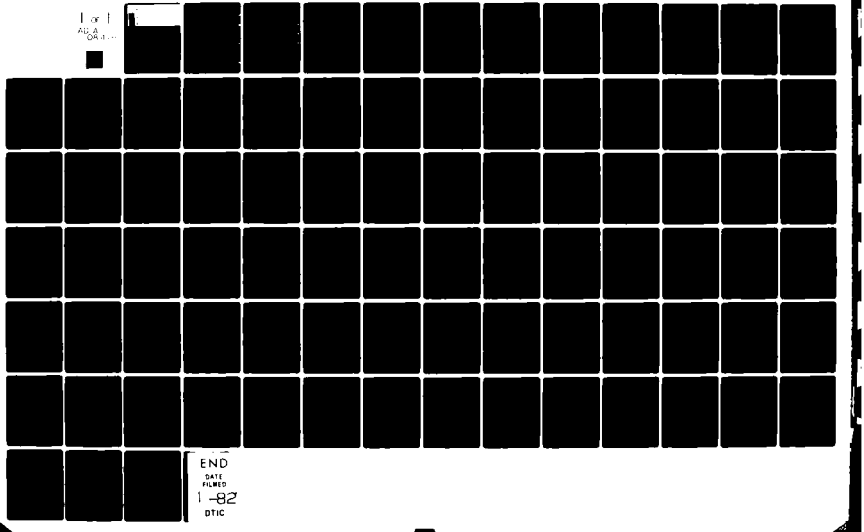

END
DATE FILMED
1-82
DTIC

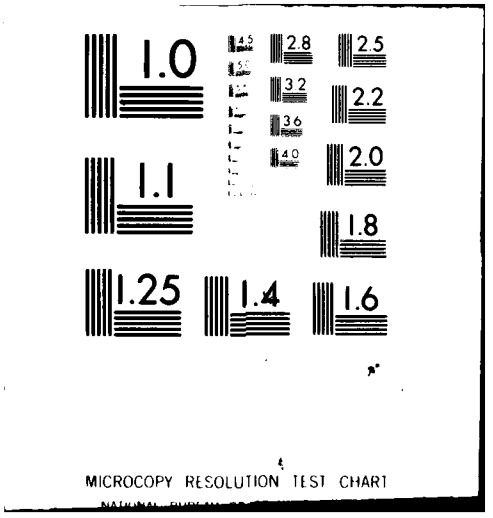
1.0
1.1
1.25
1.4
1.6
1.8
2.0
2.2
2.5
2.8
3.2
3.6
4.0
MICROCOPY RESOLUTION TEST CHART

INSTITUTE
FOR
AEROSPACE STUDIES

UNIVERSITY OF TORONTO

AFOSR-TR- 81 -0787

LEVEL II 13

ON A DUSTY-GAS SHOCK TUBE

by

H. Miura and I. I. Glass

(12) 86

May, 1981

UTIAS Report No. 250
CN ISSN 0082-5255

UNCLASSIFIED
SECURITY CLASSIFICATION OF THIS PAGE *(When Data Entered)*

REPORT DOCUMENTATION PAGE		READ INSTRUCTIONS BEFORE COMPLETING FORM
1. REPORT NUMBER AFOSR-TR- 81-0787	2. GOVT ACCESSION NO. AD-A103418	3. RECIPIENT'S CATALOG NUMBER
4. TITLE *(and Subtitle)* ON A DUSTY-GAS SHOCK TUBE		5. TYPE OF REPORT & PERIOD COVERED Interim
		6. PERFORMING ORG. REPORT NUMBER UTIAS Report No. 250
7. AUTHOR(s) H. Miura and I. I. Glass		8. CONTRACT OR GRANT NUMBER(s) AFOSR 77-3303
9. PERFORMING ORGANIZATION NAME AND ADDRESS University of Toronto, Institute for Aerospace Studies, 4925 Dufferin Street, Downsview, Ontario Canada, M3H 5T6		10. PROGRAM ELEMENT, PROJECT, TASK AREA & WORK UNIT NUMBERS 61102F 2307/A1
11. CONTROLLING OFFICE NAME AND ADDRESS Air Force Office of Scientific Research/NA, Bldg. 410, Bolling Air Force Base, DC. U.S.A. 20332		12. REPORT DATE May 1981
		13. NUMBER OF PAGES 74
14. MONITORING AGENCY NAME & ADDRESS*(if different from Controlling Office)*		15. SECURITY CLASS. *(of this report)* UNCLASSIFIED
		15a. DECLASSIFICATION DOWNGRADING SCHEDULE

16. DISTRIBUTION STATEMENT *(of this Report)*

Approved for public release; distribution unlimited.

17. DISTRIBUTION STATEMENT *(of the abstract entered in Block 20, if different from Report)*

18. SUPPLEMENTARY NOTES

19. KEY WORDS *(Continue on reverse side if necessary and identify by block number)*

1. Dusty-gas shock waves; 2. Dusty-gas shock-tube flows, 3. Nonequilibrium dusty-gas flows; 4. Shock-wave and contact-front transitions.

20. ABSTRACT *(Continue on reverse side if necessary and identify by block number)*

Analytical and numerical methods were used to investigate the flow induced by a shock wave in a shock-tube channel containing air laden with suspended small solid particles. Exact results are given for the frozen and equilibrium shock-wave properties as a function of diaphragm-pressure ratio and shock-wave Mach numbers. The driver contained air at high pressure. A modified random-choice method together with an operator-splitting technique show clearly both the decay of a discontinuous frozen shock wave and a contact discontinuity and —

DD FORM 1 JAN 73 1473 EDITION OF 1 NOV 65 IS OBSOLETE

UNCLASSIFIED
SECURITY CLASSIFICATION OF THIS PAGE *(When Data Entered)*

the formation of a stationary shock structure and an effective contact front of finite thickness.

The effects of particle diameter, particle-number density and diaphragm-pressure ratio on the transitional behaviour of the flow are investigated in detail. The alteration of the flow properties due to the presence of particles is discussed in detail and compared with classical shock-tube flows.

A

Qualified requestors may obtain additional copies from the Defense Documentation Center, all others should apply to the National Technical Information Service.

Conditions of Reproduction:

Reproduction, translation, publication, use and disposal in whole or in part by or for the United States Government is permitted.

Approved for public release; distribution unlimited.

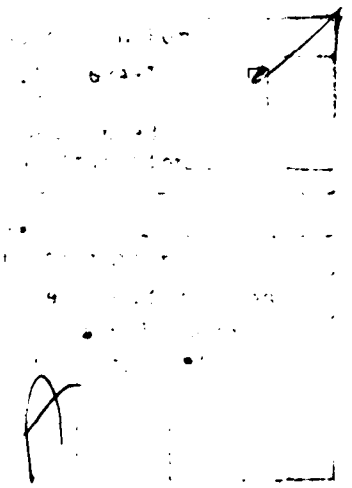

Chief, Technical Information Division

ON A DUSTY-GAS SHOCK TUBE

by

H. Miura and I. I. Glass

Submitted February, 1981

May, 1981

UTIAS Report No. 250
CN ISSN 0082-5255

Acknowledgements

We wish to express our appreciation to Mr. T. Saito for valuable advice on using the random-choice method for this problem.

One of us (H. Miura) is grateful to the University of Osaka Prefecture, Sakai, Japan, for making possible his leave at UTIAS.

The financial support received from the Natural Sciences and Engineering Research Council of Canada, the U.S. Air Force under Grant [redacted]-AFOSR-77-3303, the U.S. Army Research Office, and the Defence Research Establishment, Suffield, is acknowledged with thanks.

Summary

Analytical and numerical methods were used to investigate the flow induced by a shock wave in a shock-tube channel containing air laden with suspended small solid particles. Exact results are given for the frozen and equilibrium shock-wave properties as a function of diaphragm-pressure ratio and shock-wave Mach numbers. The driver contained air at high pressure. A modified random-choice method together with an operator-splitting technique show clearly both the decay of a discontinuous frozen shock wave and a contact discontinuity and the formation of a stationary shock structure and an effective contact front of finite thickness.

The effects of particle diameter, particle-number density and diaphragm-pressure ratio on the transitional behaviour of the flow are investigated in detail. The alteration of the flow properties due to the presence of particles is discussed in detail and compared with classical shock-tube flows.

Contents

Notation

a_e = equilibrium speed of sound

a_f = frozen speed of sound

C_m = specific heat of solid material

C_p = gas specific heat at constant pressure

C_v = gas specific heat at constant volume

D = drag force acting on a particle

d = diameter of particles

k = gas thermal conductivity

ℓ = reference length [Eq. (22)]

m = mass of a particle

n_p = particle number density

p = gas pressure

Q = rate of heat transfer to a particle

R = gas constant

T = gas temperature

t = time from diaphragm rupture

u = gas velocity

u_s = propagation velocity of shock wave

v = velocity of particles

x = space coordinate measured from diaphragm

θ = temperature of particles

μ = gas viscosity

ρ = gas density

ρ_p = density of solid particles

σ = mass concentration of particles

Dimensionless Quantities

C_D = drag coefficient of a particle

M_s = u_s/a_{1_f} or u_s/a_{1_e}

Nu = Nusselt number of a particle

P = p/p_1

P_{21} = p_2/p_1

P_{41} = p_4/p_1

Pr = gas Prandtl number

Re = Reynolds number of a particle

T = T/T_1 or Θ/T_1

T_{21} = T_2/T_1

T_{31} = T_3/T_1

U = u/a_1 or v/a_1

U_{21} = u_2/a_1

X = x/ℓ

α = ratio of mass concentrations of particles to gas [Eq. (19)]

β = ratio of specific heats of two phases [Eq. (18)]

γ = gas specific heat ratio

γ_e = specific heat ratio of an effective perfect gas

Γ = ρ/ρ_1 or σ/σ_1

Γ_{21} = ρ_2/ρ_1

Γ_{31} = ρ_3/ρ_1

τ = $t/(\ell/a_{1_f})$

Note: P_{21}, T_{21}, U_1 and Γ_{21} can have frozen and equilibrium values; at equilibrium $\Gamma_{21} = \rho_2/\rho_1 = \sigma_2/\sigma_1$.

1. INTRODUCTION

When a gas carries a lot of solid particles, they significantly affect the flow through the transfer of momentum and heat from or to the gas. Shock waves propagating in such a dusty gas are characterized by a transition region orders thicker than that caused by viscosity and heat conduction in a pure gas. Across the transition front, the interaction of the gas and the particles leads to an equilibrium state of the mixture. The structure of stationary shock waves (Refs. 1-5) and its formation by a moving piston (Refs. 5, 6) have been studied theoretically on the assumption that the formulae for the drag and the rate of heat transfer for a single spherical particle placed in a steady flow can still be applied to the motion of many particles contained in a dusty gas.

Some experimental studies of shock waves in a dusty gas inside a shock tube were done in order to get some data on the interaction of the two phases (Refs. 7-10). Some of the results showed an effective drag coefficient, obtained from the observation of the acceleration of the particles behind the shock waves, which differed appreciably from that for a single particle. However, there were many factors influencing the results and a definitive conclusion on the appropriate drag coefficient to be used is not available as yet.

Recently, numerical analyses followed these experimental studies. The shock-tube problem for a dusty gas was solved numerically by Otterman and Levine (Ref. 11) using the particle-in-cell method. They investigated the difference in the transient flow field due to different assumptions of the drag and the heat transfer coefficients. Outa, Tajima and Morii (Ref. 10) made a numerical analysis of the penetration of a shock wave into a dusty-gas region for comparison with their experimental results. Satofuka and Tokita (Ref. 12) discussed the efficiency of various numerical techniques applied to the case when both sides of a diaphragm are filled with a dusty gas.

The work of Otterman and Levine provided a rough sketch of the transient flow behaviour in a shock tube. However, they treated cases of unusually high mass-loading ratio and their numerical results include obscure points regarding the frozen shock front and the delay of particle acceleration.

At present, a more extensive and clear analytical study is required for comparison with experimental results. In this paper, we consider the classical problem of the shock tube where the driver contains high-pressure air and the channel contains a dusty gas, as would be the case in actual experiments. The effects of the ratio of mass concentrations, the size of the particles and the diaphragm pressure ratio upon the flow characteristics are fully discussed. Working curves are produced for the physical properties as a function of the initial conditions and the diaphragm pressure ratio. The transitions through the shock front and contact region as well as the rarefaction wave are studied in detail as functions of time. Some of the randomness produced by mesh size and drag relations on physical properties are also shown.

The study of shock waves in dusty gases provides a good introduction to real-gas effects. Frozen shock waves, transition to equilibrium flow, frozen and equilibrium sound speeds and dispersed shock waves are all encountered and well illustrated by analogy with real-gas flows.

2. ANALYTICAL CONSIDERATIONS

We consider the transient flow occurring after diaphragm rupture in a shock tube (Fig. 1). In order to formulate the motion of the mixture, we must make several assumptions (Refs. 1-6). The gas is assumed perfect and its viscosity and heat conductivity are neglected except for the interaction with the particles. The particles are assumed to be spheres of uniform size and their number is so large that the flow may be treated as a continuum. The volume occupied by the particles is neglected.

Let p, ρ, T, u be the pressure, density, temperature and velocity of the gas, and σ, Θ, v be the mass concentration, temperature and velocity of the particles, respectively. Using the assumptions stated above, we can express the equations of motion of mass, momentum and energy for either the gas or the particles as follows:

$$\frac{\partial \rho}{\partial t} + \frac{\partial}{\partial x}(\rho u) = 0 \tag{1}$$

$$\frac{\partial \sigma}{\partial t} + \frac{\partial}{\partial x}(\sigma v) = 0 \tag{2}$$

$$\frac{\partial}{\partial t}(\rho u) + \frac{\partial}{\partial x}(\rho u^2) + \frac{\partial p}{\partial x} = -\frac{\sigma}{m} D \tag{3}$$

$$\frac{\partial}{\partial t}(\sigma v) + \frac{\partial}{\partial x}(\sigma v^2) = \frac{\sigma}{m} D \tag{4}$$

$$\frac{\partial}{\partial t}\left\{\rho\left(C_v T + \frac{1}{2}u^2\right)\right\} + \frac{\partial}{\partial x}\left\{\rho u\left(C_p T + \frac{1}{2}u^2\right)\right\} = -\frac{\sigma}{m}(vD + Q) \tag{5}$$

$$\frac{\partial}{\partial t}\left\{\sigma\left(C_m \Theta + \frac{1}{2}v^2\right)\right\} + \frac{\partial}{\partial x}\left\{\sigma v\left(C_m \Theta + \frac{1}{2}v^2\right)\right\} = \frac{\sigma}{m}(vD + Q) \tag{6}$$

The thermally perfect equation of state for the gas is given by

$$p = \rho R T \tag{7}$$

The interaction of the two phases is incorporated in the terms of the drag and the heat transfer on the right-hand sides of Eqs. (3)-(6). Specification of the dependence of D and Q on the flow quantities is needed to obtain a closed set of equations. While various formulae valid for a single sphere exist (Refs. 3, 4), attention should be paid to the fact that in the present transient case the Reynolds number of the particle takes on a high value initially because of the large difference in velocity between the two phases. We assume that

$$D = \frac{\pi}{8} d^2 \rho (u-v) |u-v| C_D$$

$$= \frac{\pi}{8} d^2 \rho (u-v) |u-v| (0.48 + 28\ Re^{-0.85}) \tag{8}$$

for the drag (Ref. 13) and

$$Q = \pi d \mu C_p Pr^{-1} (T-\Theta) Nu$$

$$= \pi d \mu C_p Pr^{-1} (T-\Theta)(2.0 + 0.6\ Pr^{1/3}\ Re^{1/2}) \tag{9}$$

for the heat transfer (Ref. 14), where Re is the Reynolds number based on the diameter of the particle and the relative velocity of the particle to the gas

$$Re = \rho |u-v| d / \mu \tag{10}$$

and Pr is the Prandtl number

$$Pr = \mu C_p / k \tag{11}$$

The viscosity and the thermal conductivity of the gas are assumed constant for stationary shock waves (Ref. 9), since the change in temperature of the gas is small over the relaxation region. In the present case, however, the particles interact not only with a hot compressed gas between the shock front and the contact front but also with a cold expanding gas behind the contact front. In addition, the temperature of the gas varies with time. Therefore, the variations of the viscosity and the thermal conductivity with temperature must be taken into account. With air (Ref. 15) inside the tube

$$\mu = 1.71 \times 10^{-4} \times \left(\frac{T}{273} \right)^{0.77} \text{ poise} \tag{12}$$

and

$$Pr = 0.75 \tag{13}$$

The high pressure air in the driver obeys Eqs. (1), (3) and (5) with $\sigma = 0$, and Eq. (7).

The initial conditions at $t = 0$ are as follows:

$$\begin{aligned} &\frac{p}{p_1} = \frac{\rho}{\rho_1} = \frac{T}{T_1} = \frac{\sigma}{\sigma_1} = \frac{\Theta}{T_1} = 1, \qquad u = v = 0 \text{ for } x > 0 \\ &\frac{p}{p_4} = \frac{\rho}{\rho_4} = \frac{T}{T_4} = 1, \qquad u = 0,\ \sigma = 0 \text{ for } x < 0 \end{aligned} \tag{14}$$

It is assumed here that the gas and the particles initially are in equilibrium. The system of equations (1)-(7) for seven unknowns (p, ρ, T, u, σ, Θ, v) together with the supplementary equations (8)-(13) subject to the initial conditions can be solved numerically. We apply the random-choice method (Refs. 16-19) to the present problem, for it describes discontinuities clearly without the use of implicit or explicit artificial viscosity. An operator-splitting technique makes its application possible (Refs. 18, 19). The solution is obtained by solving the two sets of equations alternately in each time step, that is, the equations derived from Eqs. (1)-(6) with the right-hand sides omitted and the equations obtained by omitting the derivatives with respect to x.

The element of the random-choice method, which solves the former set, is to determine by means of random sampling the solution at the middle point between the two adjacent points where the solution is known at a previous time. The initial condition in this calculation is taken as a step-like discontinuity. The procedure for the gas phase has been written in a few papers (Refs. 17-19) and is omitted in this paper.

On the other hand, a difficulty arises in the treatment of the equations for the particles in this stage, which are reduced to

$$\begin{aligned} \frac{\partial \sigma}{\partial t} + \frac{\partial}{\partial x}(\sigma v) &= 0 \\ \frac{\partial v}{\partial t} + v\frac{\partial v}{\partial x} &= 0 \\ \frac{\partial \Theta}{\partial t} + v\frac{\partial \Theta}{\partial x} &= 0 \end{aligned} \tag{15}$$

A discontinuous initial condition would result in a multivalued solution for the velocity v. The flow variables of the particles are continuous and we assume the initial condition of linear distribution only for the particles in order to avoid this difficulty. Consider two adjacent points with distance Δx apart, where the solution is known. We take the following initial conditions:

$$\begin{aligned} v &= (v_r - v_\ell)\frac{x}{\Delta x} + \frac{1}{2}(v_r + v_\ell) \\ \Theta &= (\Theta_r - \Theta_\ell)\frac{x}{\Delta x} + \frac{1}{2}(\Theta_r + \Theta_\ell) \\ \sigma &= (\sigma_r - \sigma_\ell)\frac{x}{\Delta x} + \frac{1}{2}(\sigma_r + \sigma_\ell) \end{aligned} \tag{16}$$

where the subscripts r and ℓ refer to the two points $x = \pm \frac{1}{2}\Delta x$ (for convenience), respectively. The solution of Eq. (15) subject to the condition (16) is given by

$$v = \frac{1}{\Delta x + (v_r - v_\ell)t} \left\{(v_r - v_\ell)x + \frac{\Delta x}{2}(v_r + v_\ell)\right\}$$

$$\theta = \frac{1}{\Delta x + (v_r - v_\ell)t} \left\{(\theta_r - \theta_\ell)x + \frac{\Delta x}{2}(\theta_r + \theta_\ell) + (\theta_\ell v_r - \theta_r v_\ell)t\right\} \qquad (17)$$

$$\sigma = \frac{\Delta x}{\{\Delta x + (v_r - v_\ell)t\}^2} \left\{(\sigma_r - \sigma_\ell)x + \frac{\Delta x}{2}(\sigma_r + \sigma_\ell) + (\sigma_\ell v_r - \sigma_r v_\ell)t\right\}$$

Random sampling of the solution between the two points determines the values of flow variables at the middle point a little time later. Two repetitions of this procedure bring about a time evolution by a time step, say, Δt. The time step must be appropriately small so that the so-called Courant-Friedrichs-Lewy condition is satisfied, otherwise the result loses physical meaning. Although most points are treated in this way, the point bordering the region of the dusty gas is an exception. Since the diffusion of concentration is not considered, we must take a discontinuous initial condition at this point so as to get a clear boundary of the particle cloud.

The other portion of the operator-splitting technique is accomplished by integration of the equations with respect to time. This procedure must be carefully done for moving discontinuities, because it may produce a significant error of the first order. Consider the case when a discontinuous surface passes across a point in a time of Δt. The surface should be regarded to have moved over the distance Δx between the middle points on both sides of the point. Therefore, the contribution to the integration in Δt at the point must be considered separately for the two halves of $\frac{1}{2}\Delta t$.

3. RESULTS AND DISCUSSIONS

An assignment of several parameters is needed for the numerical calculations. We take air ($\gamma = 1.4$) as the gas in both the driver and the driven sections. The gas is assumed to be at room temperature ($T_1 = T_4$) before diaphragm rupture. The initial pressure p_1 in the driven section is taken to be one atmosphere. Further, we restrict ourselves to the case where the ratio of specific heats of the two phases

$$\beta = C_m/C_v \qquad (18)$$

is unity. The remaining factors, on which flow behaviours depend, are the ratio of mass concentration

$$\alpha = \sigma_1/\rho_1 \qquad (19)$$

the diameter of the particles d and the diaphragm pressure ratio

$$P_{41} = p_4/p_1 \qquad (20)$$

The results for the case of $\alpha = 1$, $d = 10\ \mu m$ and $P_{41} = 10$ are presented in Figs. 2-6. Normalized quantities are used in all the figures. Flow quantities, except the velocity, are referred to corresponding values in the stationary region (1) ahead of the shock wave. The velocity is normalized by the speed of sound in the gas phase, i.e., the so-called frozen speed of sound:

$$a_{1_f} = \sqrt{\gamma p_1/\rho_1} \tag{21}$$

The distance x is also measured in units of

$$\ell = \frac{8m}{\pi \rho_1 d^2} = \frac{4}{3} \cdot \frac{\rho_p}{\rho_1} d \tag{22}$$

and the time t in ℓ/a_{1_f}. [Note the value of ℓ can be obtained from Eq. (4)]. Numerical calculations have been done in the manner stated in the previous section. A mesh size Δx of 0.1 is used together with time step Δt as large as the Courant-Friedrichs-Lewy condition may allow.

Flow structures after a small time has elapsed after the diaphragm rupture are shown in Fig. 2, for the case of $P_{41} = 10$, $\alpha = 1$, $d = 10\ \mu m$ for a time $\tau = 4$. Under these conditions with $p_1 = 1$ atm and $T_1 = 300$ K, using glass beads, the number density to provide $\alpha = 1$ would be 0.94×10^6/cc; $\ell = 2.72$ cm; $a_{1_f} = 350$ m/s and $\tau = 4 \equiv 3.11 \times 10^{-4}$ sec (see Table 1 for further details). The dashed lines are for the classical shock-tube problem. The solid lines show the frozen shock wave as an abrupt change followed by a gradual approach to equilibrium. In this case the flow is far from equilibrium. Note in Fig. 2(b) the particle concentration rises gradually though the shock front, reaches a maximum at the contact front and then drops to zero at the driver gas. It should be noted that the rarefaction is weaker than for the gas case only. In addition there are spurious numerical oscillations near the tail of the wave in all flow properties. Only the gas responds to the abrupt change at the instant of diaphragm rupture, while the particles cannot folow any sudden change. After the frozen shock front has passed by, the velocity and temperature of the particles are raised gradually through interaction with the gas. On the other hand, the gas is decelerated and loses energy. A comparison of the results with the solution for a pure gas exhibits a decay of the frozen shock front due to this interaction. The velocity of propagation of the shock wave also diminishes as can be seen by looking at the values of X for both cases. The deceleration of the gas results in a compression and its pressure away from the frozen shock front attains a higher value than in the case of a pure gas. The rarefaction wave weakens as a result. Some particles cross the frozen contact surface and drop to zero in the cold gas. Thus the temperature of these particles drops. However, the gas temperature [see Fig. 2(c)] also drops but not as low as for the frozen flow since the particles act as a heat reservoir.

Subsequent transitional behaviours of the physical quantities are shown in Figs. 3-5 for increasing time τ. Both the velocities and temperatures of the gas and the particles behind the frozen shock front approach each other with time and a new uniform region in equilibrium forms some distance behind the discontinuous frozen shock front. An almost stationary shock structure of finite thickness can be seen in Fig. 5. For our case of $\rho_p = 2.5$ g/cm^3, this state is attained

after 2.49×10^{-3} sec and the thickness of the shock transition is about 34 cm. If, for example, ρ_p is made smaller for $\alpha = 1$, the particle number density will increase and the transition length will decrease.

It is very useful to assume that everywhere the particles reach the equilibrium-flow limit of the gas velocity and temperature. This must occur because the flow except for relaxation regions of finite length must approach this limit after a sufficient time elapses. The mixture in this limit behaves effectively as a perfect gas with the specific heat ratio given by (Ref. 4)

$$\gamma_e = (\gamma + \alpha\beta)/(1 + \alpha\beta) \tag{23}$$

and the speed of sound by

$$a_{1_e} = \sqrt{\frac{\gamma + \alpha\beta}{(1 + \alpha)(1 + \alpha\beta)} \cdot \frac{p_1}{\rho_1}} \tag{24}$$

The shock-tube solution for this equilibrium-flow limit is also shown in Fig. 5 for comparison. The agreement of the equilibrium flow limit and the numerical results is very good indeed. Besides the relaxation region of the shock wave, the contact surface also has a structure of finite thickness. The particles in this layer are in equilibrium with the gas. The structure of the effective contact surface must depend on how the particles have interacted with the gas.

A wave diagram is shown in Fig. 6. The paths of the discontinuous frozen and equilibrium shock fronts are shown. For comparison the present numerical results are also shown. As noted on Fig. 6, the present data shows the relaxation distance between the present frozen shock and the idealized equilibrium gas-particle front. It shows that the present frozen shock moves at a velocity closer to the idealized equilibrium shock front than the perfect gas frozen shock wave after a sufficient time has elapsed. At times close to zero it would move closer to the perfect gas shock.

The path of the contact surface has been made possible by choosing a point on its transition region such that the temperature equals the original gas temperature T_1. Consequently, the results by definition must lie on our equilibrium contact front path for convenience of illustration. The results for the tail of the rarefaction wave were obtained by extrapolating the straight lines of the pressure curves in regions (2) and (3), the uniform states, until it hit the rarefaction wave profile. It can be seen that the agreement with the idealized equilibrium value is very good by large. Note that the tail of this wave is weaker than the perfect gas tail. Of course the head of the rarefaction wave is identical for all three flows as shown.

The changes in temperature and pressure of the gas immediately behind the frozen shock front as it moves are shown in Fig. 7. They start from values for a pure gas and approach finally the values calculated from the shock speed attained in the idealized equilibrium-flow limit.

Small random disturbances in the numerical results are characteristic of the use of the random-choice method. Taking a smaller mesh size makes the disturbances smaller. (We confirmed this by comparing the results with those for a half and quarter-size mesh smaller, although only for a short time owing to the increased cost of the computations - see Figs. 8 and 9.)

It should be noted that the thermal equilibration between the two phases is achieved faster than the equilibration of velocity (see Figs. 2c, d and 3c, d). This fact is also reflected in that longer length from the discontinuous shock front is needed for velocity equilibration than for temperature equilibration (see Figs. 5c and 5d).

Next, we investigate the influence of the size of the particles on the transition of the flow. The results for the cases of d = 20 μm (see Figs. 10-12) and d = 40 μm (see Figs. 13-15) with other parameters unchanged, are shown in Figs. 10-15, respectively. It is interesting to find almost similar flow fields at $\tau = 4$ in the three cases of 10-40 μm. Note that the actual times and distances are different for different particle diameters, being proportional to the diameter according to Eq. (22). This is nearly true for later times as well. This similarity may be related to the constancy of the drag coefficient of the particles for large Reynolds numbers. The rate of heat transfer is much greater for smaller particles. For example, a comparison of Figs. 2c and 13c soon show that the 10 μm particle differs greatly from the frozen value but the 40 μm particle is very close to the frozen value.

The results at $\tau = 32$ may be compared with the structure of a stationary shock wave. It can be seen that the stationary shock values are almost achieved. The length of the relaxation region is naturally longer for larger particles on account of their larger inertia. Alternatively, the relaxation length depends on the diameter d [Eq. (22)]. However it is found to lie between d and d^2. As seen from Figs. 7, 12 and 15, the time required for the stationary shock wave to form also depends on the diameter of the particles. However, it is not a linear relation. The time τ for the 20 μm particle to achieve equilibrium is much less than a factor of two for the 10 μm particles. Nevertheless the actual time is longer than two but less than four.

Calculations have been done for cases of different ratios of mass concentrations with the remaining parameters the same as the first case. The results for $\alpha = 0.4$ and $\alpha = 2.0$ are shown in Figs. 16-18 and 19-21 respectively. It can be seen from comparison of the flow fields at $\tau = 4$ that a larger mass concentration of particles causes in the gas phase larger deviations from the frozen flow. However, the final quasi-equilibrium state is accomplished more quickly when α is small. For example, compare median curves through Figs. 18, 7 and 21 and it will be clear that equilibrium is faster for the small loading ratio $\alpha = 0.4$. The effect of the mass concentration of particles on the thickness of the stationary shock wave is not so apparent. In the case when $\alpha = 2.0$, the propagation of the shock wave becomes so slow that the discontinuous jump in the gas phase cannot be supported (see Fig. 20). The transition to the fully dispersed shock wave is characteristic of this case. The contact surface consists of a region of dusty gas of finite thickness which is followed by a discontinuity in the gas phase (see Figs. 20b and 20c).

The difference in transitional behaviour due to the strength of the diaphragm pressure ratio is studied next. The results for the cases of $p_{41} = 5.0$ and $p_{41} = 20.0$ are shown in Figs. 22-24 and 25-27, respectively. The length of the relaxation

region of the stationary shock wave forming after a sufficient time is larger for weaker shock waves (see Figs. 23 and 26), i.e., smaller diaphragm pressure ratio. When the diaphragm pressure ratio is lower than a critical value, the shock wave is weak and the decay due to absorption of energy by the particles is so large that the shock wave becomes fully dispersed, that is, the frozen shock front disappears. In fact, the case of $p_{41} = 5.0$ lies in this range. Comparison of the changes in the pressure jump at the frozen shock front with time clarifies that the stationary shock wave forms also in a shorter time for a higher diaphragm pressure ratio (see Figs. 7, 24 and 27).

Finally, several figures (Figs. 28-34) are presented illustrating the effect of the existence of particles upon the uniform states between the shock wave, the contact surface and the rarefaction wave for the idealized gas-particle equilibrium flow limit. Flow quantities are given by the exact classical shock-tube solution (Ref. 20) (see Appendix B) for the effective perfect gas based on γ_e and a_{1f} (see Table 2). Variations of shock Mach numbers based on the frozen or the equilibrium speed of sound with the diaphragm pressure ratio are shown in Fig. 28 for values of α over the range $0 \leq \alpha \leq 2$. The particles reduce the velocity of propagation of a shock wave and since the speed of sound of the gas is fixed the Mach number M_s falls with increasing α for a fixed p_{41}. The reason lies in the fact that the particles absorb kinetic and thermal energy. However, the equilibrium speed of sound becomes much smaller and as a result the effective shock Mach number increases with α for a fixed p_{41}. The shock speed is even less than the frozen speed of sound if the amount of particles is sufficiently large. Then, the shock wave becomes dispersed without a discontinuous frozen front. The region below the dashed line $M_s = 1$, is that of dispersed shock waves over the p_{41} range. The variations of flow quantities behind the shock wave with diaphragm pressure ratio are illustrated in Figs. 29-32. The flow quantities of the gas immediately behind the frozen shock front are also plotted. The temperature and the velocity reduce as α takes on larger value. On the contrary, the equilibrium pressure and density increase owing to compression. It should be noted that at equilibrium the frozen values of the pressure and the density of the gas decreases with particle concentration. The density and the temperature between the contact surface and the rarefaction wave are plotted in Figs. 33 and 34. The presence of particles bring about compressive effects on the flow in this region, such that these values increase with particle concentration for a given diaphragm pressure ratio.

4. CONCLUSIONS

Flow properties in a shock tube, in which many solid particles are suspended in the driven section, were analyzed numerically. Use was made of the random-choice method modified so as to be applicable to a dusty gas together with an operator splitting technique.

The particles remove momentum and energy from the gas behind the shock wave. As a result, the strength of the discontinuous frozen shock wave in the gas phase decays. If the number of particles is sufficiently large or the shock is fairly weak, the frozen shock decays to a Mach wave and the shock wave becomes fully dispersed. The deceleration of the gas, while the particles accelerate behind the shock wave, produces a compression and the equilibrium pressure becomes higher than for the case of a pure gas at some distance from the front. In this manner a thick stationary structure arises, where the particles finally reach the same velocity and temperature as the gas. On the other side of the contact front the compressive effect weakens the strength of the rarefaction wave.

Some particles remain in the contact region, such that they interact with the hot gas in front of it and with the cold gas behind it. Thus, the sharp discontinuities in temperature and density of the gas become transitional and a contact region of finite thickness appears. For the cases considered here, with larger drag values, it is possible for the particles to vanish abruptly at the cold side of the contact region. As a consequence, there is a sudden discontinuity in temperature and density typical of a contact surface (see Fig. 20).

The influence of particle diameter, particle-number density and diaphragm pressure upon the transient properties of the flow have been studied with the following conclusions. Particles of large size increase the time required for the flow to be in quasi-equilibrium and also increase relaxation length or time to the final stationary shock wave. The degree of increase varies with particle diameter d and lies between d and d^2. When the particle number density is large, variations in the flow quantities occur quickly but the final equilibrium flow values are reached after a longer time. Strong shock waves have much shorter relaxation lengths.

The flow quantities in the equilibrium-flow limit were calculated from exact shock-tube relations. The speed of sound and the specific-heat ratio of this effective perfect gas take on fairly low values owing to the increase of the effective molecular weight. The increase in pressure and density of the dust-laden gas from its frozen values at the shock wave can be quite large. The temperature and velocity on the other hand decrease.

The results obtained in this paper have been based, in particular, on the assumption that the drag force and the rate of heat transfer to the particles are given by Eqs. (8) and (9) (see Appendix C for other assumptions). However, there are many causes in practice to make these assumptions questionable. Among these are non-spherical shape of particles, variation in local distribution of particle-size, interaction between particles, rotation of particles and electrostatic forces. Nevertheless, the quantitative and qualitative nature of the flow in a dusty-gas shock tube has been made clear in our study.

Undoubtedly improvements will be made in the future to take into account some of the above non-ideal properties of the particles. It is possible that even volume and partial-pressure effects will be considered in future for comparison with the present study.

REFERENCES

1. Carrier, G. F. — "Shock Waves in a Dusty Gas", Journal of Fluid Mechanics, Vol. 4, 1958, pp. 376-382.

2. Marble, F. E. — "Dynamics of a Gas Containing Small Solid Particles", Combustion and Propulsion AGARD Colloq. 5th, Pergamon Press, 1963, pp. 175-213.

3. Kriebel, A. R. — "Analysis of Normal Shock Waves in Particle Laden Gas", Trans. ASME, Journal of Basic Engineering, Vol. 86, 1964, pp. 655-665.

4. Rudinger, G. — "Some Properties of Shock Relaxation in Gas Flows Carrying Small Particles", The Physics of Fluids, Vol. 7, 1964, pp. 658-663.

5. Miura, H. — "Weak Shock Waves in a Dusty Gas", Journal of the Physical Society of Japan, Vol. 33, 1972, pp. 1688-1692.

6. Rudinger, G.
Chang, A. — "Analysis of Nonsteady Two-Phase Flow", The Physics of Fluids, Vol. 7, 1964, pp. 1747-1754.

7. Crowe, C. T.
Nicholls, J. A.
Morrison, R. B. — "Drag Coefficients of Inert and Burning Particles Accelerating in Gas Streams", 9th Int. Symp. Combust., Academic Press, 1963, pp. 395-406.

8. Selberg, B. P.
Nicholls, J. A. — "Drag Coefficient of Small Spherical Particles", AIAA Journal, Vol. 6, 1968, pp. 401-408.

9. Rudinger, G. — "Effect[illegible] Coefficient for Gas-Particle Flow in Shock Tubes", Trans. ASME, Journal of Basic Eng., Vol. 92, 1970, pp. 165-172.

10. Outa, E.
Tajima, K.
Morii, H. — "Experiments and Analyses on Shock Waves Propagating through a Gas-Particle Mixture", Bulletin of the JSME, Vol. [illegible] 76, pp. 384-394.

11. Otterman, B.
Levine, A. S. — "Analysis of Gas-Solid Particle Flows in Shock Tubes", AIAA Journal, Vol. 12, 1974, pp. 579-580.

12. Satofuka, N.
Tokita, K. — "Finite Difference Calculation of Gas-Particle Flows in Shock Tubes", The Memoirs of the Faculty of Industrial Arts, Kyoto Technical University, Vol. 28, 1979, pp. 28-3[illegible].

13. Gilbert, M.
Davis, L.
Altman, D. — "Velocity Lag of Particles in Linearly Accelerated Combustion Gases", Jet Propulsion, Vol. 25, 1955, p. 26.

14. Knudsen, J. G.
Katz, D. L.
"Fluid Mechanics and Heat Transfer", McGraw-Hill, New York, 1958.

15. Chapman, S.
Cowling, T. G.
"The Mathematical T heory of Non-Uniform Gases", Cambridge Univ. Press, 1961.

16. Glimm, J.
"Solutions in the Large for Nonlinear Hyperbolic Systems of Equations", Comm. on Pure and Appl. Math., Vol. 18, 1965, pp. 697-715.

17. Chorin, A. J.
"Random Choice Solution of Hyperbolic Systems", Journal of Computational Physics, Vol. 22, 1976, pp. 517-533.

18. Sod, G. A.
"A Numerical Study of a Converging Cylindrical Shock", Journal of Fluid Mechanics, Vol. 83, 1977, pp. 785-794.

19. Saito, T.
Glass, I. I.
"Applications of Random-Choice Method to Problems in Shock and Detonation-Wave Dynamics", UTIAS Report No. 240, 1979.

20. Glass, I. I.
Hall, J. G.
Handbook of Supersonic Aerodynamics, Section 18, Shock Tubes, Government Printing Office, Washington, D.C., 1959.

APPENDIX A

LIST OF NUMERICAL PROGRAMS

In each time step, four calculations are done in order: integration of inhomogeneous equations for $\frac{1}{2}\Delta t$, two applications of random-choice procedure to homogeneous equations and integration of inhomogeneous equations for $\frac{1}{2}\Delta t$. Godunov's iterative procedure (Refs. 17-19) is used in solving the Riemann problem for the gas.

APPENDIX A

```
C       INFINITE SHOCK TUBE (DUSTY GAS)
C       PARTICLES CONTAINED ONLY IN LOW PRESSURE SIDE
        COMMON/A/GA,GB,GC,GD,GE,GF
        COMMON/C/ZUS,XA,RS,UL,PL,[illegible]
        DIMENSION PO(1003),RO(1003),TO(1003),UO(1003),
       1 ZPO(1003),ZTO(1003),ZUO(1003),XS(1003),
       2 X(1003),T(1003),PT(1003),TT(1003),
       3 XCD(500),ZTCD(500),ZCUD(500),
       4 GP(5),GR(5),GT(5),GU(5),GX(5)
        DOUBLE PRECISION DSEED
C       CONSTANTS
        NN=1000
        NS=1000
        NA=NN/2
        NT=NA+1
        NC=NN+1
        NCHART=NC-5
        TCHART=40.0
        UC=1.0
        DX=0.1
        NU=2
        KA=7
        KD=3
        DSEED=123457.D0
        GA=1.4
        GB=0.5*(GA+1.0)
        GC=0.5*(GA-1.0)
        GD=SQRT(GA)
        GE=GC/GA
        GF=GC/GB
        ALFA=1.0
        BETA=1.0
        ETAM=1.0E-3
        FG1=1.225E-3*[illegible]/1.71E-4/((300.0/273.0)**0.760)
        FG2=6.0*1.71E-4*((300.0/273.0)**0.760)*GA/0.75/DIA/DIA/
       1 3.49E4/1.225E-3
        FG3=0.6*(0.75**(1.0/3.0))
C       INITIAL CONDITIONS
        PL=10.0/GA
        RL=10.0
        TL=1.0
        UL=0.0
        ZRL=0.0
        ZTL=0.0
        ZUL=0.0
        PR=1.0/GA
        RR=1.0
        TR=1.0
        UR=0.0
        ZRR=1.0
        ZTR=TR
        ZUR=UR
        PPI=RL
        RRI=UR
        DO 10 I=1,NA
        PO(I)=PL
        RO(I)=RL
        TO(I)=TL
```

```
      UC(I)=UL
      ZRC(I)=ZRL
      ZTC(I)=ZTL
      ZUC(I)=ZUL
      KZ(I)=1
      X(I)=(FLOAT(I-NB)+0.5)*DX
   10 CONTINUE
      DO 20 I=NB,NC
      PC(I)=PR
      RC(I)=RR
      TC(I)=TR
      UC(I)=UR
      ZRC(I)=ZRR
      ZTC(I)=ZTR
      ZUC(I)=ZUR
      KZ(I)=2
      X(I)=(FLOAT(I-NB)+0.5)*DX
   20 CONTINUE
      ISHOCK=NB+L
      CALL PLOTST('//AERO1//MIURA',14)
      CALL PLOT(0.0,1.0,-3)
      CALL FACTOR(0.05)
      HP4=10.0
      HP2F=5.333
      HP2E=2.640
      HGE=(GA+ALFA*BETA)/(1.0+ALFA*BETA)
      HT2E=(HGE+1.0+(HGE-1.0)*HP2E)/(HGE+1.0+(HGE-1.0)/HP2E)
      HT2F=(GA+1.0+(GA-1.0)*HP2F)/(GA+1.0+(GA-1.0)/HP2F)
      HT3E=(HP2E/HP4)**(1.0-1.0/GA)
      HT3F=(HP2F/HP4)**(1.0-1.0/GA)
      HUSE=SQRT((1.0+0.5*(1.0+1.0/HGE)*(HP2E-1.0))*(1.0+ALFA*BETA
     1 /GA)/(1.0+ALFA)/(1.0+ALFA*BETA))
      HUSF=SQRT(1.0+0.5*(1.0+1.0/GA)*(HP2F-1.0))
      HU2F=(HP2F-1.0)*SQRT(2.0/GA/((GA+1.0)*HP2F+GA-1.0))
      HU2E=(HP2E-1.0)*SQRT(2.0/HGE/((HGE+1.0)*HP2E+HGE-1.0)
     1 *(1.0+ALFA*BETA/GA)/(1.0+ALFA)/(1.0+ALFA*BETA))
      HR2F=HUSF/(HUSF-HU2F)
      HR2E=HUSE/(HUSE-HU2E)
      HP3E=HP2E/HT3E
      HP3F=HP2F/HT3F
      T(1)=0.0
      PI(1)=HP2F
      TI(1)=HT2F
      PC(NC+1)=0.0
      PC(NC+2)=2.0
      RC(NC+1)=0.0
      RC(NC+2)=2.0
      TC(NC+1)=0.0
      TC(NC+2)=0.5
      UC(NC+1)=0.0
      UC(NC+2)=0.2
      ZRC(NC+1)=0.0
      ZRC(NC+2)=2.5
      ZTC(NC+1)=0.0
      ZTC(NC+2)=0.5
      ZUC(NC+1)=0.0
      ZUC(NC+2)=0.2
      X(NC+1)=-50.0
```

```
      X(NC+2)=10.0
      TLIST=4.0
      TAULA=4.0
C     TIME STEP
      DO 100 NT=2,NS
      NZ=ISHOCK+5
      NI=NC-NZ
      IF(NT.LE.6)GO TO 31
      ZA=0.0
      DO 30 I=N1,N2
      ZB=ABS(UO(I))+SQRT(GA*PO(I)/RO(I))
      IF(ZB.GT.ZA)ZA=ZB
   30 CONTINUE
      DT=CN*DX/ZA
      GO TO 32
   31 DT=0.05*DX
   32 T(NT)=T(NT-1)+DT
      DS=0.5*DT
C     I-SWEEP(FIRST)
      DO 100 I=N1,ISHOCK
      IF(KZ(I).EQ.1)GO TO 100
      PA=PO(I)
      RA=RO(I)
      UA=UO(I)
      TA=GA*PA/RA
      ZRA=ZRO(I)
      ZTA=ZTO(I)
      ZUA=ZUO(I)
      FRE=FG1*RA*ABS(UA-ZUA)/(TA**0.768)
      IF(FRE.LT.1.0E-6)GO TO 162
      FCD=0.48+28.0/(FRE**0.85)
      FF1=RA*(UA-ZUA)*ABS(UA-ZUA)*FCD
      FNU=2.0+FG3*(FRE**0.5)
      GO TO 163
  162 FF1=0.0
      FNU=2.0
  163 FF2=FG2*(TA**0.768)*FNU*(TA-ZTA)
      ZUO(I)=ZUA+DS*FF1
      UO(I)=UA-DS*ALFA*ZRA/RA*FF1
      ZTO(I)=ZTA+DS*FF2
      PO(I)=PA-GC*RA*(UO(I)**2)-(UA**2))-2.0*GC*ALFA*ZRA*ZUA*FF1*DS
     1 -ALFA*FETA/CA*ZRA*FF2*DS
  100 CONTINUE
C     FIRST STEP
      NO=MAX0(NO,...,KA)
      CC=C...(...)
      S=(CC*FLOAT(NO))/FLOAT(KA)-0.5
      XA=S*DX
      N3=N1+1
      PL=PO(N1)
      RL=RO(N1)
      UL=UO(N1)
      ZRL=ZRO(N1)
      ZTL=ZTO(N1)
      ZUL=ZUO(N1)
      KZL=KZ(N1)
      DO 40 I=N3,N2
      PR=PO(I)
```

```
      PR=PO(I)
      UR=UO(I)
      ZRR=ZRO(I)
      ZTR=ZTO(I)
      ZUR=ZUO(I)
      KZR=KZ(I)
      IF(ABS(PR-PRI).LT.1.0E-4)GO TO 40
      IF(ABS(RR-RRI).LT.1.0E-4)GO TO 40
      CALL CENTR
      PO(I)=P
      RO(I)=R
      UO(I)=U
      IF(KZR.EQ.1)GO TO 45
      IF(KZL.EQ.1)GO TO 43
      IF(ABS(RR-RRI).LT.1.0E-4)GO TO 41
      ZUZ=DX+(ZUR-ZUL)*DS
      ZUO(I)=((ZUR-ZUL)*XA+0.5*DX*(ZUR+ZUL))/ZUZ
      ZTO(I)=((ZTR-ZTL)*XA+0.5*DX*(ZTR+ZTL)+(ZTL*ZUR-ZTR*ZUL)*DS)/ZUZ
      ZRO(I)=((ZRR-ZRL)*XA+0.5*DX*(ZRR+ZRL)+(ZRL*ZUR-ZRR*ZUL)*DS)*DX
     1 /ZUZ**2
      GO TO 49
   41 XZ=ZUL*DS
      IF(ABS(RL-RRI).LT.1.0E-4)GO TO 601
      ISHOCK=I
      GO TO 602
  601 ISHOCK=I-1
  602 IF(XA.GT.XZ)GO TO 42
      ZUO(I)=ZUL
      ZTO(I)=ZTL
      ZRO(I)=ZRL
      GO TO 510
   42 ZUO(I)=ZUR
      ZTO(I)=ZTR
      ZRO(I)=ZRR
      GO TO 510
   43 XZ=ZUR*DS
      IF(XA.GT.XZ)GO TO 46
      ZUO(I)=ZUL
      ZTO(I)=ZTL
      ZRO(I)=ZRL
      KZ(I)=KZL
      GO TO 49
   46 ZUO(I)=ZUR
      ZTO(I)=ZTR
      ZRO(I)=ZRR
      KZ(I)=KZR
   49 PL=PR
      RL=RR
      UL=UR
      ZRL=ZRR
      ZTL=ZTR
      ZUL=ZUR
      KZL=KZR
   40 CONTINUE
C     SECOND STEP
  510 NU=MOD(NU+K3,KA)
      GG=GGUBS(DSEED)
      S=(GG+FLOAT(NU))/FLOAT(KA)-0.5
```

```
      XA=S*DX
      PL=PU(N1)
      RL=RU(N1)
      UL=UU(N1)
      ZRL=ZRU(N1)
      ZTL=ZTU(N1)
      ZUL=ZUU(N1)
      N2=N2(N1)
      DO 50 I=N1,N2
      PR=PU(I+1)
      RR=RU(I+1)
      UR=UU(I+1)
      ZRR=ZRU(I+1)
      ZTR=ZTU(I+1)
      ZUR=ZUU(I+1)
      N2R=N2(I+1)
      IF(ABS(RR-RM1).LT.1.0E-4)GO TO 50
      IF(ABS(RL-RM1).LT.1.0E-4)GO TO 50
      CALL GLIMM
      PU(I)=P
      RU(I)=R
      UU(I)=U
      IF(N2R.GT.1)GO TO 51
      IF(N2L.EQ.1)GO TO 55
      IF(ABS(R-RM1).LT.1.0E-4)GO TO 51
      ZUZ=DX+(ZUR-ZUL)*05
      ZUU(I)=((ZUR-ZUL)*XA+0.5*DX*(ZUR+ZUL))/ZUZ
      ZTU(I)=((ZTR-ZTL)*XA+0.5*DX*(ZTR+ZTL)+(ZTL*ZUR-ZTR*ZUL)*DX)/ZUZ
      ZRU(I)=((ZRR-ZRL)*XA+0.5*DX*(ZRR+ZRL)+(ZRL*ZUR-ZRR*ZUL)*DX)*
     1 /ZUZ**2
      GO TO 55
   51 N2=N2L+1
      IF(ABS(R-RM1).LT.1.0E-4)GO TO 511
      ISHOCK=1
      GO TO 512
  511 ISHOCK=I-1
  512 IF(XA.GT.X2)GO TO 57
      ZUU(I)=ZUL
      ZTU(I)=ZTL
      ZRU(I)=ZRL
      GO TO 58
   57 ZUU(I)=ZUR
      ZTU(I)=ZTR
      ZRU(I)=ZRR
      GO TO 58
   55 XA=ZUL*DX
      IF(XA.GT.X2)GO TO 56
      ZUU(I)=ZUL
      ZTU(I)=ZTL
      ZRU(I)=ZRL
      N2(I)=N2L
      ISUBI=I+1
      GO TO 59
   56 ZUU(I)=ZUR
      ZTU(I)=ZTR
      ZRU(I)=ZRR
      N2(I)=N2R
      ISUBI=I
```

```
   59 [illegible]
      [illegible]
      [illegible]
      [illegible]
      [illegible]
      [illegible]
      [illegible]
   50 CONTINUE
C     [illegible]
  620 [illegible] I=1,ISHOCK
      IF(N[illegible](I).EQ.1)GO TO 61
      PA=P0(I)
      [illegible]A=R0(I)
      UA=U0(I)
      TA=[illegible]PA/[illegible]A
      [illegible](I)
      ZTA=ZT0(I)
      ZUA=[illegible](I)
      FR[illegible]A*ABS(UA-ZUA)/(TA**0.768)
      [illegible](FR[illegible].LT.1.0E-5)GO TO 62
      [illegible]=0.40+20.0/(FRE**0.85)
      [illegible]1=RA*(UA-ZUA)*ABS(UA-ZUA)*CD
      FNU=2.0+0.3*(FRE**0.5)
      GO TO 63
   62 FFI=0.0
      FNU=2.0
   63 FF2=[illegible]G2*(TA**0.763)*FNU*(TA-ZTA)
      ZU0(I)=ZUA+DS*FF1
      U0(I)=UA-DS*ALFA*RA/RA[illegible]
      ZT0(I)=ZTA+DS*FF2
      P0(I)=PA-GC[illegible]A*((U0(I)**2)-(UA**2))-2.0*GC*ALFA*ZRA*ZUA*FF[illegible]
     1 -ALFA[illegible]TA/GA[illegible]FF2*DS
   61 [illegible](I)=GA*P0(I)/R0(I)
   60 CONTINUE
      IF(NT.GT.2)GO TO 701
      PT(NT)=[illegible]
      TT(NT)=[illegible]
      [illegible] 702
  701 PT(NT)=P0(ISHOCK)*GA
      TT(NT)=T0(ISHOCK)
  702 IF([illegible]I)GO TO [illegible]
      IF(T(NT).GT.T[illegible]I)GO TO 701
C     [illegible]
      WRITE(6,500)NT,T(NT),ISHOCK,PT(NT),TT(NT)
  500 FORMAT(1H ,10X,I[illegible],F[illegible])
      IF(T(NT).LT.TLIST)GO TO 100
      WRITE(6,[illegible])T(NT)
  [illegible] FORMAT(1H[illegible] =,[illegible])
      [illegible]=TLIST+[illegible]
      DO 70 I=1,[illegible]
      [illegible](I)=[illegible]*GA
   70 CONTINUE
      [illegible]=I[illegible]+2
      DO [illegible] J=1,[illegible]
      I=[illegible]-1+J
      X[illegible](J)=X(I)
      ZT[illegible](J)=ZT0(I)
      ZU[illegible](J)=ZU0(I)
```

```
   72 CONTINUE
      XDD(NDUST+1)=-50.0
      XDD(NDUST+2)=10.0
      ZDD(NDUST+1)=3.0
      ZDD(NDUST+2)=0.3
      ZDD(NDUST+1)=3.0
      ZDD(NDUST+2)=0.2
      CALL AXIS(0.0,0.0,1HX,-1,10.0,0.0,-50.0,10.0)
      CALL AXIS(0.0,0.0,1HR,+1,5.0,90.0,0.0,2.5)
      CALL PLOT(10.0,0.0,3)
      CALL PLOT(10.0,5.0,2)
      CALL PLOT(0.0,5.0,2)
      CALL LINEST(-1)
      CALL LINE(X,RC,NC,1,0,0)
      CALL LINEST(0)
      CALL LINE(X,ZC,NC,1,0,0)
      CALL PLOT(0.0,0.0,-3)
      CALL AXIS(0.0,0.0,1HX,-1,10.0,0.0,-50.0,10.0)
      CALL AXIS(0.0,0.0,1HZ,+1,5.0,90.0,0.0,2.5)
      CALL PLOT(10.0,0.0,3)
      CALL PLOT(10.0,5.0,2)
      CALL PLOT(0.0,5.0,2)
      CALL LINEST(-1)
      CALL LINE(X,RC,NC,1,0,0)
      CALL LINEST(0)
      CALL PLOT(10.0,0.0,-3)
      CALL AXIS(0.0,0.0,1HX,-1,10.0,0.0,-50.0,10.0)
      CALL AXIS(0.0,0.0,1HT,+1,5.0,90.0,0.0,2.5)
      CALL PLOT(10.0,0.0,3)
      CALL PLOT(10.0,5.0,2)
      CALL PLOT(0.0,5.0,2)
      CALL LINEST(-1)
      CALL LINE(X,TC,NC,1,0,0)
      CALL LINEST(0)
      CALL LINE(XDD,ZDD,NDUST,1,0,0)
      CALL PLOT(0.0,-5.0,-3)
      CALL AXIS(0.0,0.0,1HX,-1,10.0,0.0,-50.0,10.0)
      CALL AXIS(0.0,0.0,1HG,+1,5.0,90.0,0.0,2.5)
      CALL PLOT(10.0,0.0,3)
      CALL PLOT(10.0,5.0,2)
      CALL PLOT(0.0,5.0,2)
      CALL LINEST(-1)
      CALL LINE(X,GC,NC,1,0,0)
      CALL LINEST(0)
      CALL LINE(XDD,ZDD,NDUST,1,0,0)
      CALL PLOT(10.0,0.0,-3)
      DO 71 I=1,NC
      PL(I)=PL(I)/GA
   71 CONTINUE
      VP(7)=0.0
      VP(8)=2.5
      VR(7)=0.0
      VR(8)=2.5
      VT(7)=0.0
      VT(8)=0.2
      GL(7)=0.0
      GL(8)=0.2
      GX(7)=-50.0
```

```
      GX(1)=10.0
      IF(T(NT).GT.(TAIDA+1.0))GO TO 75
      HP2=HP21
      HA2=HA2F
      HA3=HA3F
      HT2=HT2F
      HT3=HT3F
      HO2=HO2F
      HO3=HO3F
      GO TO 74
   73 IF(T(NT).LT.17.0)GO TO 100
      HP2=HP2L
      HA2=HA2L
      HA3=HA3L
      HT2=HT2L
      HT3=HT3L
      HO2=HO2L
      HO3=HO3L
   74 GX(1)=T(NT)
      GP(1)=HP2
      GA(1)=HA2
      GT(1)=HT2
      GO(1)=HO2
      GU(1)=0.0
      GX(2)=(100-EXP(HP2/100.0))*T(NT)
      GP(2)=HP2
      GA(2)=HA2
      GT(2)=HT3
      GO(2)=HO2
      DO 75 J=2,5
      GX(J)=GX(1)+0.2*(GX(2)-GX(1))*(1.0AT(J-1)
      GA=(7.0-GX(J))/T(NT)*(GA-1.0))/(GA+1.0)
      GX(J)=((GA+(2.0/(GA-1.0)))*HP2
      GP(J)=(HP2*(1.0-GA))*(GX(J)**GA)
      GT(J)=GP(J)/GX(J)
      GU(J)=2.0/(GA+1.0)*(GX(J)/T(NT)+1.0)
   75 CONTINUE
      CALL PLOT(-2.0,0.0,-3)
      CALL PLINE(GX,GP,6,1,0)
      CALL PLOT(0.0,15.0,-3)
      CALL PLINE(GX,GP,6,1,0)
      CALL PLOT(13.0,0.0,-3)
      CALL PLINE(GX,GT,6,1,0)
      CALL PLOT(0.0,-15.0,-3)
      CALL PLINE(GX,GO,6,1,0)
      CALL PLOT(-13.0,0.0,-3)
      GX(1)=GX(6)
      GP(1)=HP2
      GA(1)=HA2
      GT(1)=HT2
      GO(1)=HO2
      GX(2)=HA2+T(NT)
      GP(2)=HP2
      GA(2)=HA3
      GT(2)=HT3
      GO(2)=HO2
      GX(3)=GX(6)
      GP(3)=HP2
      GA(3)=HA2
```

```
      GI(4)=GI(3)
      GC(4)=GC(3)
      GX(4)=GX(3)+GT(3,3)
      GP(4)=GP(3)
      GR(4)=GR(3)
      GI(4)=GI(3)
      GC(4)=GC(3)
      GX(5)=GX(4)
      GP(5)=1.0
      GR(5)=1.0
      GI(5)=1.0
      GC(5)=0.0
      GX(6)=50.0
      GP(6)=1.0
      GR(6)=1.0
      GI(6)=1.0
      GC(6)=0.0
      CALL GASHL(GX,GP,6,1)
      CALL PLOT(0.0,0.0,-3)
      CALL GASHL(GX,GR,6,1)
      CALL PLOT(15.0,0.0,-3)
      CALL GASHL(GX,GI,6,1)
      CALL PLOT(0.0,-5.0,-3)
      CALL GASHL(GX,GC,6,1)
      CALL PLOT(15.0,0.0,-3)
  100 CONTINUE
  201 CALL AXIS(0.0,0.0,'TIME',-4,5.0,0.0,0.0,0.0)
      CALL AXIS(0.0,0.0,'AMP',+3,5.0,90.0,1.0,0.4)
      CALL PLOT(5.0,0.0,3)
      CALL PLOT(5.0,5.0,2)
      CALL PLOT(0.0,5.0,2)
      PT(NT+1)=1.0
      PT(NT+2)=.1
      T(NT+1)=0.0
      T(NT+2)=0.0
      CALL LINTYP(-1)
      CALL LINE(T,PT,NT,1,0,0)
      CALL LINTYP(0)
      CALL PLOT(0.0,0.0,-3)
      CALL AXIS(0.0,0.0,'AMPLITUDE',+9,5.0,0.0,0.0,0.0)
      CALL AXIS(0.0,0.0,'FREQUENCY',+9,5.0,90.0,1.0,0.1)
      CALL PLOT(5.0,0.0,3)
      CALL PLOT(5.0,5.0,2)
      CALL PLOT(0.0,5.0,2)
      PT(NT+1)=1.0
      PT(NT+2)=0.1
      CALL LINTYP(-1)
      CALL LINE(T,PT,NT,1,0,0)
      CALL LINTYP(0)
      CALL PLEND
      STOP
      END
```

```
      SUBROUTINE GLIMM
      COMMON/A/GA,GB,GC,GD,GE,GF
      COMMON/B/DS,XA,RL,UL,PL,RR,UR,PR,R,U,P
C     SOLUTION OF RIEMANN PROBLEM BY GODUNOV'S ITERATIVE METHOD
      AA=1.0
      EP=1.0E-6
      IS=40
      CL=SQRT(PL*RL)
      CR=SQRT(PR*RR)
    5 IT=0
      PA=0.5*(PL+PR)
   10 IT=IT+1
      PA=AMAX1(EP,PA)
      WL=CL*FY(PA/PL)
      WR=CR*FY(PA/PR)
      PE=(UL-UR+PR/WR+PL/WL)/(1.0/WR+1.0/WL)
      PS=PE-PA
      IF(ABS(PS).LT.EP)GO TO 20
      PA=PA+AA*PS
      IF(IT.LE.IS)GO TO 10
      AA=0.5*AA
      IF(AA.LT.EP)GO TO 20
      GO TO 5
   20 UA=(PL-PR+WR*UR+WL*UL)/(WR+WL)
C     [illegible]
      XX=UA*DS
      IF(XA.GE.XX)GO TO 70
      IF(PA.LT.PL)GO TO 40
      W=UL-WL/RL
      XX=W*DS
      IF(XA.GT.XX)GO TO 30
      R=RL
      U=UL
      P=PL
      GO TO 200
   30 R=WL/(UA-W)
      U=UA
      P=PA
      GO TO 200
   40 W=SQRT(GA*PL/RL)
      XX=(UL-W)*DS
      IF(XA.GE.XX)GO TO 50
      R=RL
      U=UL
      P=PL
      GO TO 200
   50 CC=PL/(RL**GA)
      RA=(PA/CC)**(1.0/GA)
      WA=SQRT(GA*PA/RA)
      XX=(UA-WA)*DS
      IF(XA.GE.XX)GO TO 60
      U=(XA/DS [illegible] (CC*GC)/GF
      R=((U-XA/DS)**2/GA/CC)**(0.5/GC)
      P=CC*(R**GA)
      GO TO 200
   60 R=RA
      U=UA
      P=PA
```

```
      GO TO 200
   70 IF(PA.LT.PR)GO TO 140
      U=UI+CR/[illegible]
      XX=[illegible]DS
      IF(XA.LT.XX)GO TO 130
      R=[illegible]
      U=UR
      P=PR
      GO TO 200
  130 R=GF/(U-UA)
      U=UA
      P=PA
      GO TO 200
  140 R=SQRT(GA*PF/RR)
      XX=(UR+S)*DS
      IF(XA.LT.XX)GO TO 150
      R=RR
      U=UR
      P=PR
      GO TO 200
  150 CC=PA/(RA**GA)
      RA=(PA/CC)**(1.0/GA)
      SS=SQRT(GA*PA/RA)
      XX=(UA+SS)*DS
      IF(XA.LT.XX)GO TO 160
      U=(XA/DS-S+GC*UA)/GB
      R=((XA/DS-U)**2/GA/CC)**(0.5/GC)
      P=CC*(R**GA)
      GO TO 200
  160 R=RA
      U=UA
      P=PA
  200 CONTINUE
      RETURN
      END
```

```
      FUNCTION FY(X)
      COMMON /A/GA,GB,GC,GD,GE,GF
      EP=1.0E-2
      IF(X.LT.1.0)GO TO 10
      FY=SQRT(GD*X+GC)
      RETURN
   10 IF((1.0-X).LT.EP)GO TO 20
      FY=GF*(1.0-X)/(1.0-(X**GE))
      RETURN
   20 FY=GD/(1.0-0.5*(GE-1.0)*(1.0-X)+(GE-1.0)*(GE-2.0)/6.0
     1 *(1.0-X)**2-(GE-1.0)*(GE-2.0)*(GE-3.0)/24.0*(1.0-X)**3)
      RETURN
      END
```

APPENDIX B

FROZEN AND EQUILIBRIUM FLOWS

The frozen-flow values at the instant of diaphragm rupture when the particles have no effect can readily be found from the relations given in Ref. 20. If it is now assumed that the velocity and the temperature of the particles are the same as those of the gas everywhere and we neglect the transition thicknesses of the shock wave and the contact region, the equilibrium-flow limit is readily found. In this limit, the pressure in the uniform region behind the shock wave p_2 must satisfy the shock-tube equation (Ref. 20):

$$\frac{p_4}{p_1} = \frac{p_2}{p_1}\left\{1 - \frac{(\gamma_4 - 1)(a_1/a_4)(p_2/p_1 - 1)}{\sqrt{2\gamma_1}\sqrt{2\gamma_1 + (\gamma_1 + 1)(p_2/p_1 - 1)}}\right\}^{-\frac{2\gamma_4}{\gamma_4 - 1}} \tag{B1}$$

where γ_1 and a_1 are now given by Eqs. (23) and (24) as γ_1 and a_1, respectively. Once p_{21} is known, the other flow quantities are obtained from the Rankine-Hugoniot relations as follows (see Ref. 20):

$$\frac{\rho_2}{\rho_1} = \frac{1 + (\gamma_1 + 1)/(\gamma_1 - 1) \times (p_2/p_1)}{(\gamma_1 + 1)/(\gamma_1 - 1) + p_2/p_1} \tag{B2}$$

$$\frac{T_2}{T_1} = \frac{p_2}{p_1} \cdot \frac{(\gamma_1 + 1)/(\gamma_1 - 1) + p_2/p_1}{1 + (\gamma_1 + 1)/(\gamma_1 - 1) \times (p_2/p_1)} \tag{B3}$$

$$\frac{u_2}{a_1} = \frac{1}{\gamma_1}\left(\frac{p_2}{p_1} - 1\right)\sqrt{\frac{2\gamma_1}{\gamma_1 + 1}\Big/\left(\frac{p_2}{p_1} + \frac{\gamma_1 - 1}{\gamma_1 + 1}\right)} \tag{B4}$$

$$\frac{u_s}{a_1} = \sqrt{\frac{\gamma_1 - 1}{2\gamma_1} + \frac{\gamma_1 + 1}{2\gamma_1} \cdot \frac{p_2}{p_1}} \tag{B5}$$

where u_s is the velocity of propagation of the shock wave.

The temperature and the density in the uniform region between the contact surface and the rarefaction wave are given by the isentropic relations (Ref. 20)

$$\frac{T_3}{T_4} = \left(\frac{p_3}{p_4}\right)^{\frac{\gamma_4 - 1}{\gamma_4}} = \left(\frac{p_2/p_1}{p_4/p_1}\right)^{\frac{\gamma_4 - 1}{\gamma_4}} \tag{B6}$$

$$\frac{\rho_3}{\rho_4} = \left(\frac{p_3}{p_4}\right)^{\frac{1}{\gamma_4}} = \left(\frac{p_2/p_1}{p_4/p_1}\right)^{\frac{1}{\gamma_4}} \tag{B7}$$

Once u_s is obtained, we can calculate the properties of the discontinuous frozen shock wave at the head of the shock front. If u_s is smaller than the frozen speed of sound a_{1_f}, the frozen shock wave reduces to a Mach wave and it is fully dispersed.

For u_s larger than a_{1_f}, the pressure immediately behind the frozen shock front is obtained from Eq. (B5) by taking a_{1_f} and γ as a_1 and γ_1 respectively. Other quantities at this position are calculated from the foregoing Rankine-Hugoniot relations for a pure gas.

To summarize, in Fig. 26a for example, the equilibrium value of pressure can be calculated at once from the shock-tube relations for the given initial conditions. Knowing the equilibrium Mach number, the frozen part of the shock front can also be immediately calculated from the shock-tube equations (since the entire equilibrium phenomenon and the frozen shock all move at the same Mach number). The transition from the frozen shock wave to equilibrium, however, must be obtained numerically. On this basis all the curves from Fig. 28 to 32 were constructed to provide exact solutions useful for the experimenter.

APPENDIX C

NONEQUILIBRIUM SHOCK-TUBE PROFILES USING STOKES' DRAG LAW

Figures 35-37 are included to illustrate how the Stokes' drag law $C_D = Re/24$ together with Nu = 2 can give erroneous results. For example, the shock transition profiles are unduly long owing to the very small drag coefficient (compare Fig. 36a with Fig. 5a). The same is true of the contact front transition (compare Fig. 36c with Fig. 5c). The change in transition is slow and the oscillations are very much reduced (compare Fig. 7 with Fig. 37).

Table 1

Some Reference Lengths, Times and Number Densities

$$\ell = \frac{4}{3} \cdot \frac{\rho_p}{\rho_1} d, \quad t = \frac{\ell}{a_{1_f}} \tau$$

$\rho_p = 2.5$ g/cm^3 (typical of crown glass), $\rho_1 = 1.23 \times 10^{-3}$ g/cm^3, $a_{1_f} = 350$ m/sec

d (μm)	10	20	40
ℓ (cm)	2.72	5.44	10.9
ℓ/a_{1_f} (sec)	0.78×10^{-4}	1.56×10^{-4}	3.11×10^{-4}
t (sec) for $\tau = 4$	3.11×10^{-4}	6.23×10^{-4}	1.25×10^{-3}
t (sec) for $\tau = 32$	2.49×10^{-3}	4.98×10^{-3}	9.96×10^{-3}
n_p (cm^{-3}) for $\alpha = 1.0$	0.94×10^{6}	1.17×10^{5}	1.46×10^{4}

Table 2

Some Properties of Idealized Equilibrium Gas-Particle Mixture

$$\gamma_e = \frac{\gamma + \alpha\beta}{1 + \alpha\beta}, \qquad a_{1_e} = \sqrt{\frac{\gamma + \alpha\beta}{(1 + \alpha)(1 + \alpha\beta)} \cdot \frac{p_1}{\rho_1}}$$

$\beta = 1$ (typical of glass), $T_1 = 300°K$

α	γ_e	a_{1_e} (m/sec)
0	1.40 (= γ)	350 (= a_{1_f})
0.2	1.33	312
0.4	1.29	283
0.6	1.25	261
0.8	1.22	244
1.0	1.20	229
2.0	1.13	182

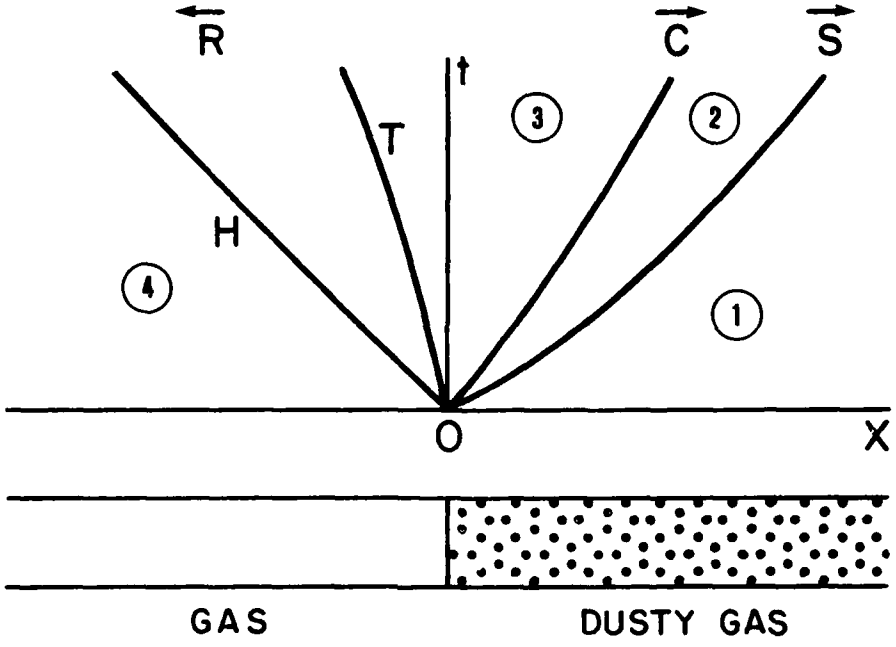

FIG. 1 SCHEMATIC DIAGRAM OF FLOW IN A DUSTY-GAS SHOCK TUBE AFTER DIAPHRAGM RUPTURE.

$\overleftarrow{R}$ = RAREFACTION WAVE; $\overrightarrow{C}$ = CONTACT FRONT; $\overrightarrow{S}$ = SHOCK FRONT; H = HEAD, T = TAIL.

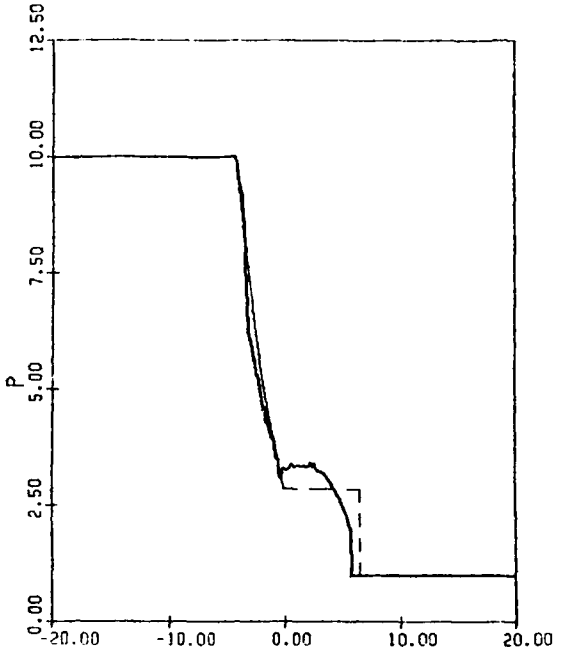

(a) Pressure

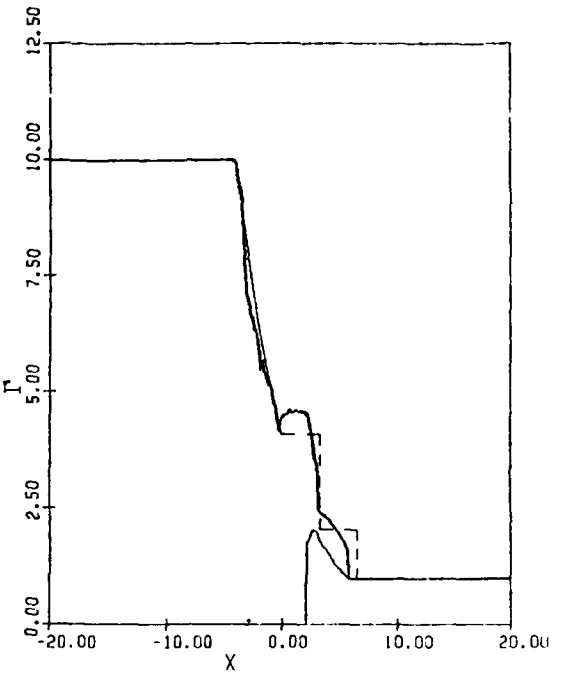

(b) Mass Concentration

(c) Temperature

(d) Velocity

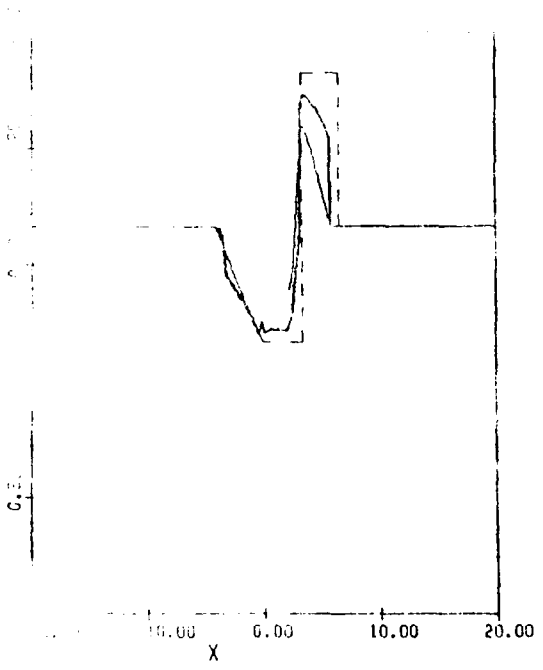

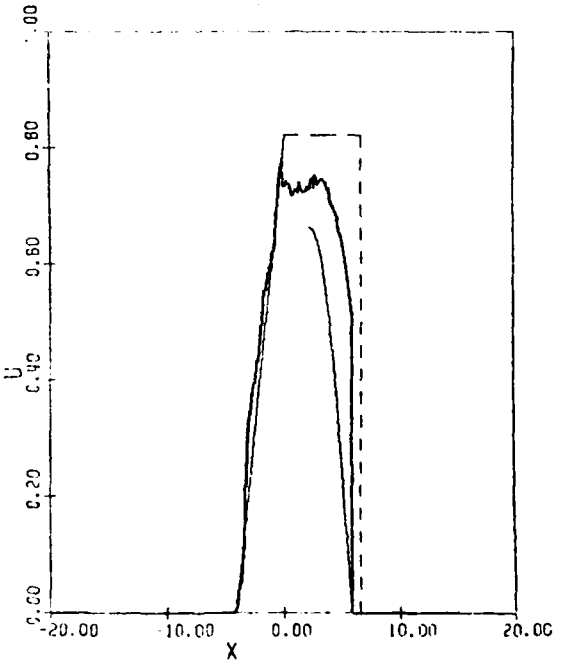

FIG. 2 FLOW QUANTITIES AT $\tau = 4$ ($\alpha = 1$, $P_{41} = 10$, d = 10 μm)

——— GAS, ——— PARTICLES, ------ FROZEN FLOW

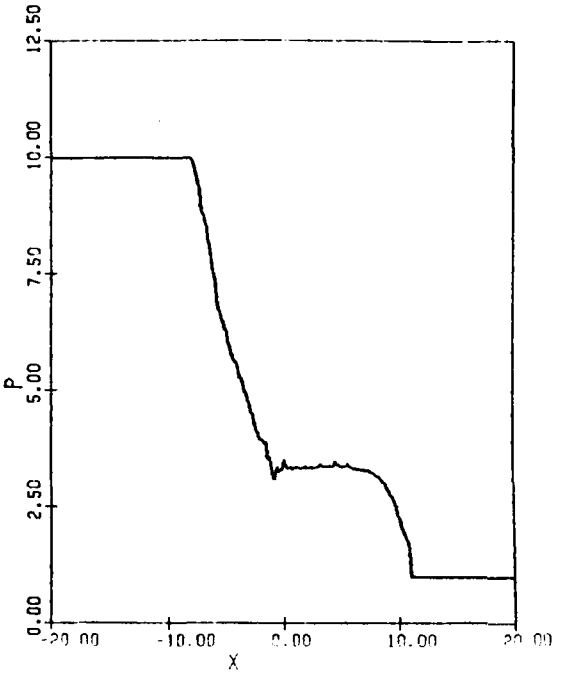

(a) Pressure

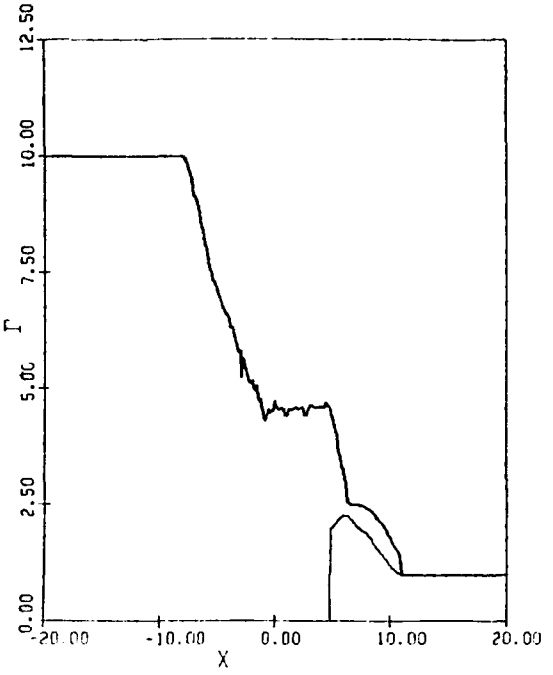

(b) Mass Concentration

(c) Temperature

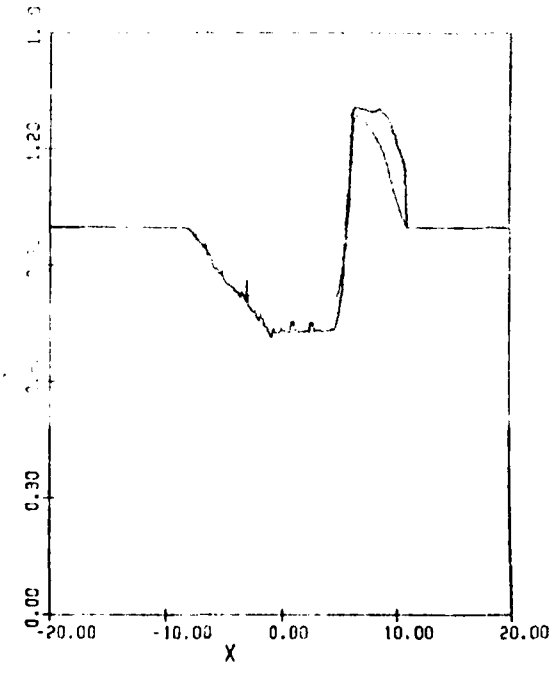

(d) Velocity

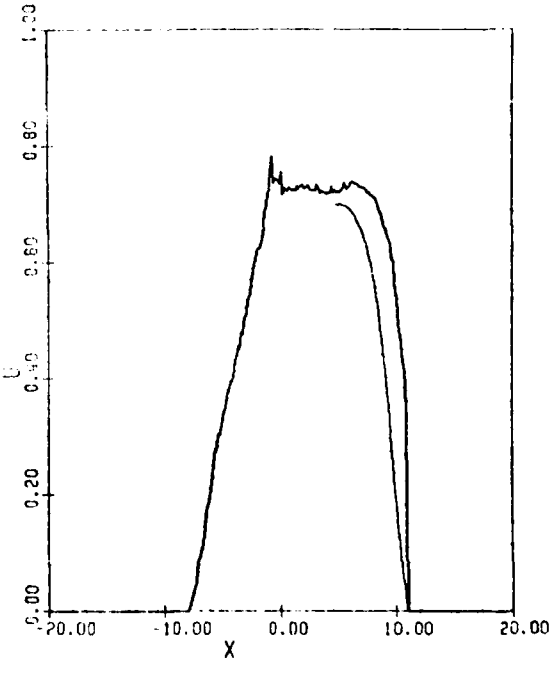

FIG. 3 FLOW QUANTITIES AT $\tau = 8$ ($\alpha = 1$, $P_{41} = 10$, d = 10 μm)
——— GAS, ——— PARTICLES.

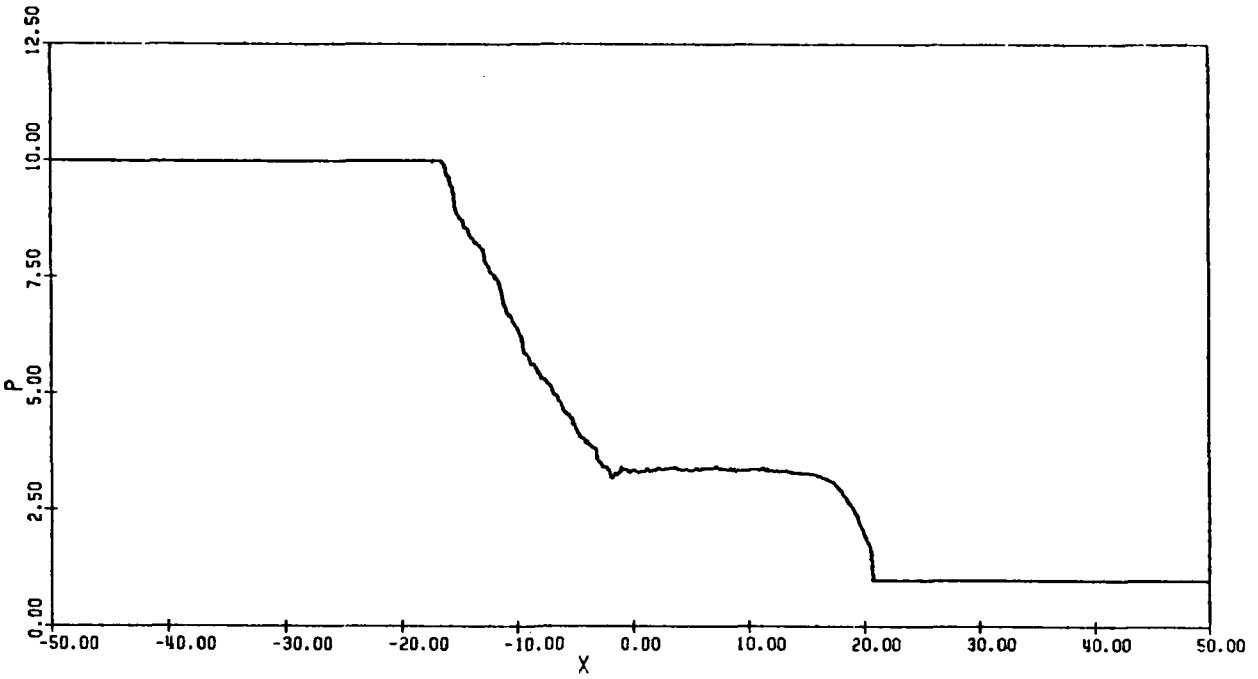

(a) Pressure

(b) Mass Concentration

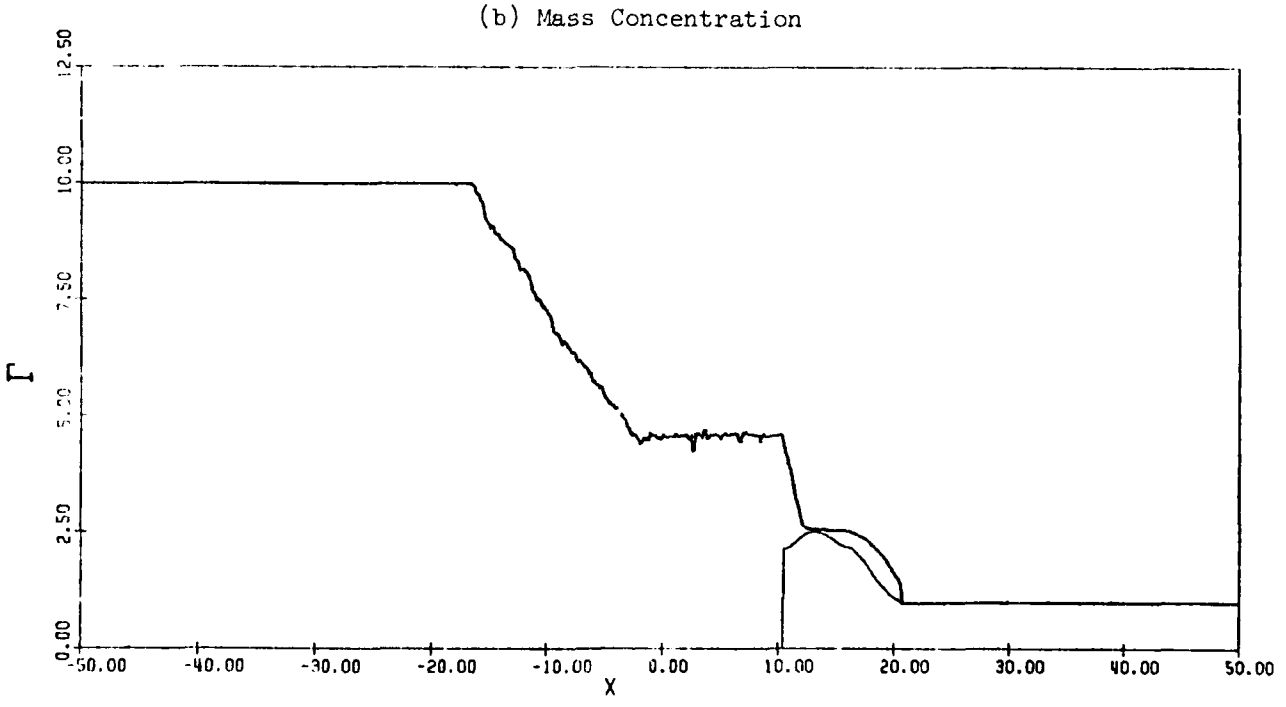

FIG. 4 FLOW QUANTITIES AT $\tau = 16$ ($\alpha = 1$, $P_{41} = 10$, $d = 10\ \mu m$)
——— GAS, ——— PARTICLES.

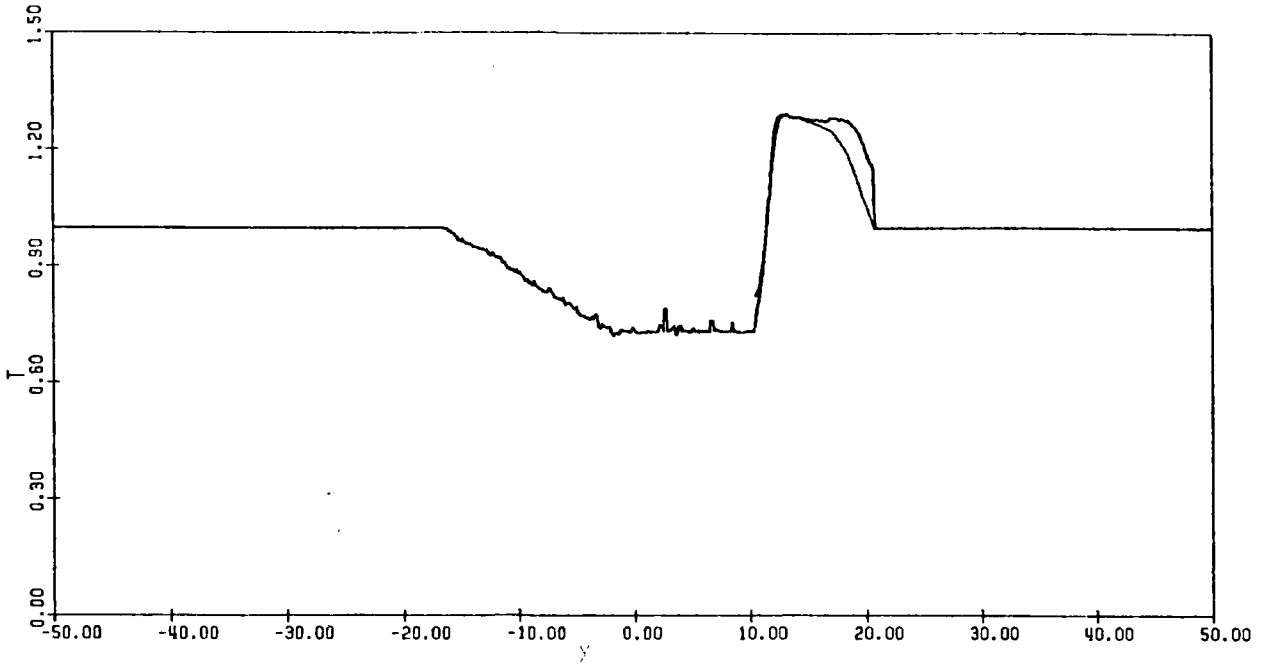

(c) Temperature

(d) Velocity

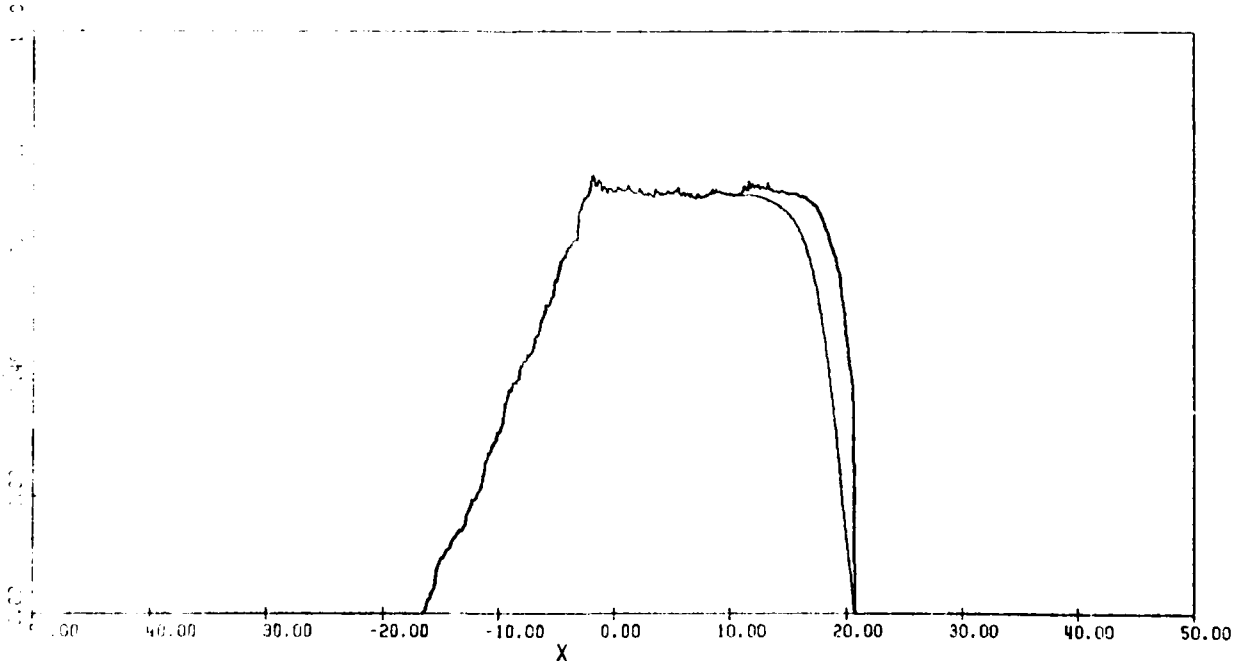

FIG. 4 (CONTINUED) FLOW QUANTITIES AT $\tau = 16$ ($\alpha = 1$, $P_{41} = 10$, $d = 10\ \mu m$)
——— GAS, ——— PARTICLES.

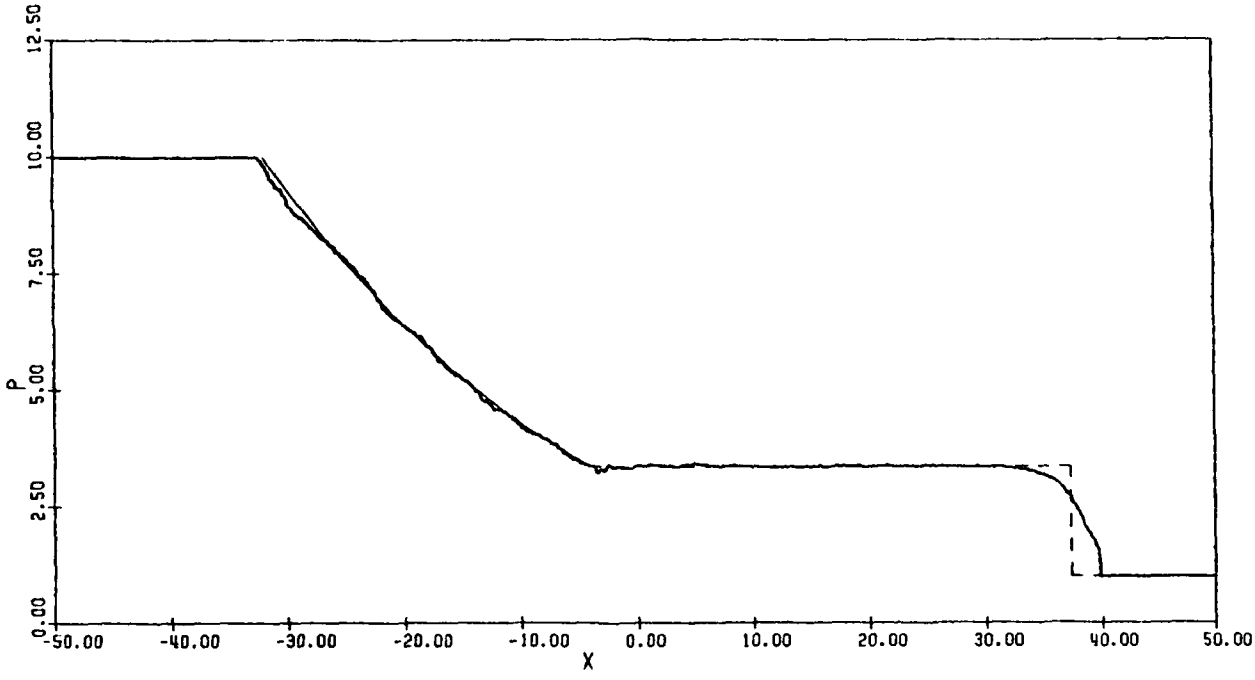

(a) Pressure

(b) Mass Concentration

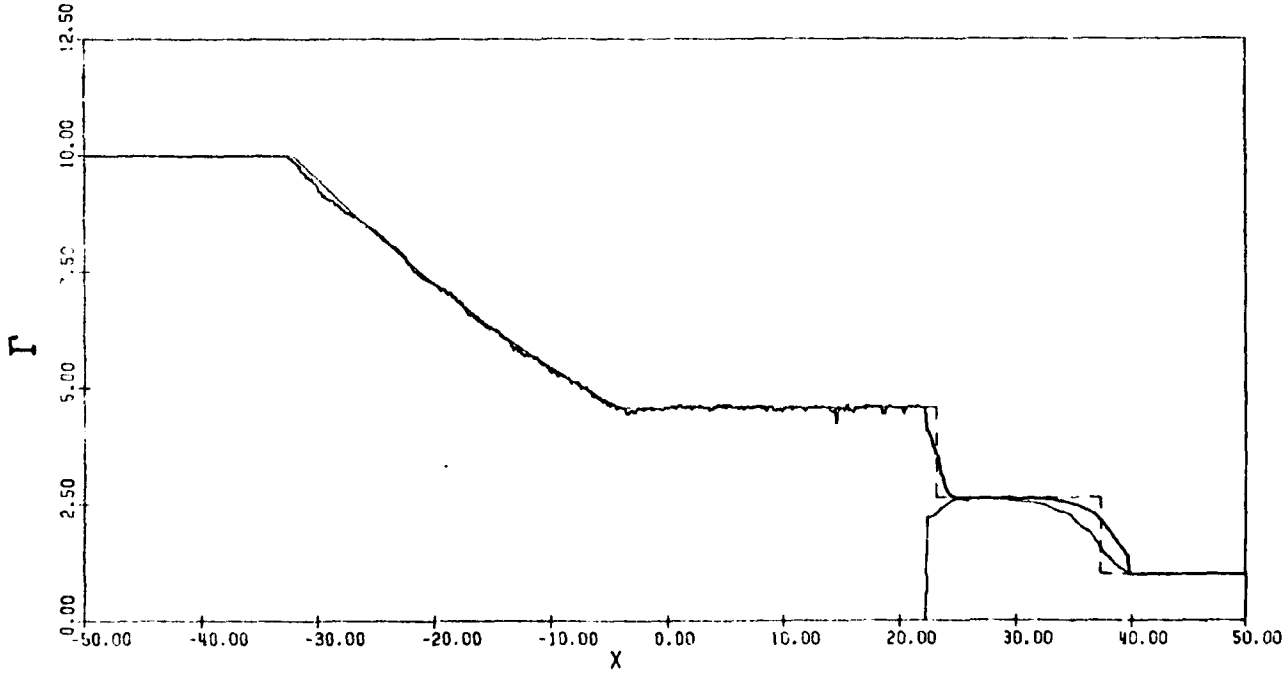

FIG. 5 FLOW QUANTITIES AT $\tau = 32$ ($\alpha = 1$, $P_{41} = 10$, $d = 10$ μm)
——— GAS, ——— PARTICLES, ------ EQUILIBRIUM FLOW

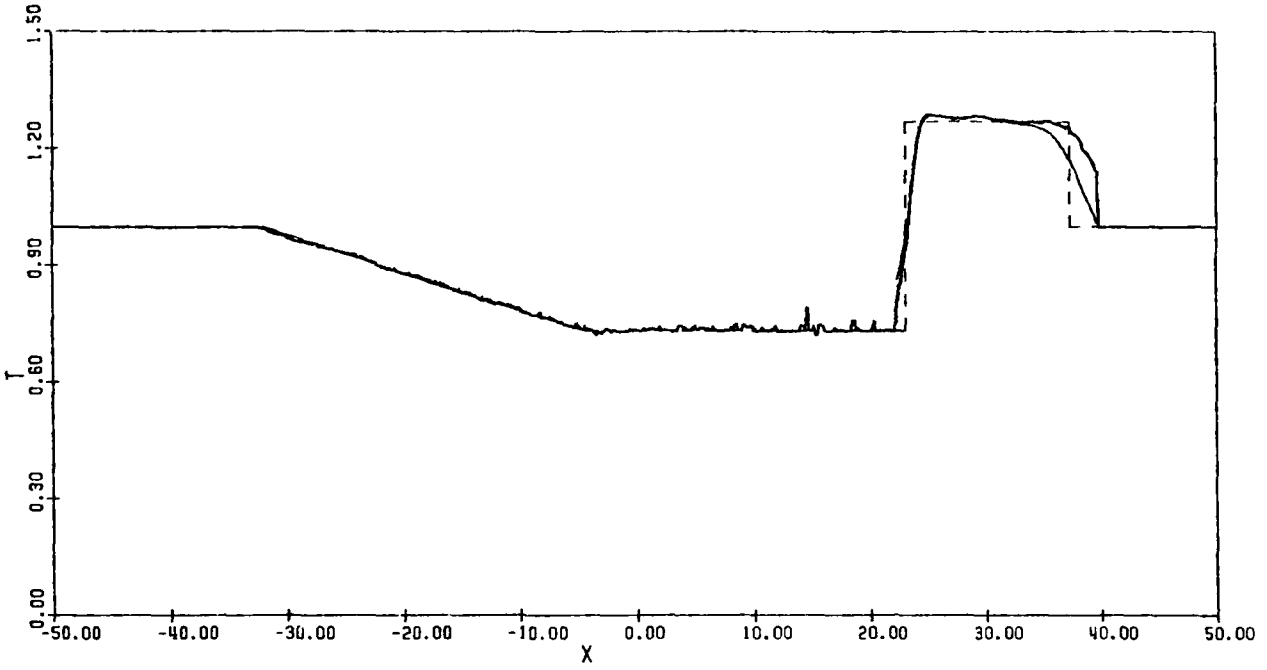

(c) Temperature

(d) Velocity

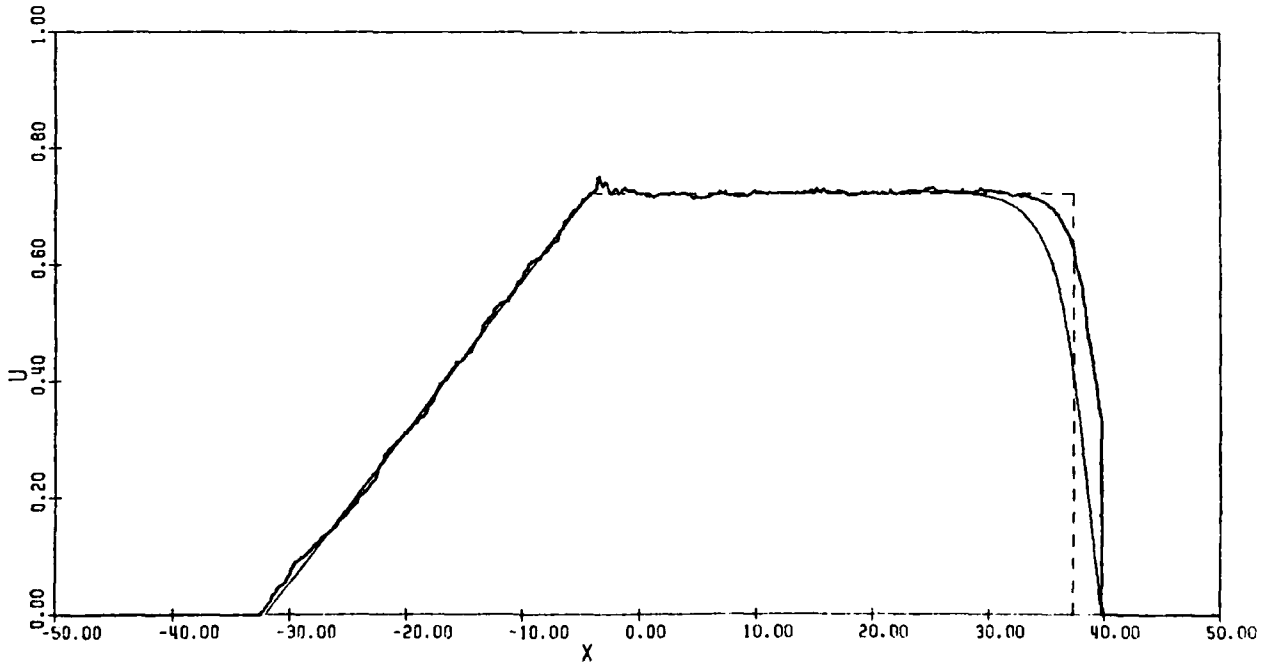

FIG. 5 (CONTINUED) FLOW QUANTITIES AT $\tau = 32$ ($\alpha = 1$, $P_{41} = 10$, $d = 10\ \mu m$).

——— GAS, ——— PARTICLES, EQUILIBRIUM FLOW.

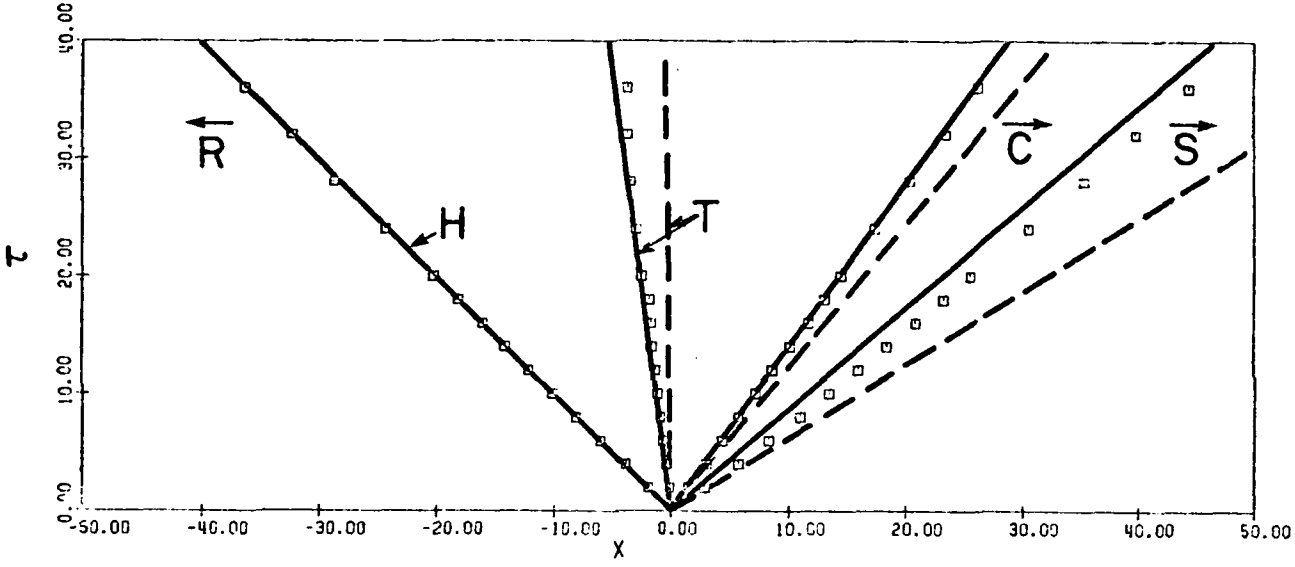

FIG. 6 WAVE DIAGRAM OF TIME-DISTANCE (τ, X) PLANE AFTER DIAPHRAGM RUPTURE (α = 1, P_{41} = 10, d = 10 μm).

□ PRESENT RESULTS, ——— EQUILIBRIUM FLOW, ------ FROZEN FLOW, R = RAREFACTION WAVE, H = HEAD, T = TAIL, c = CONTACT SURFACE, S = SHOCK FRONT. NOTE THAT THE SEPARATION BETWEEN THE PRESENT RESULTS AND THE EQUILIBRIUM LINES SHOW THE STRUCTURE OF THE SHOCK-WAVE TRANSITION.

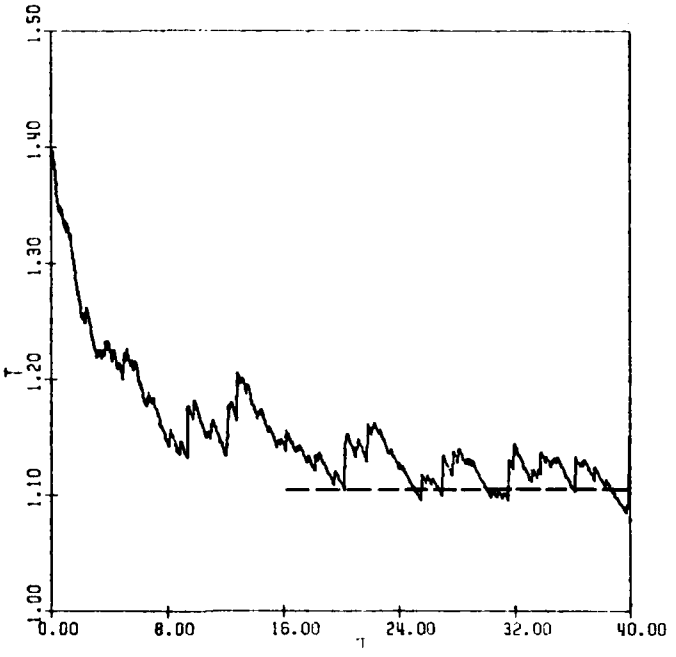

(a) Temperature

(b) Pressure

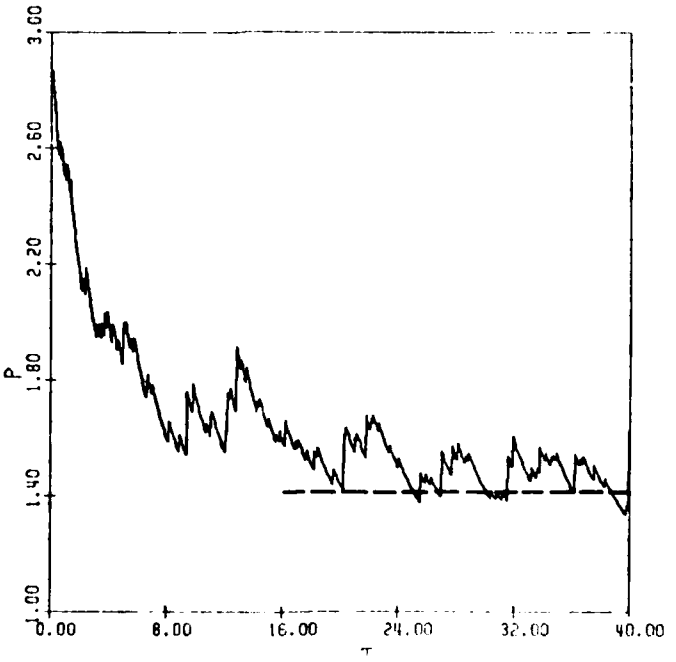

FIG. 7 VARIATIONS WITH TIME OF TEMPERATURE AND PRESSURE OF GAS JUST BEHIND DISCONTINUOUS FROZEN SHOCK FRONT (α = 1, P_{41} = 10, d = 10 μm, Δx = 0.1)

------ EXPECTED FINAL VALUE.

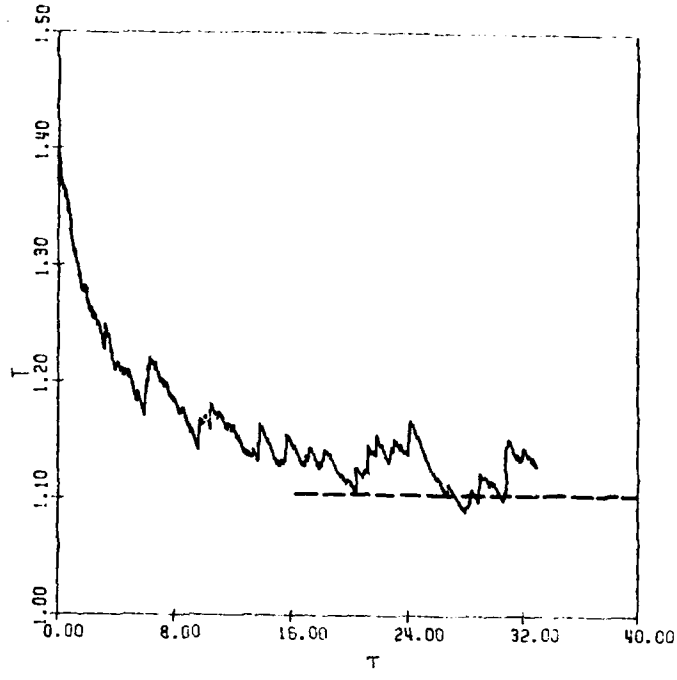

(a) Temperature

(b) Pressure

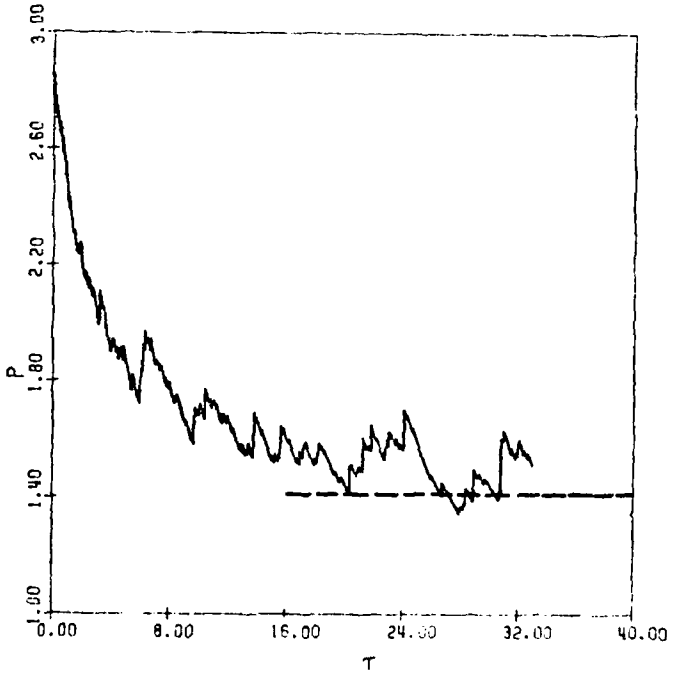

FIG. 8 VARIATION WITH TIME OF TEMPERATURE AND PRESSURE OF GAS JUST BEHIND DISCONTINUOUS FROZEN SHOCK FRONT (α = 1, P_{41} = 10, d = 10 μm, Δx = 0.05)

------ EXPECTED FINAL VALUE.

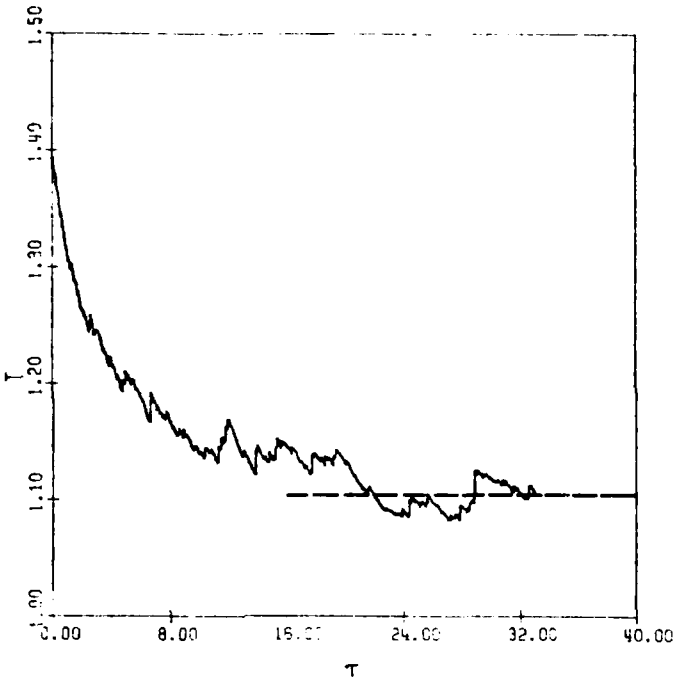

(a) Temperature

(b) Pressure

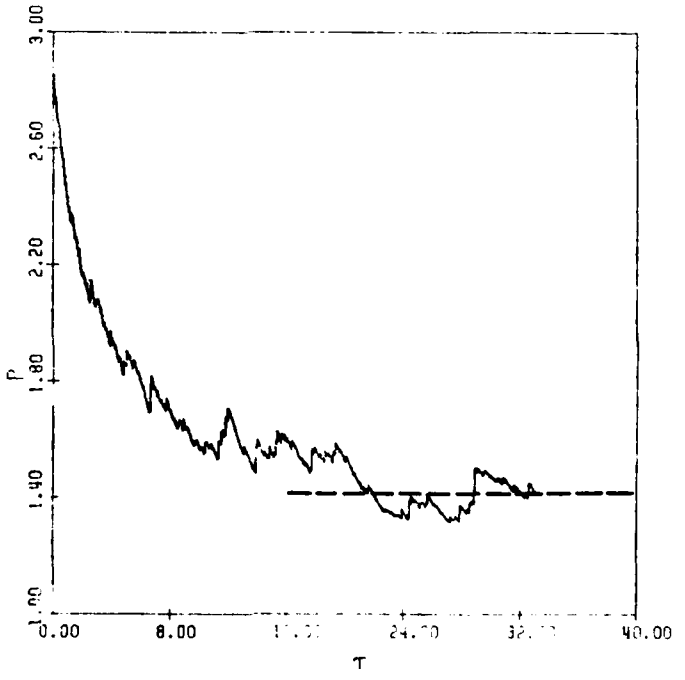

FIG. 9 VARIATION WITH TIME OF TEMPERATURE AND PRESSURE OF GAS JUST BEHIND DISCONTINUOUS FROZEN SHOCK FRONT ($\alpha = 1$, $P_{41} = 10$, $d = 10$ μm, $\Delta x = 0.025$)

------ EXPECTED FINAL VALUE.

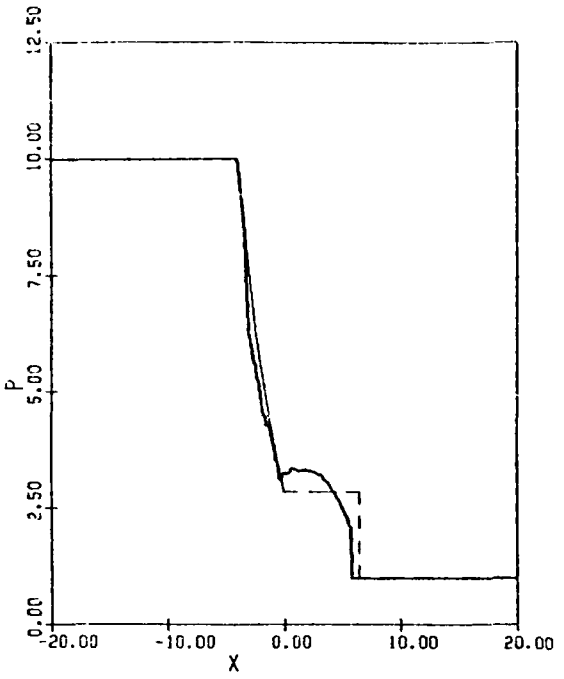

(a) Pressure

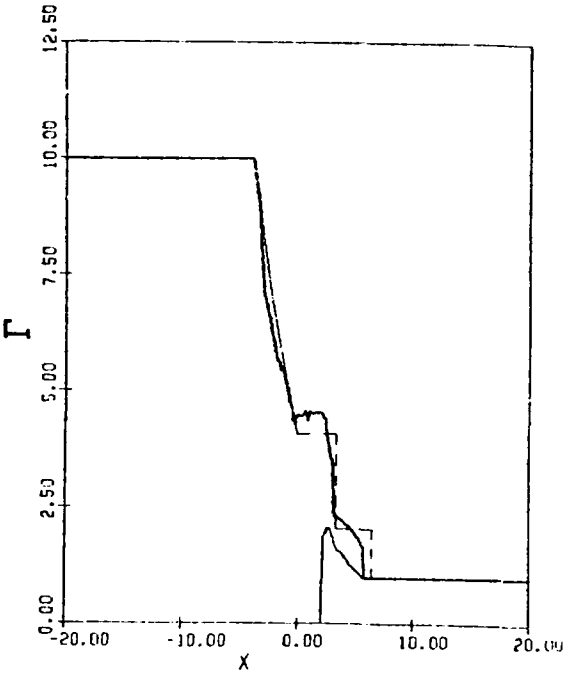

(b) Mass Concentration

(c) Temperature

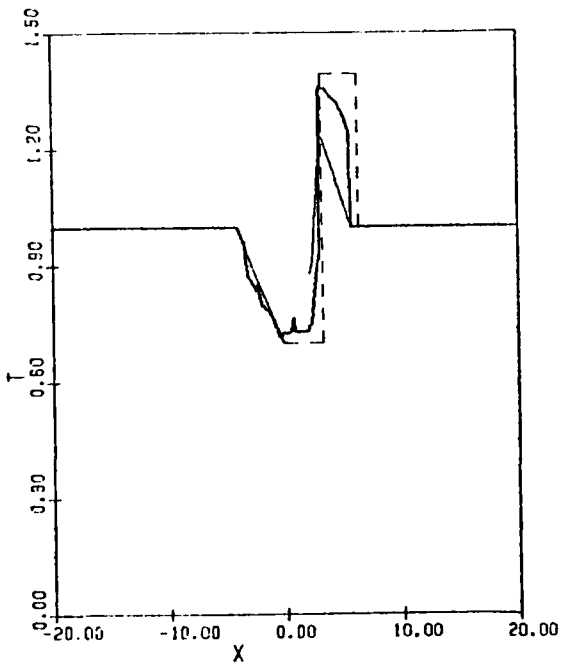

(d) Velocity

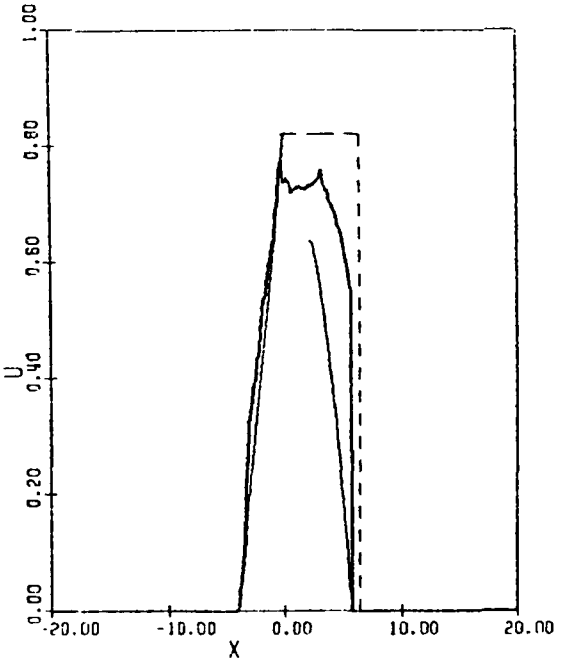

FIG. 10 FLOW QUANTITIES AT $\tau = 4$ ($\alpha = 1$, $P_{41} = 10$, d = 20 μm)
——— GAS, ——— PARTICLES, ------ FROZEN FLOW.

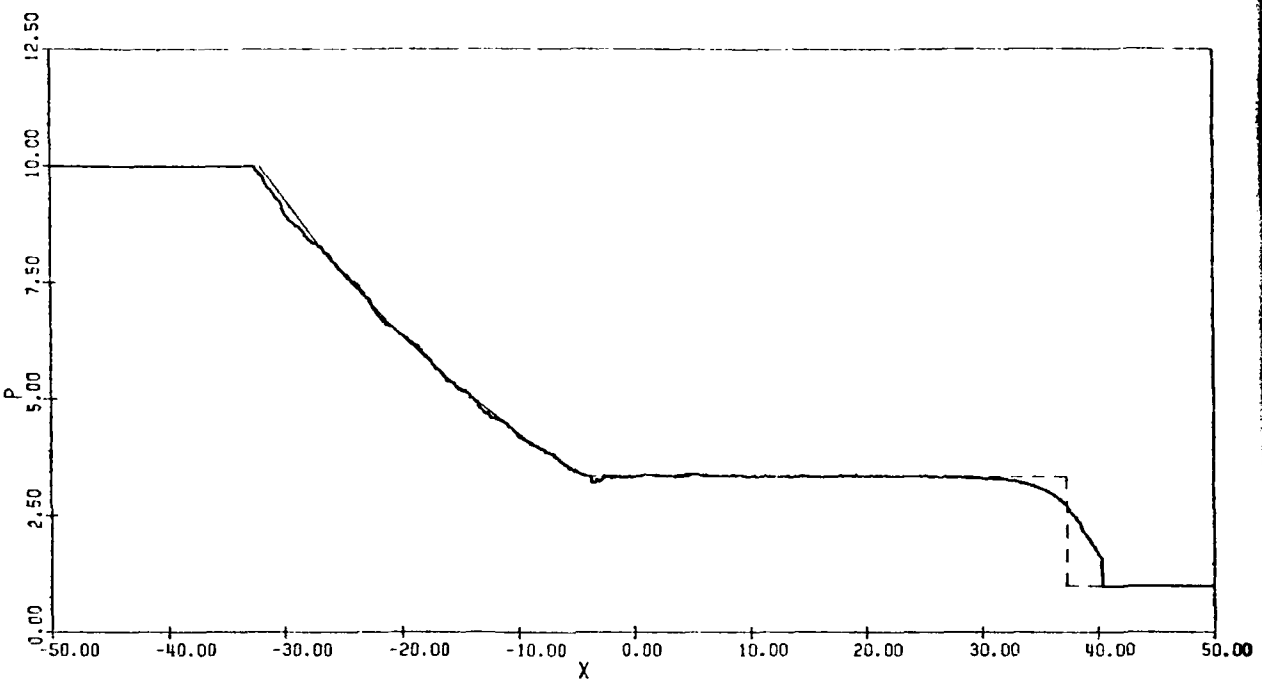

(a) Pressure

(b) Mass Concentration

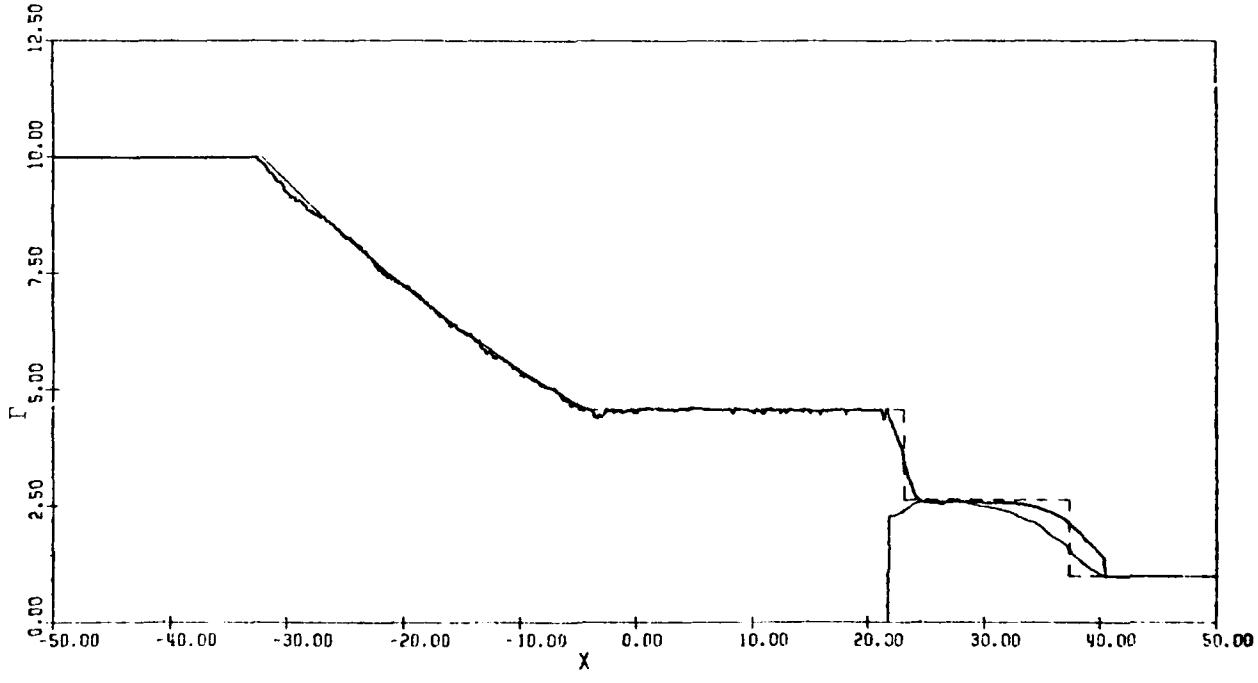

FIG. 11 FLOW QUANTITIES AT $\tau = 32$ ($\alpha = 1$, $P_{41} = 10$, d = 20 μm)
——— GAS, ——— PARTICLES, ------ EQUILIBRIUM FLOW.

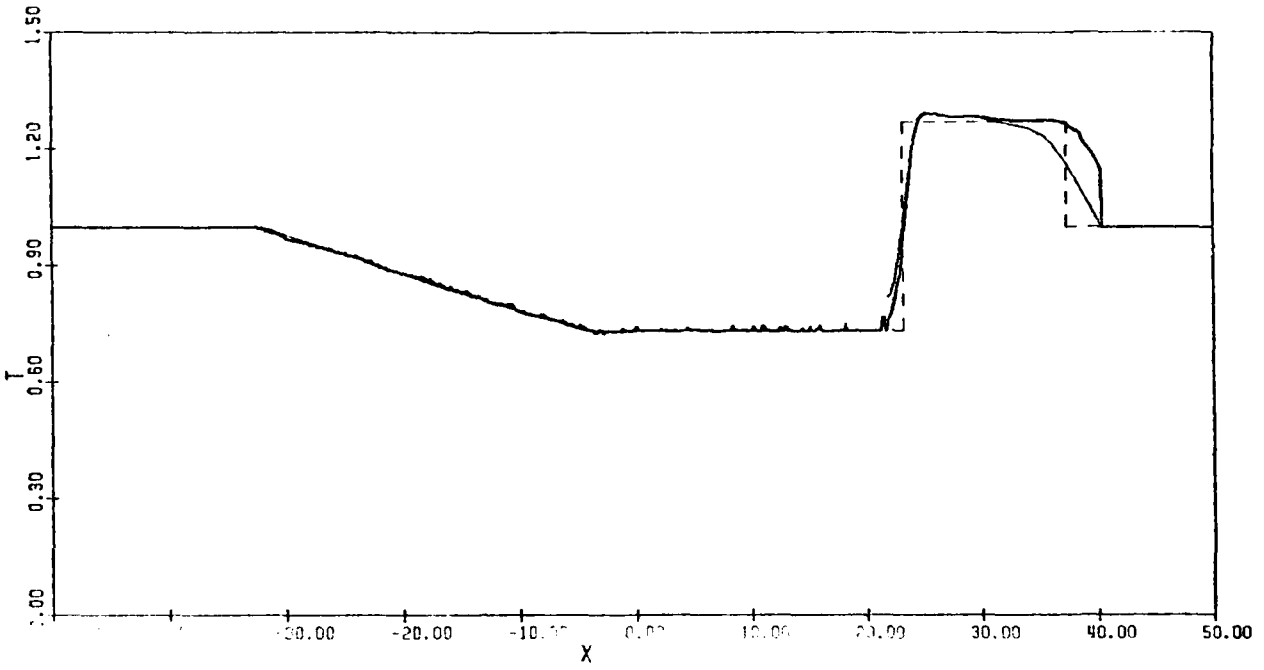

(c) Temperature

(d) Velocity

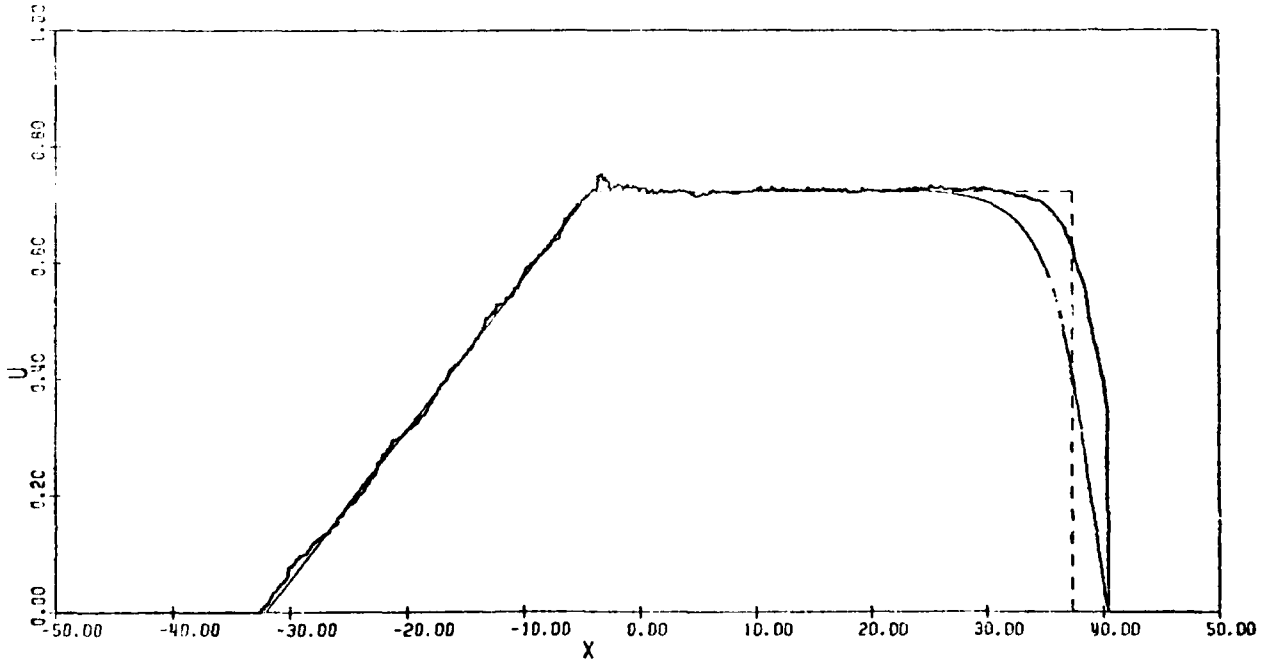

FIG. 11 (CONTINUED) FLOW QUANTITIES AT $\tau = 32$ ($\alpha = 1$, $P_{41} = 10$, $d = 20$ μm)
——— GAS, ——— PARTICLES, ------ EQUILIBRIUM FLOW.

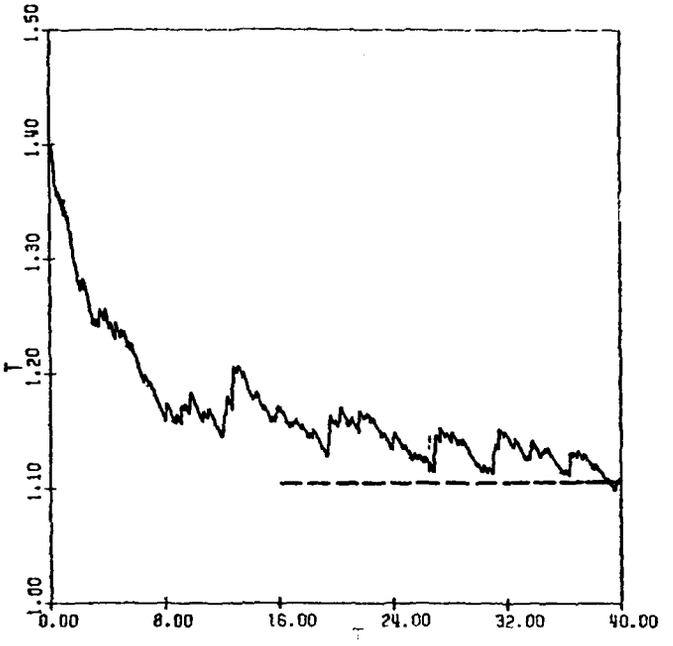

(a) Temperature

(b) Pressure

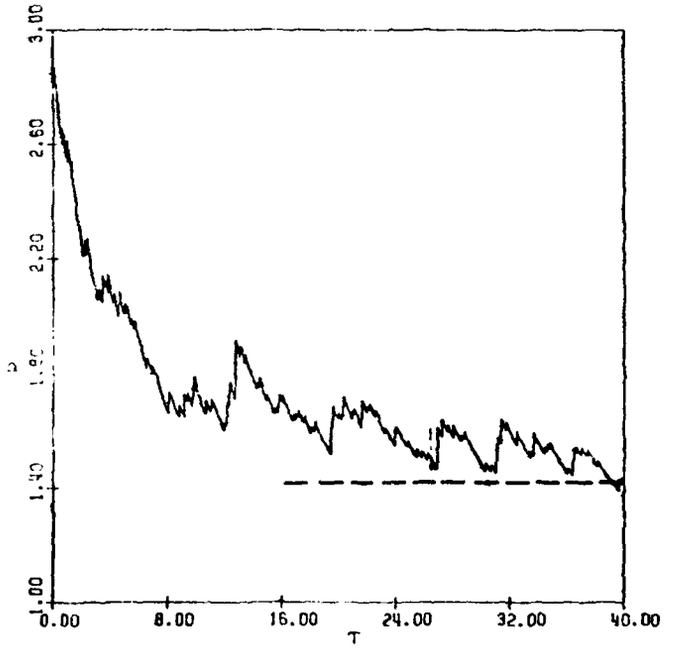

FIG. 12 VARIATIONS WITH TIME OF TEMPERATURE AND PRESSURE OF GAS JUST BEHIND DISCONTINUOUS FROZEN SHOCK FRONT (α = 1, P_{41} = 10, d = 20 μm)

------ EXPECTED FINAL VALUE.

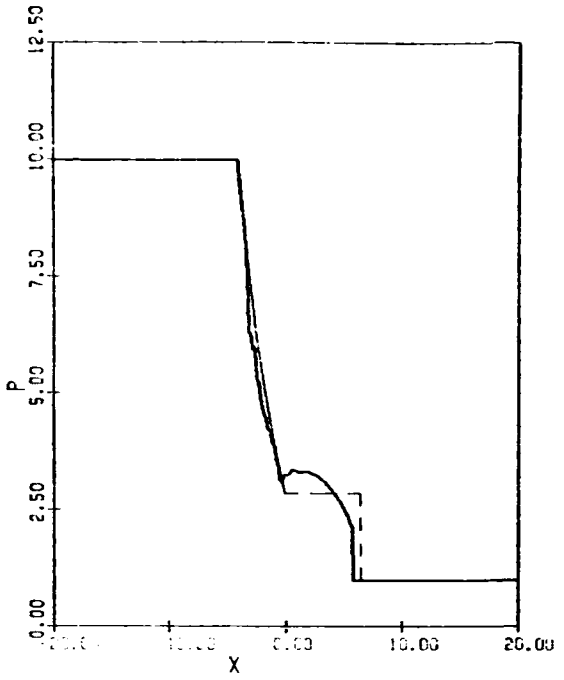

(a) Pressure

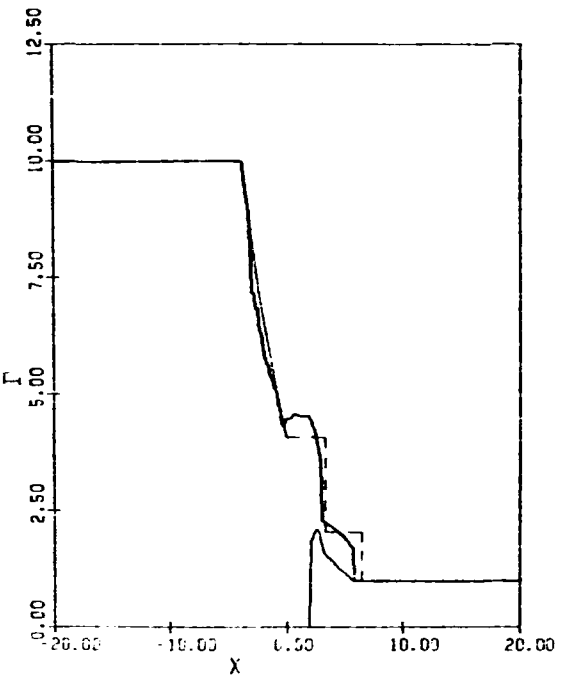

(b) Mass Concentration

(c) Temperature

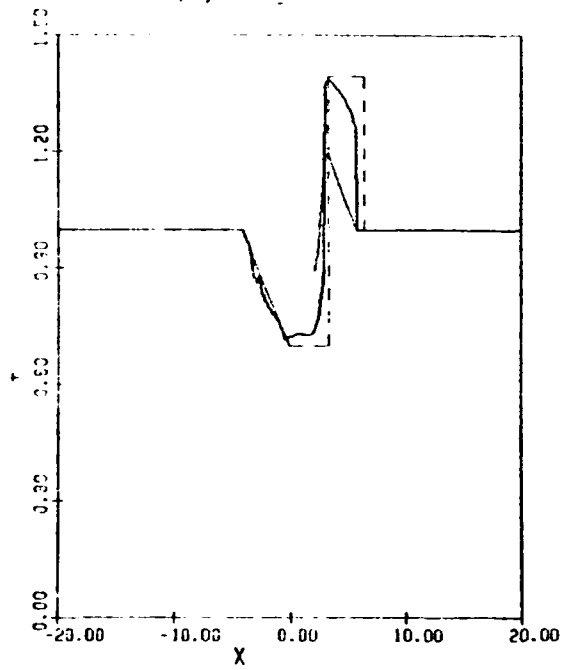

(d) Velocity

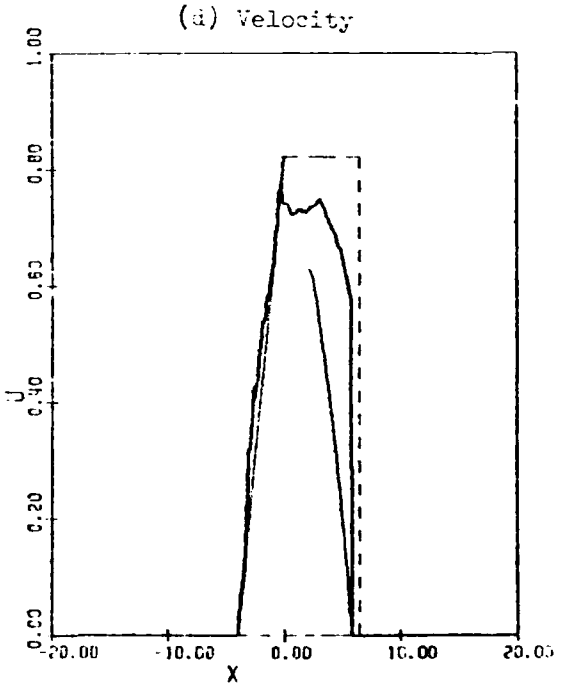

FIG. 13 FLOW QUANTITIES AT $\tau = 4$ ($\alpha = 1$, $P_{41} = 10$, d = 40 μm)

——— GAS, ——— PARTICLES, ------ FROZEN FLOW.

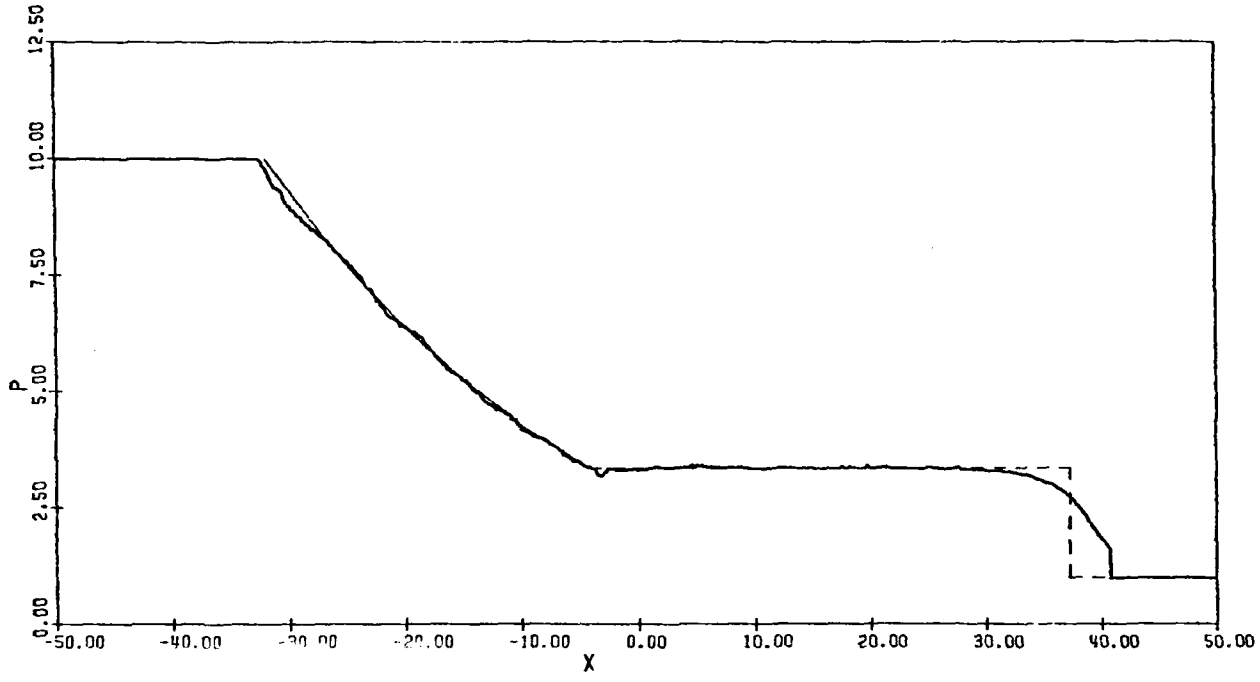

(a) Pressure

(b) Mass Concentration

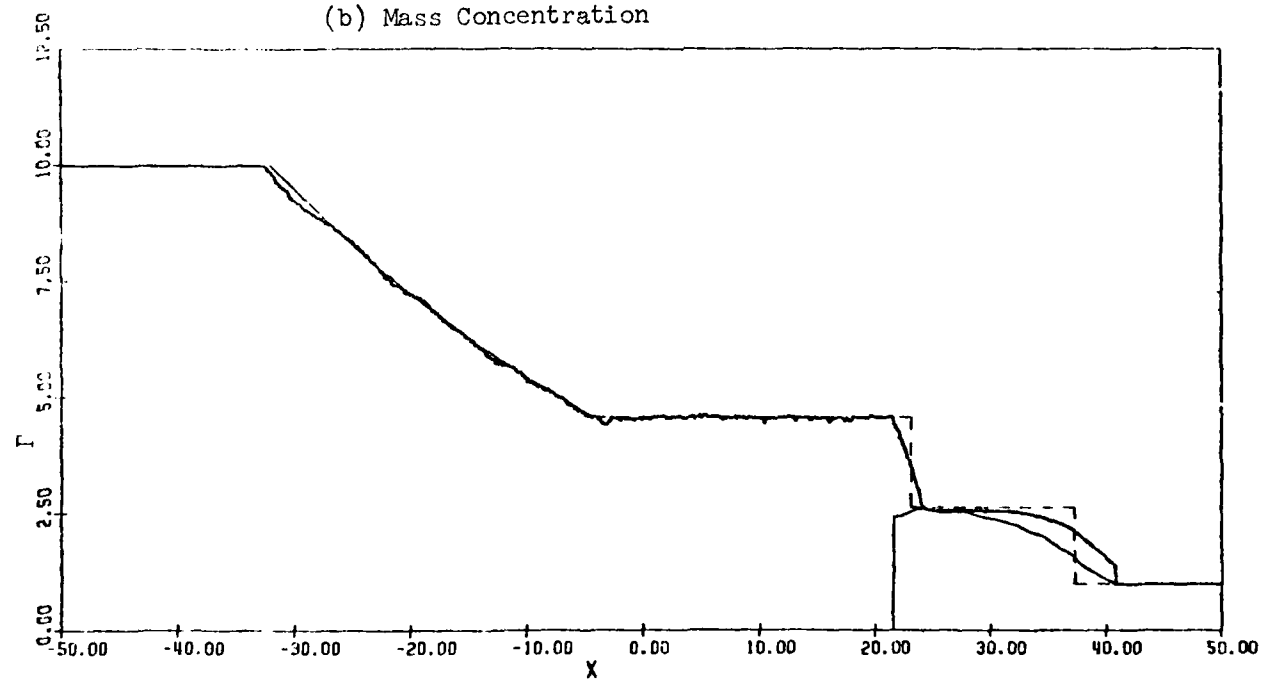

FIG. 14 FLOW QUANTITIES AT $\tau = 32$ ($\alpha = 1$, $P_{41} = 10$, $d = 40$ μm).
——— GAS, ——— PARTICLES, ------ EQUILIBRIUM FLOW.

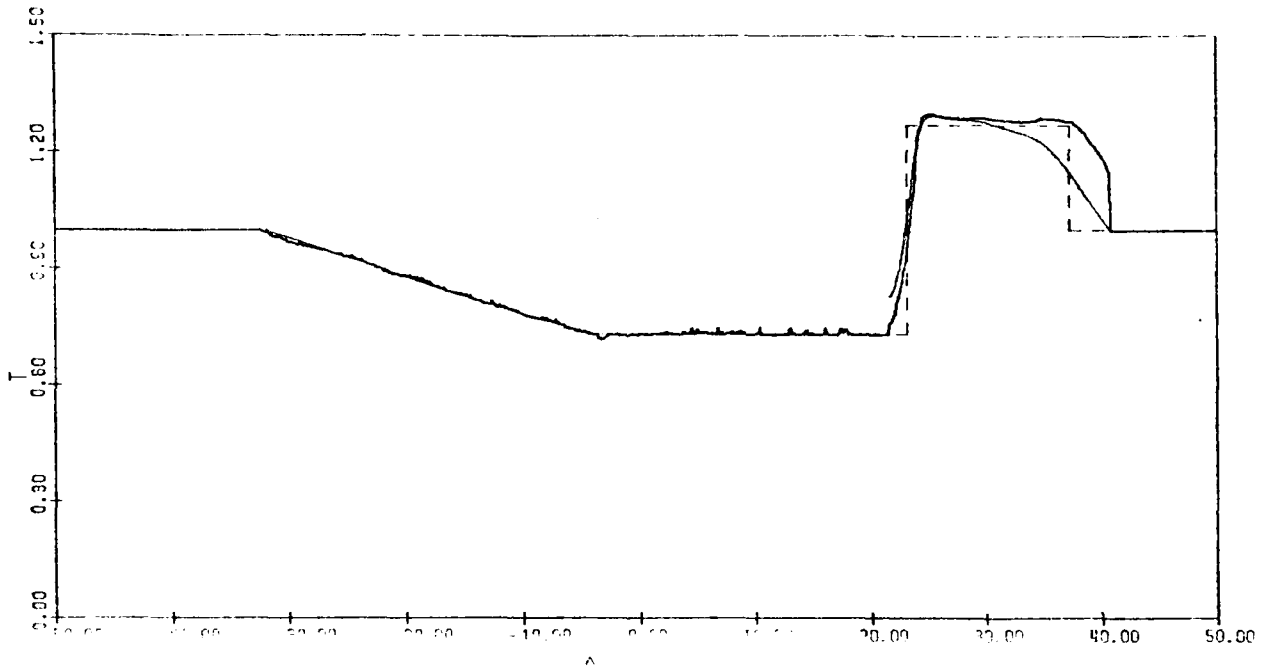

(c) Temperature

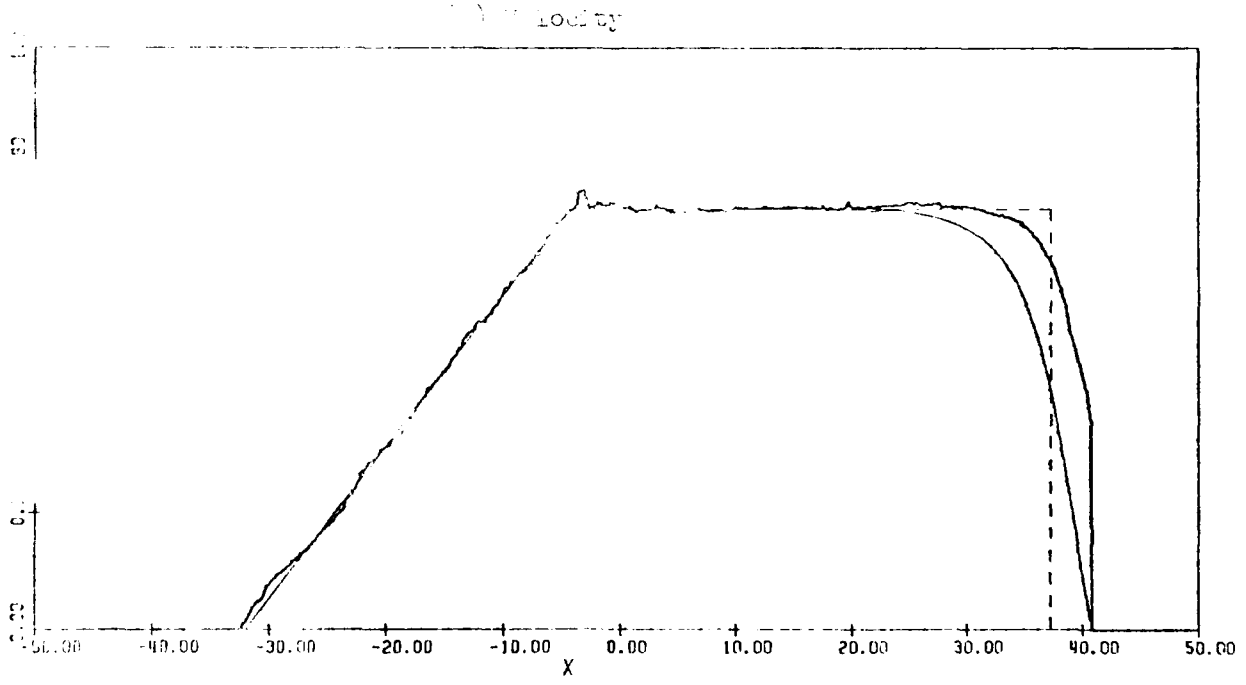

FIG. 14 (CONTINUED) FLOW QUANTITIES AT $\tau = 32$ ($\alpha = 1$, $P_{41} = 10$, $d = 40$ μm).

——— GAS, ——— PARTICLES, ------ EQUILIBRIUM FLOW.

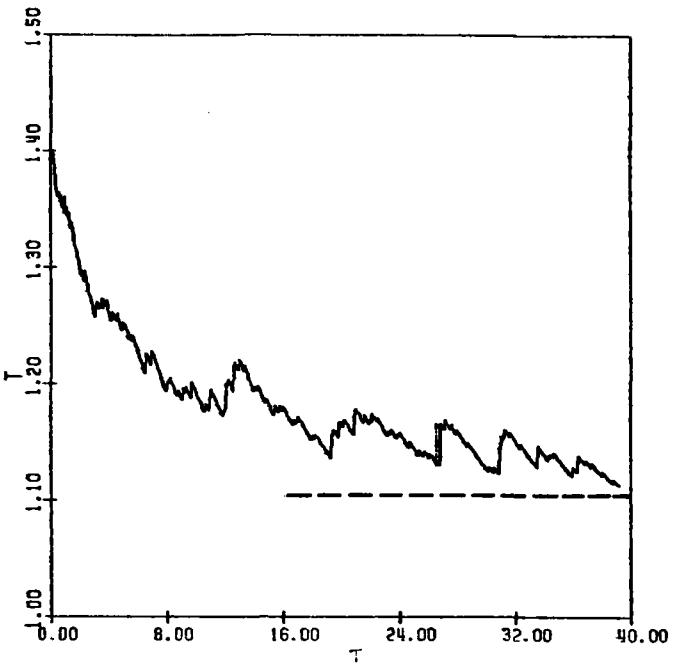

(a) Temperature

(b) Pressure

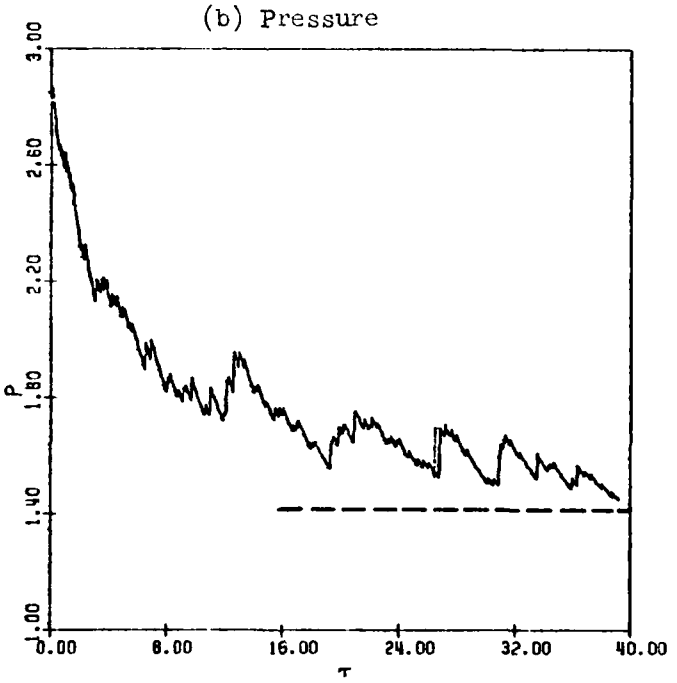

FIG. 15 VARIATIONS WITH TIME OF TEMPERATURE AND PRESSURE OF GAS JUST BEHIND DISCONTINUOUS FROZEN SHOCK FRONT (α = 1, P_{41} = 10, d = 40 μm).

------ EXPECTED FINAL VALUE.

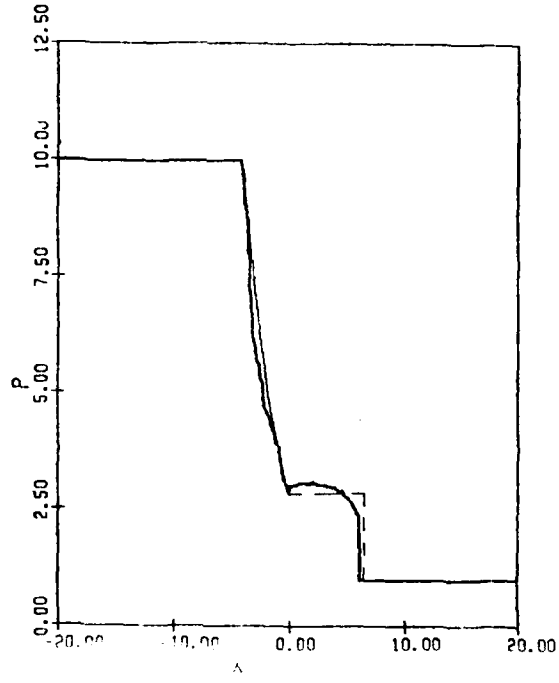

(a) Pressure

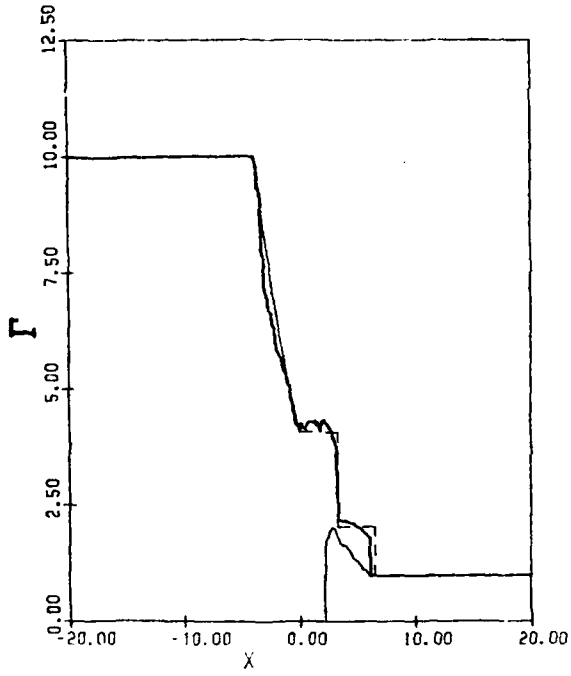

(b) Mass Concentration

(c) Temperature

(d) Velocity

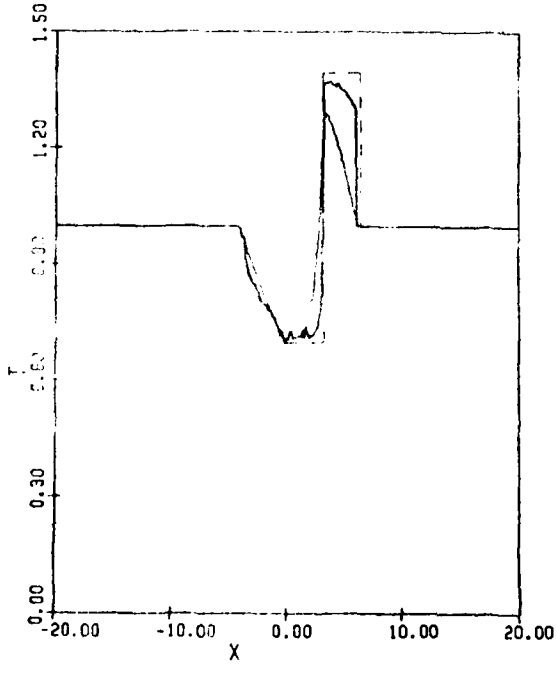

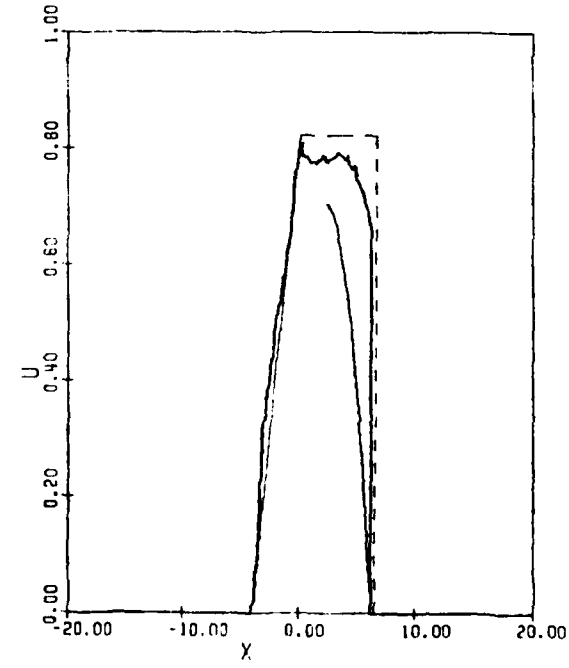

FIG. 16 FLOW QUANTITIES AT $\tau = 4$ ($\alpha = 0.4$, $P_{41} = 10$, $d = 10$ μm)
——— GAS, ——— PARTICLES, ------ FROZEN FLOW.

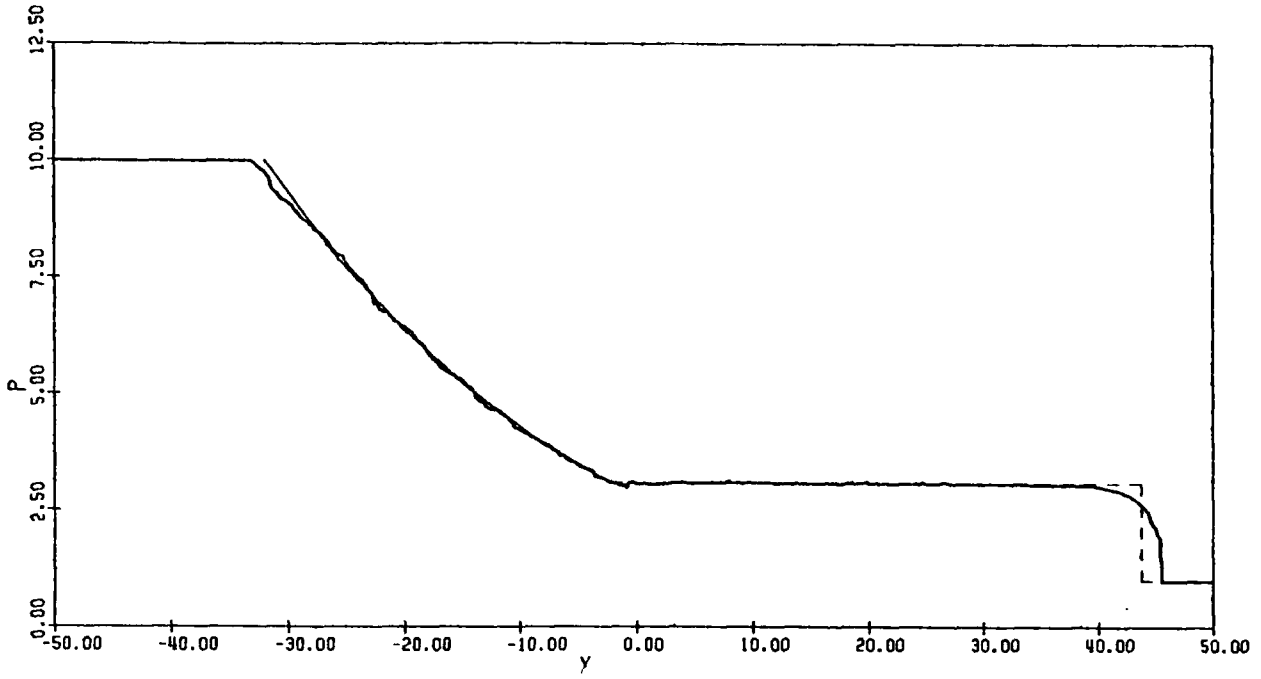

(a) Pressure

(b) Mass Concentration

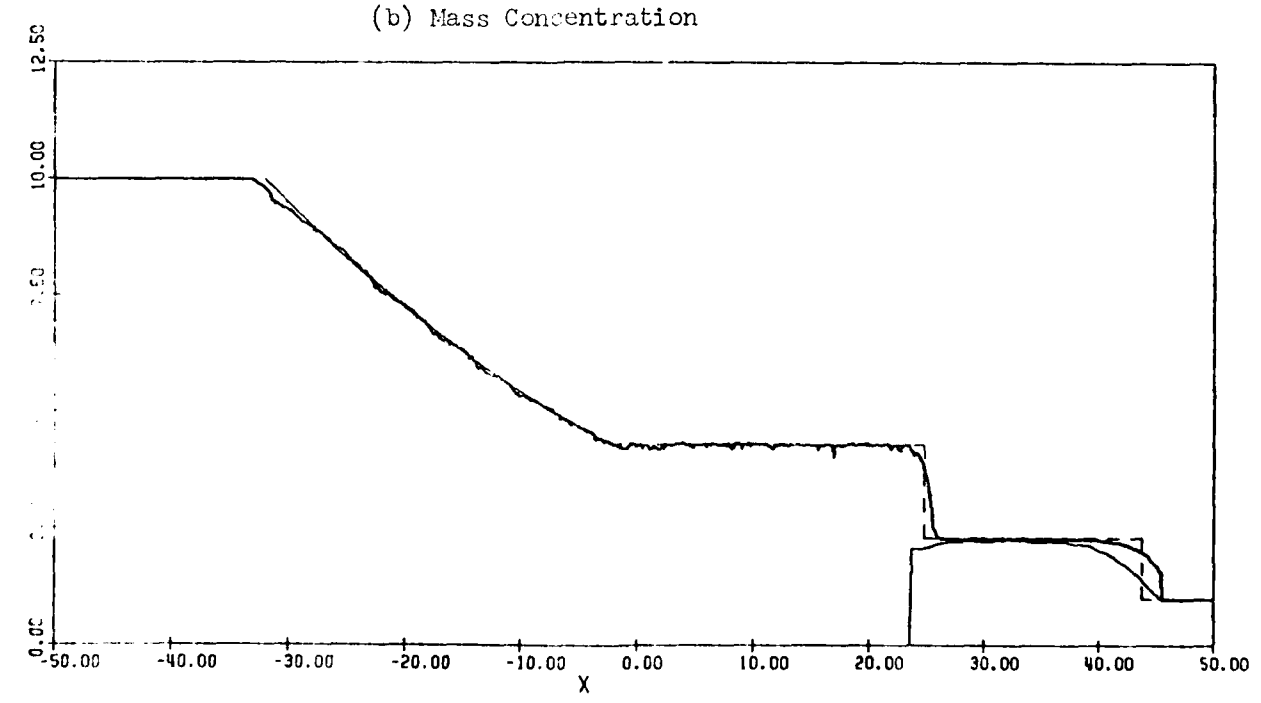

IG. 17 FLOW QUANTITIES AT $\tau = 32$ ($\alpha = 0.4$, $P_{41} = 10$, $d = 10$ μm).
——— GAS, ——— PARTICLES, ------ EQUILIBRIUM FLOW.

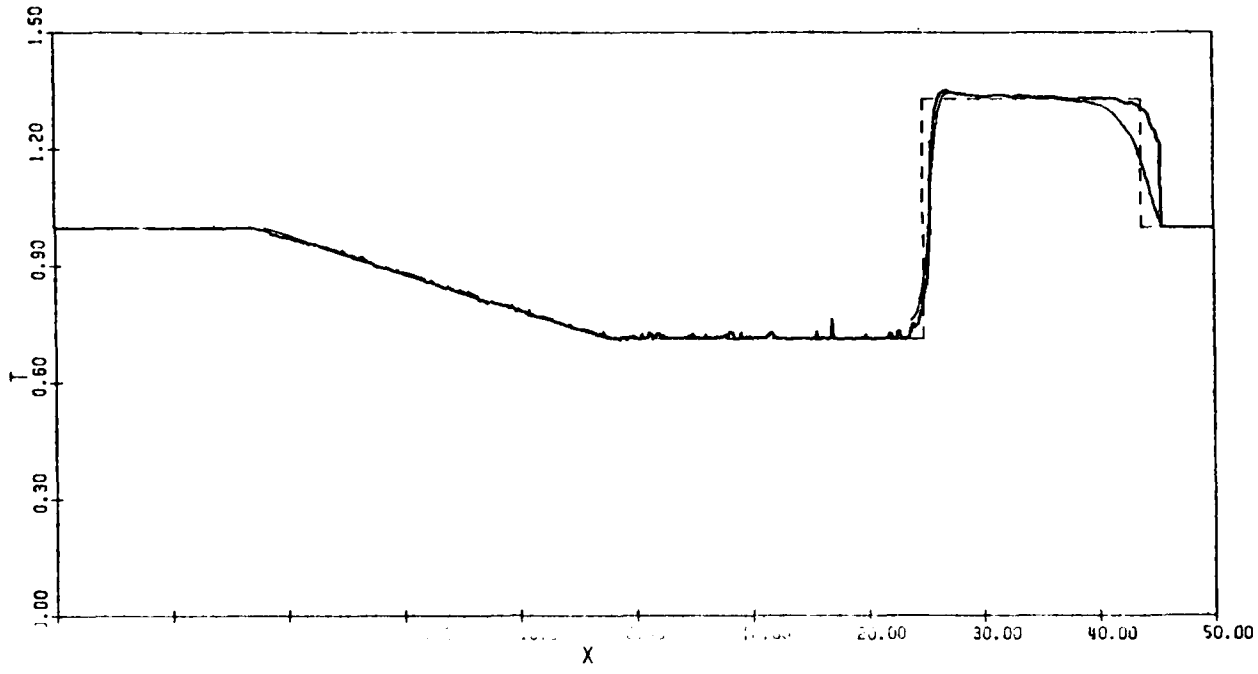

(c) Temperature

(d) Velocity

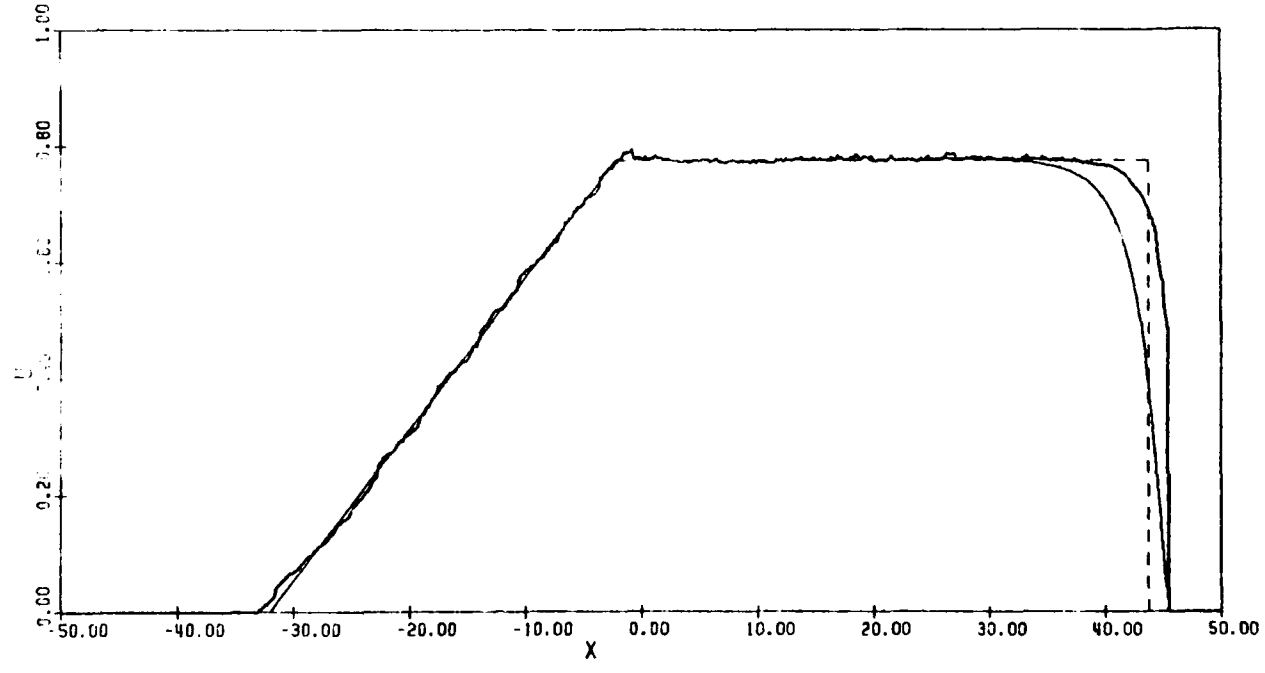

FIG. 17 (CONTINUED) FLOW QUANTITIES AT $\tau = 32$ ($\alpha = 0.4$, $P_{41} = 10$, $d = 10\ \mu m$).

——— GAS, ——— PARTICLES, ------ EQUILIBRIUM FLOW.

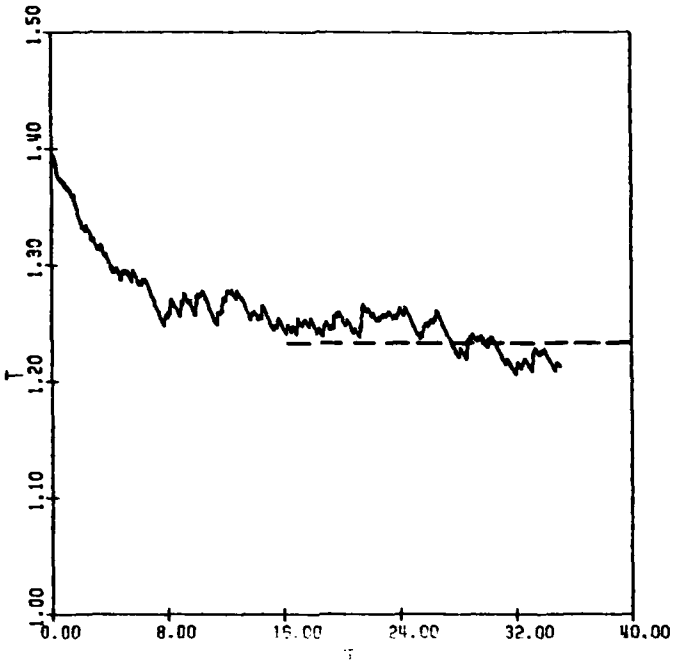

(a) Temperature

(b) Pressure

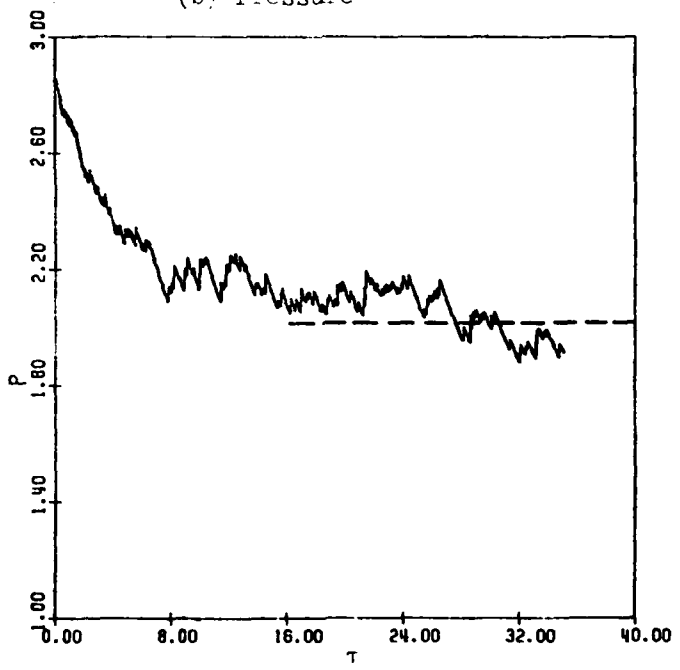

FIG. 18 VARIATIONS WITH TIME OF TEMPERATURE AND PRESSURE OF GAS JUST BEHIND DISCONTINUOUS FROZEN SHOCK FRONT (α = 0.4, P_{41} = 10, d = 10 μm).

------ EXPECTED FINAL VALUE.

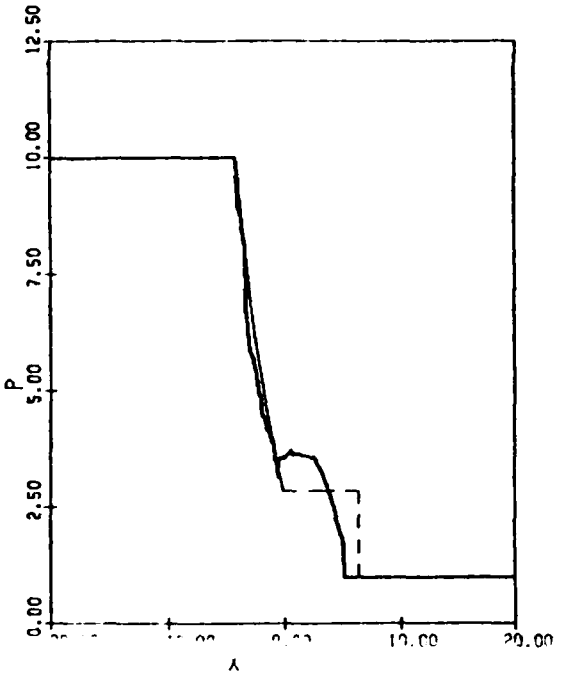

(a) Pressure

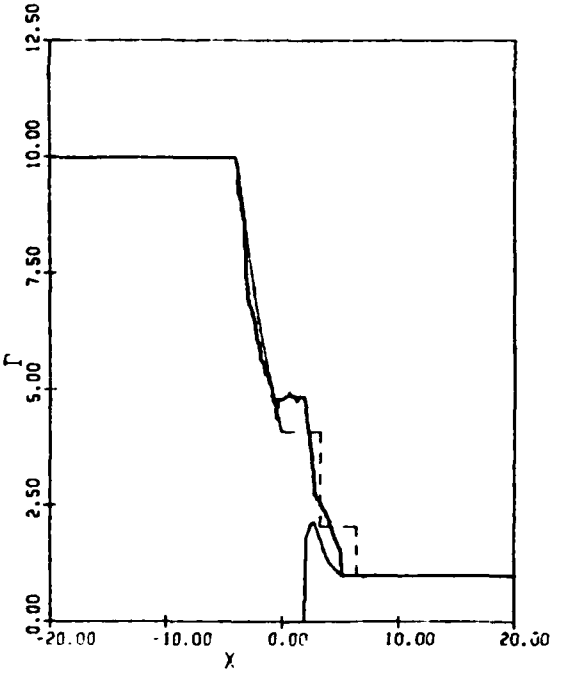

(b) Mass Concentration

( ) Temperature

(d) Velocity

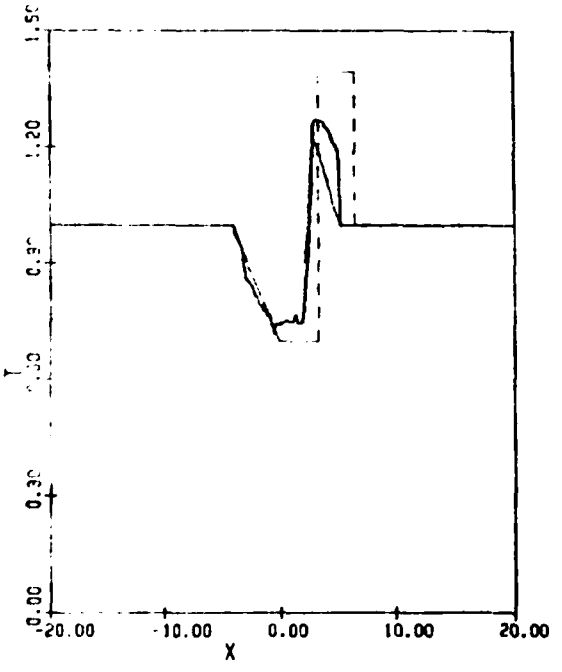

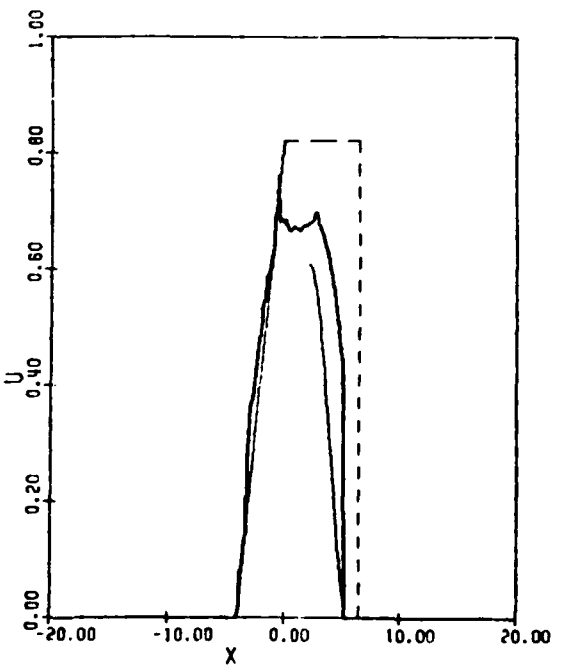

FIG. 19 FLOW QUANTITIES AT $\tau = 4$ ($\alpha = 2$, $P_{41} = 10$, $d = 10$ μm).
——— GAS, ——— PARTICLES, ------ FROZEN FLOW.

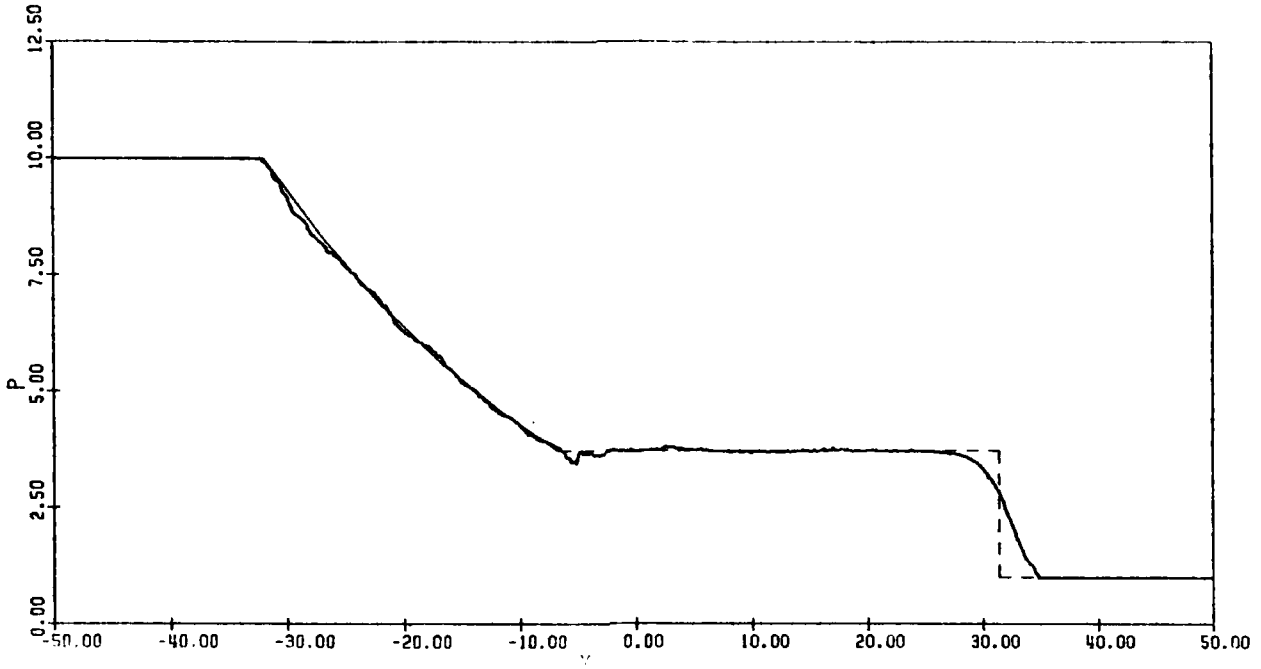

(a) Pressure

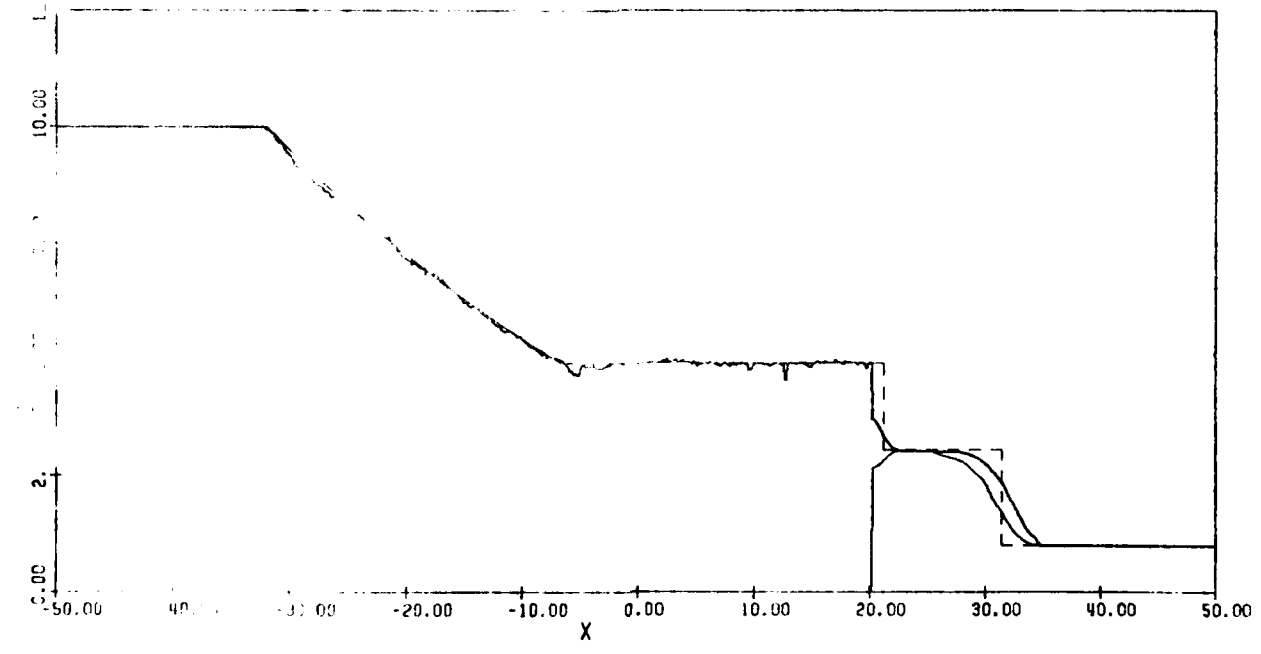

Fig. 20 FLOW QUANTITIES AT $\tau = 32$ ($\alpha = 2$, $P_{41} = 10$, $d = 10$ μm).
——— GAS, ——— PARTICLES, ------ EQUILIBRIUM FLOW.

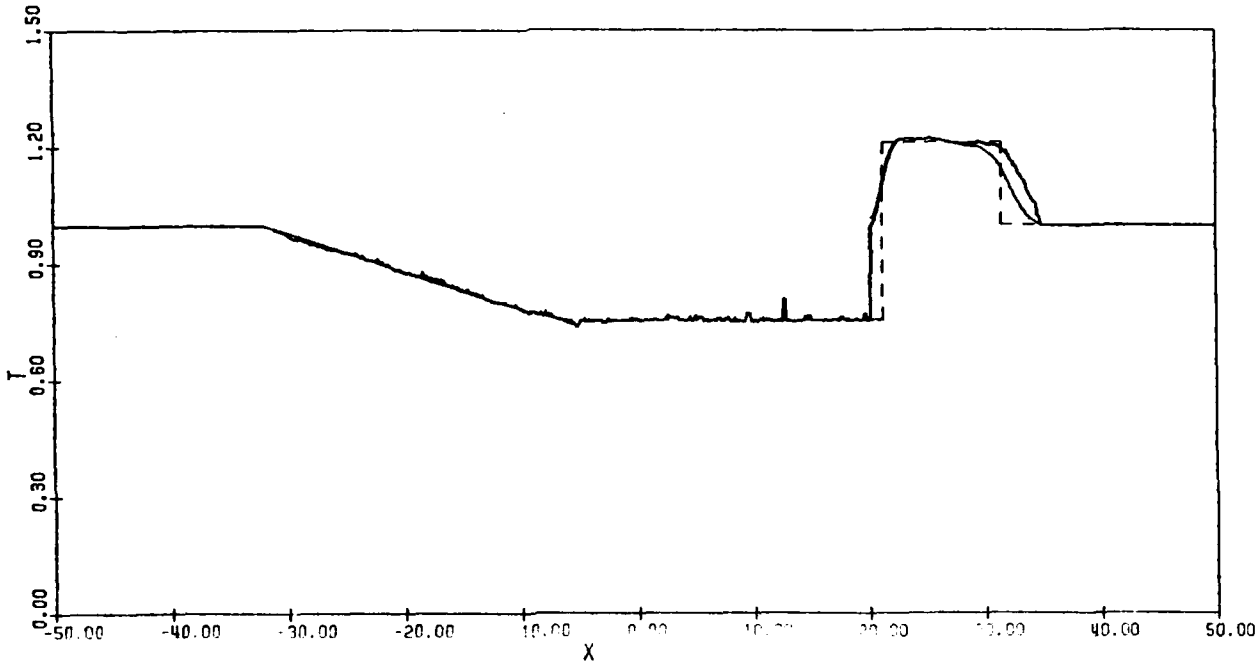

(c) Temperature

(d) Velocity

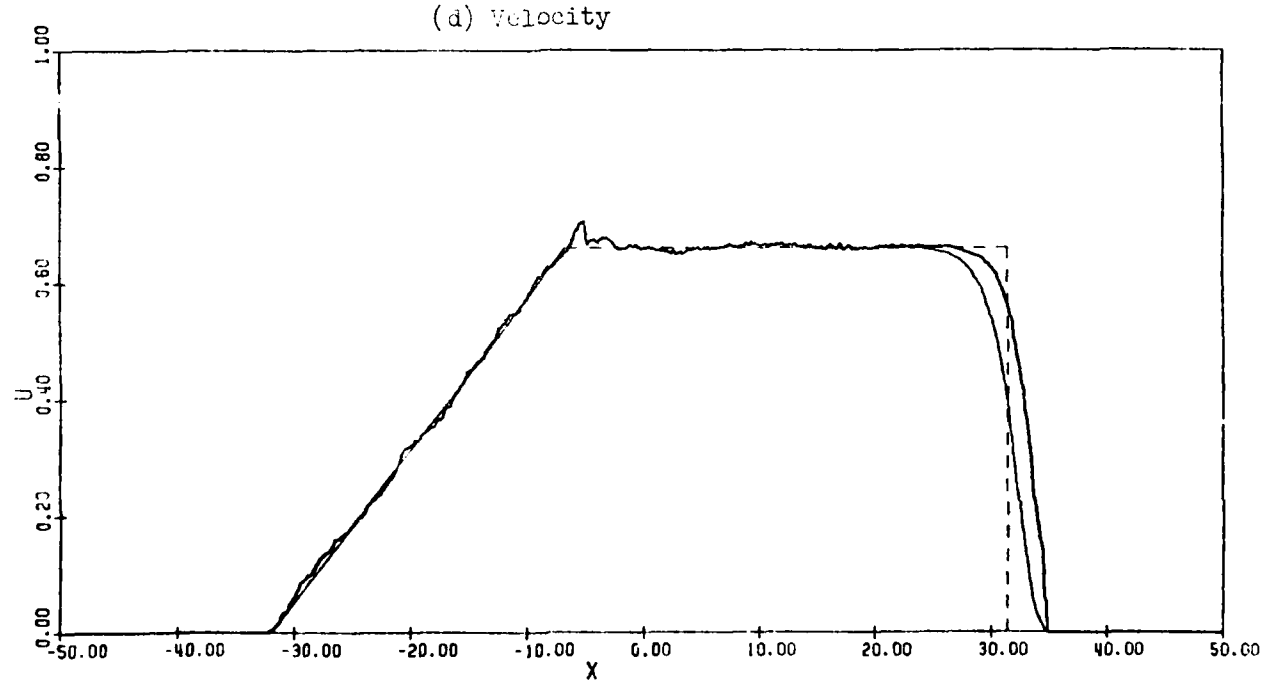

FIG. 20 (CONTINUED) FLOW QUANTITIES AT $\tau = 32$ ($\alpha = 2$, $P_{41} = 10$, $d = 10$ μm).

——— GAS, ——— PARTICLES, ------ EQUILIBRIUM FLOW.

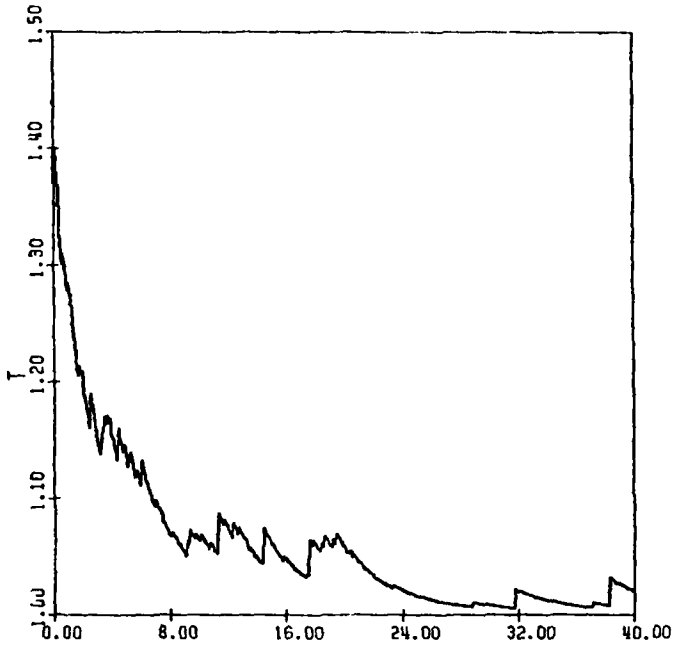

(a) Temperature

(b) Pressure

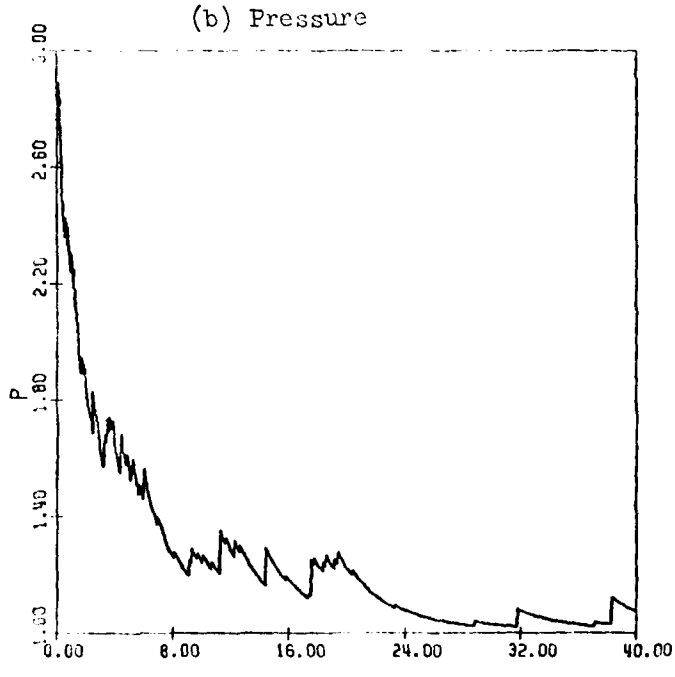

FIG. 21 VARIATIONS WITH TIME OF TEMPERATURE AND PRESSURE OF GAS JUST BEHIND DISCONTINUOUS FROZEN SHOCK FRONT ($\alpha = 2$, $P_{41} = 10$, $d = 10$ μm).

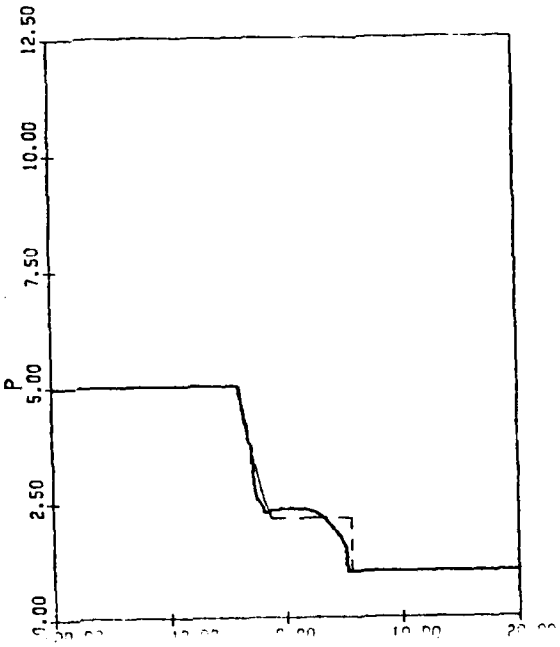

(a) Pressure

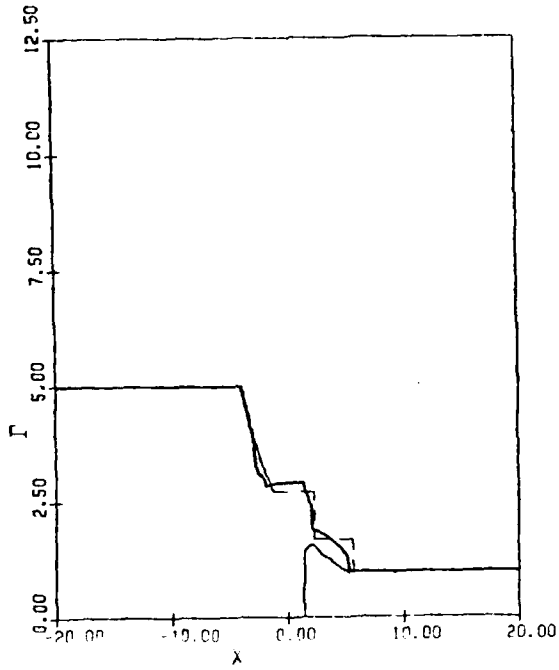

(b) Mass Concentration

(c) Temperature

(d) Velocity

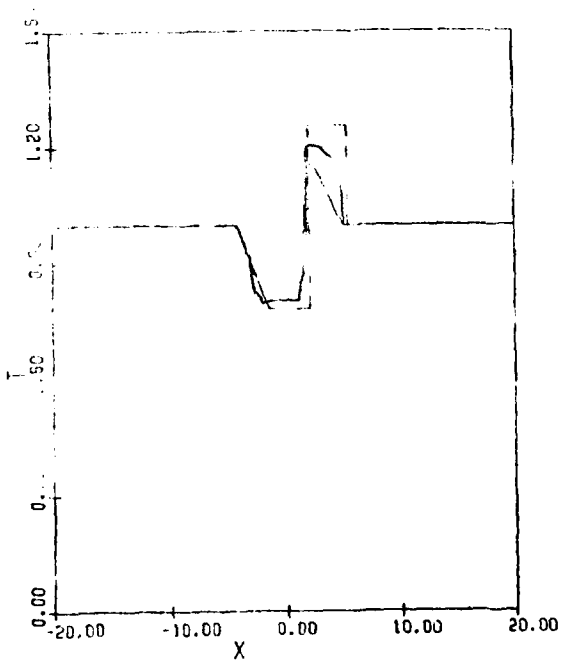

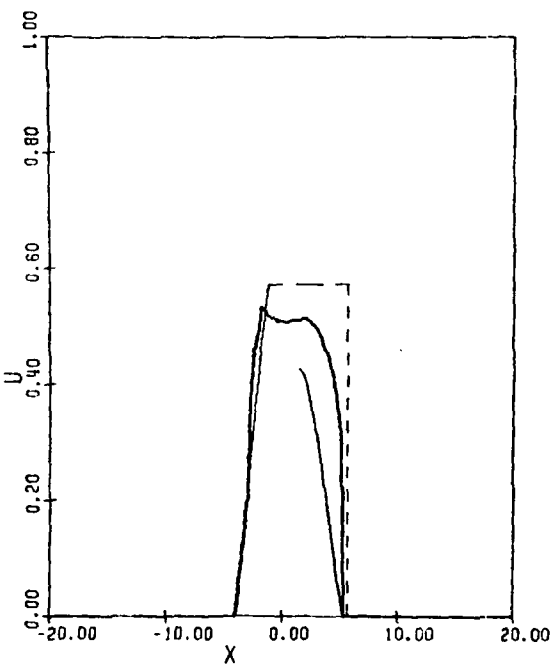

FIG. 22 FLOW QUANTITIES AT $\tau = 4$ ($\alpha = 1$, $P_{41} = 5$, d = 10 μm).
——— GAS, ——— PARTICLES, ------ FROZEN FLOW.

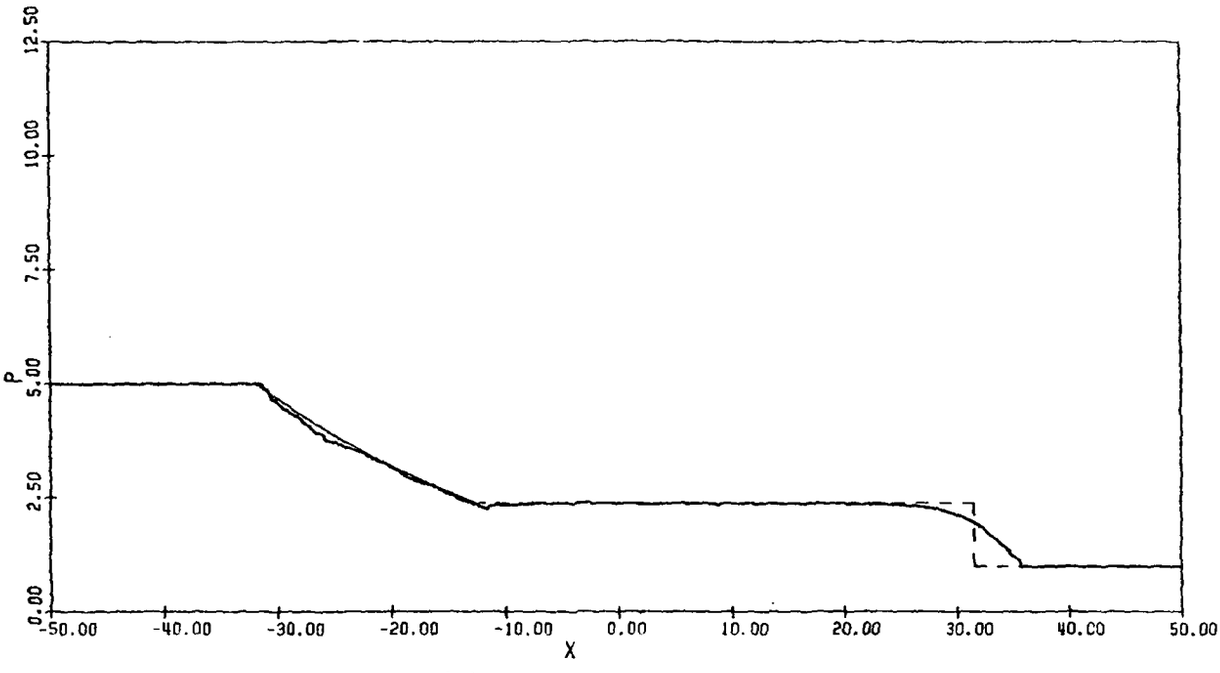

(a) Pressure

(b) Mass Concentration

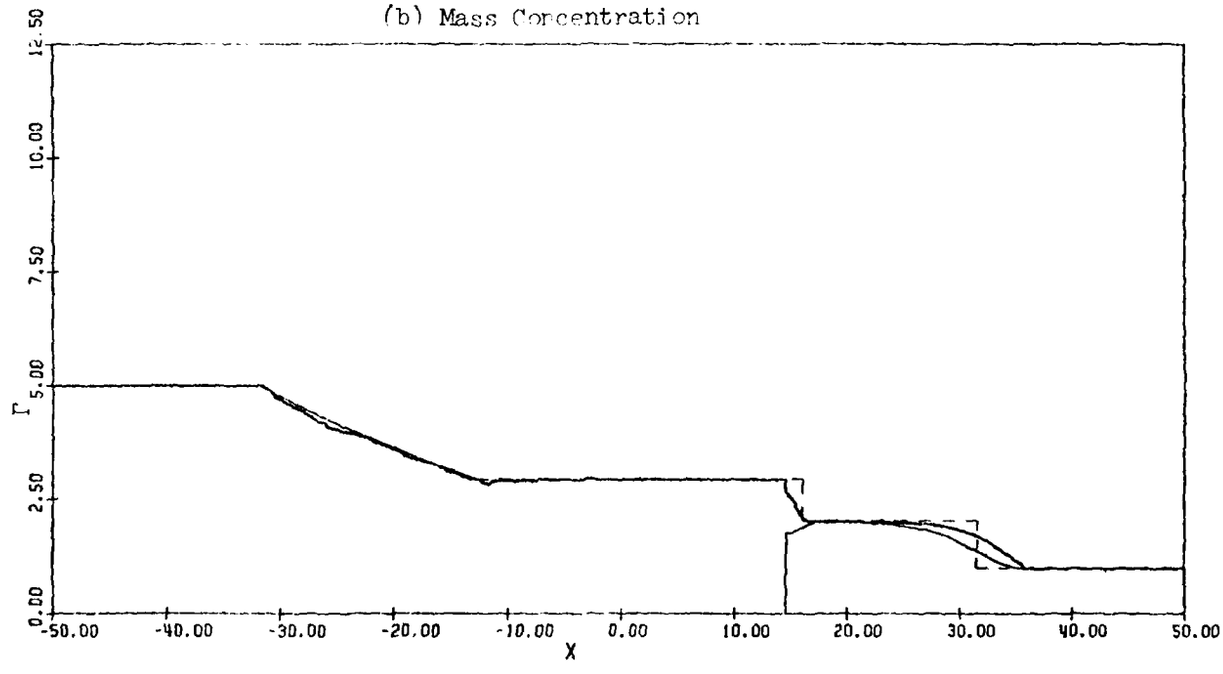

FIG. 23 FLOW QUANTITIES AT $\tau = 32$ ($\alpha = 1$, $P_{41} = 5$, $d = 10$ μm).
——— GAS, ——— PARTICLES. ------ EQUILIBRIUM FLOW.

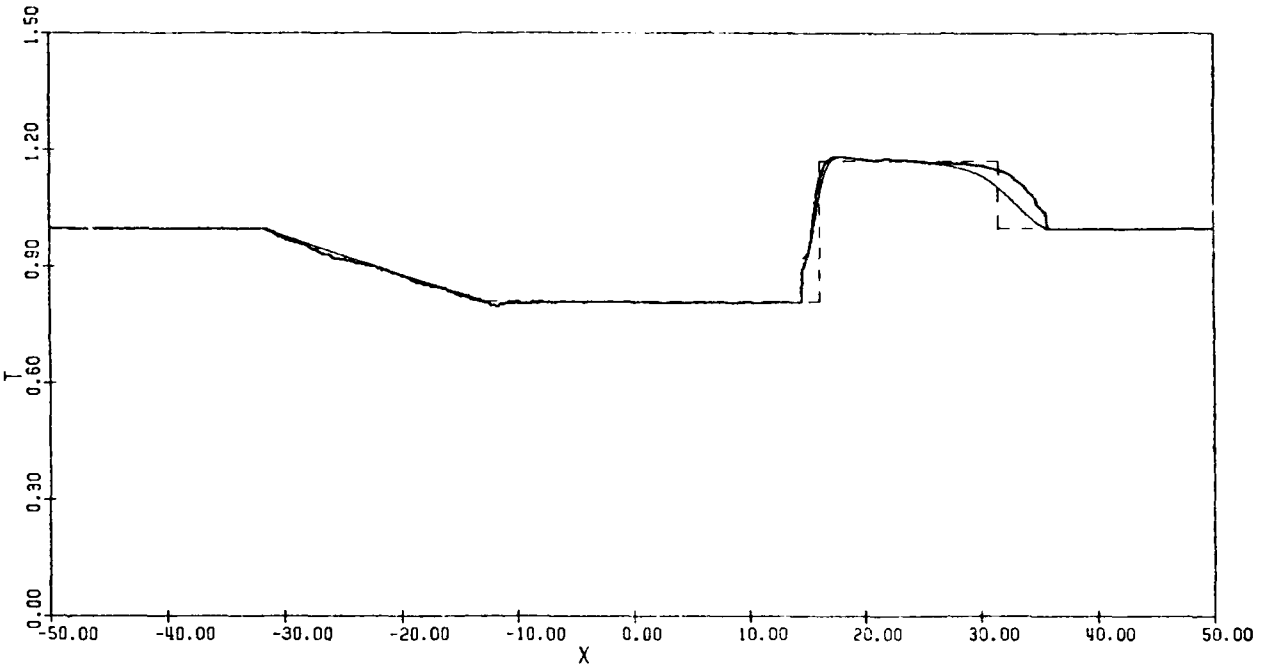

(c) Temperature

(d) Velocity

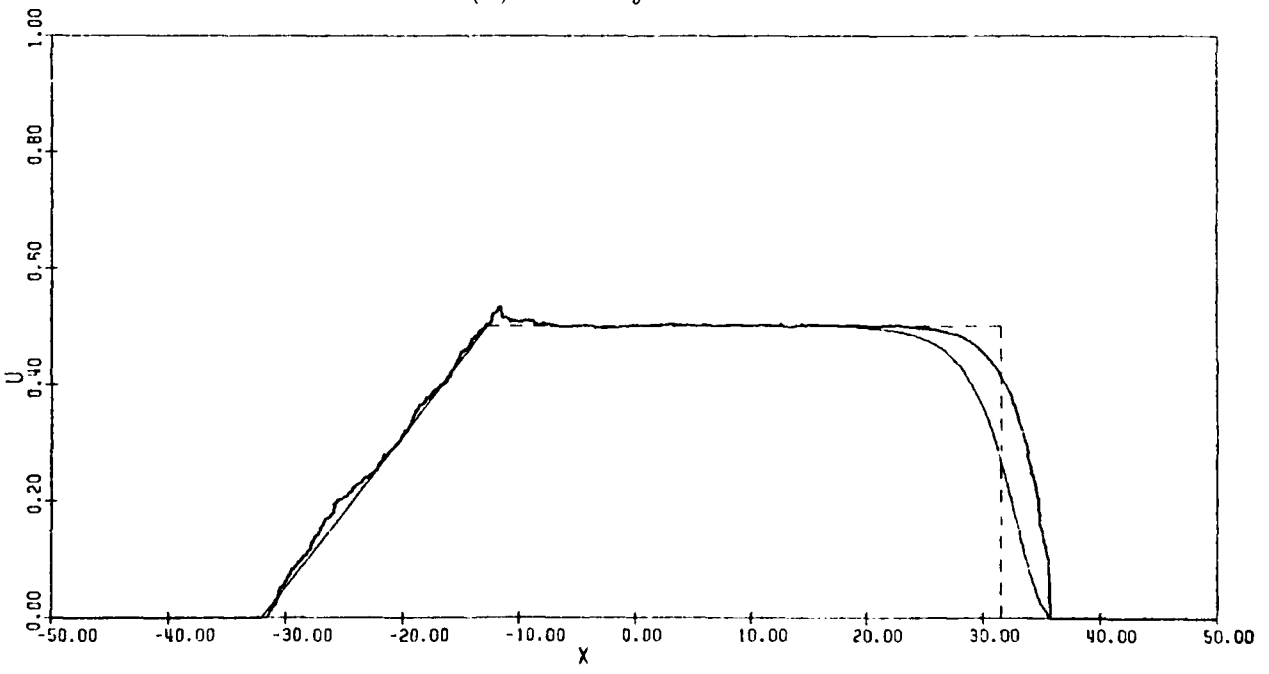

FIG. 23 (CONTINUED) FLOW QUANTITIES AT $\tau = 32$ ($\alpha = 1$, $P_{41} = 5$, $d = 10$ μm).

——— GAS, ——— PARTICLES, ------ EQUILIBRIUM FLOW.

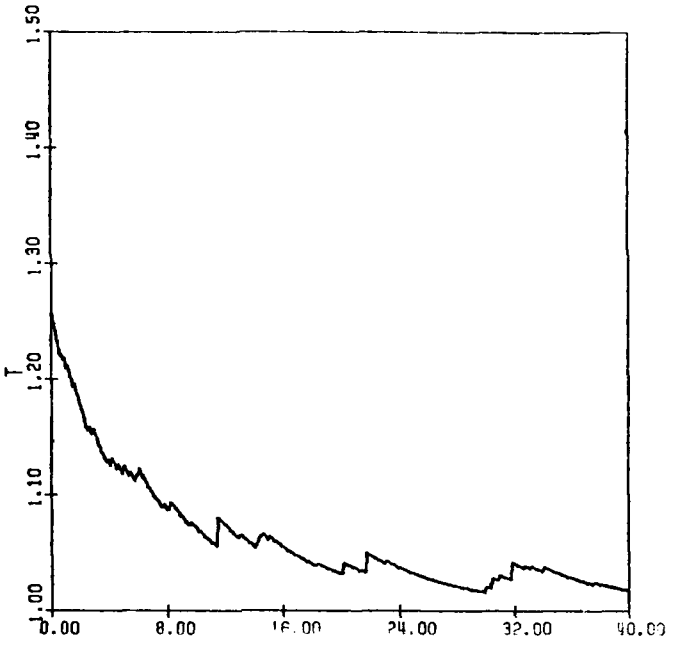

(a) Temperature

(b) Pressure

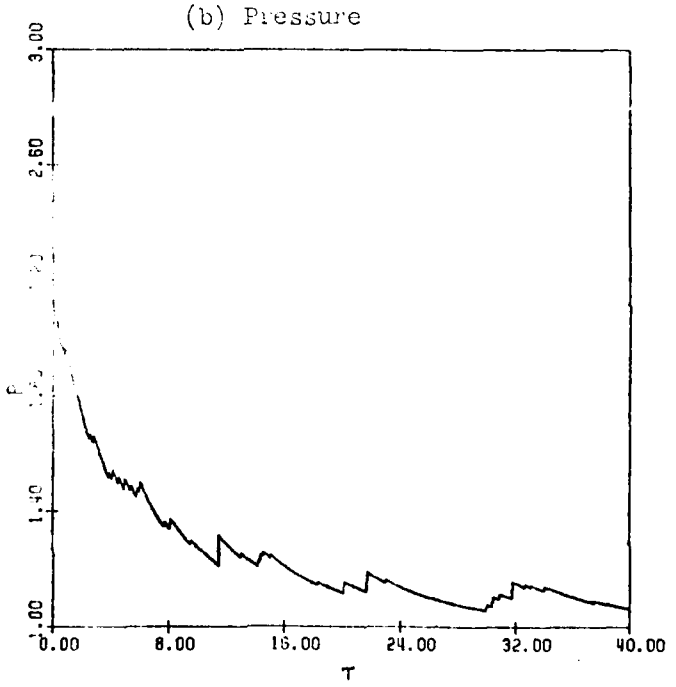

FIG. 24 VARIATIONS WITH TIME OF TEMPERATURE AND PRESSURE OF GAS JUST BEHIND DISCONTINUOUS FROZEN SHOCK FRONT (α = 1, P_{41} = 5, d = 10 μm).

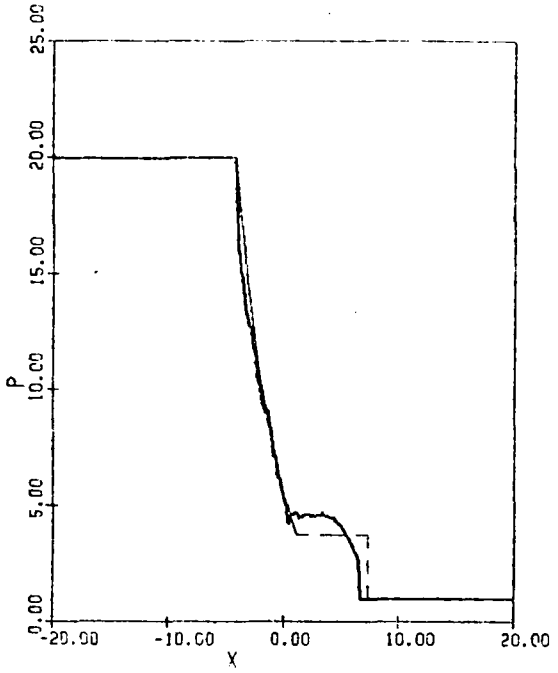

(a) Pressure

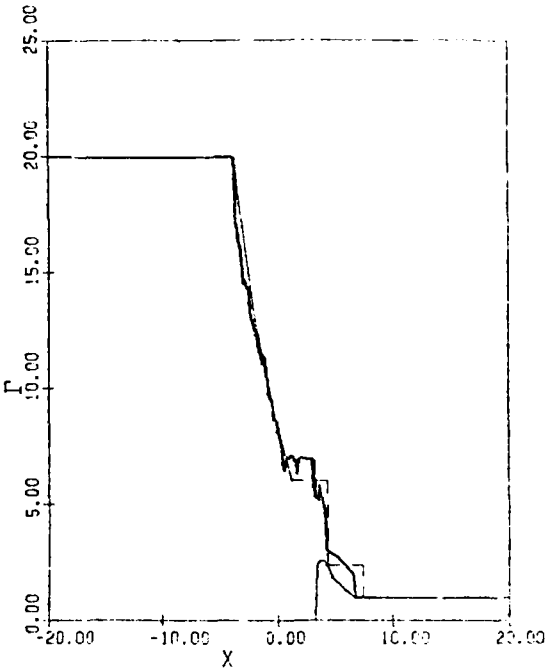

(b) Mass Concentration

(c) Temperature

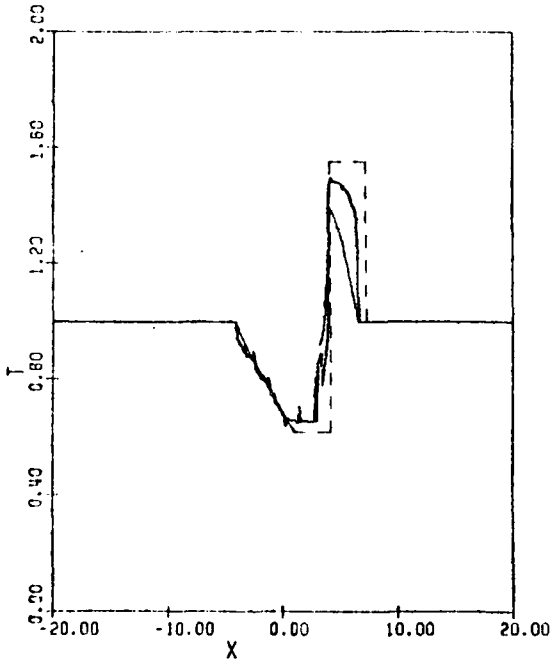

(d) Velocity

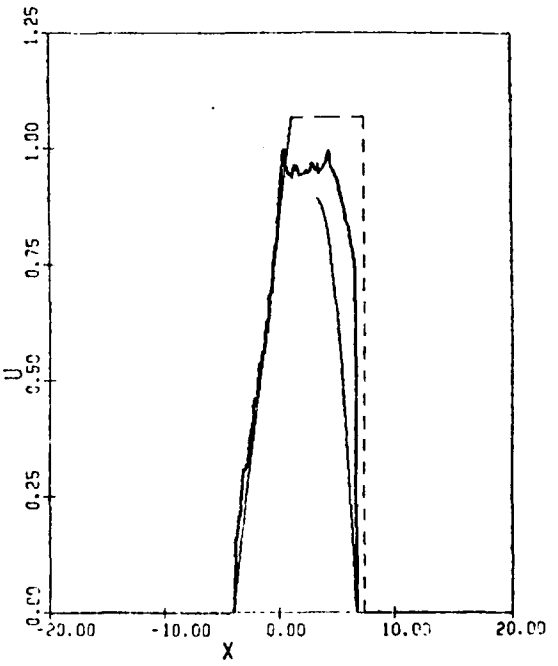

FIG. 25 FLOW QUANTITIES AT $\tau = 4$ ($\alpha = 1$, $P_{41} = 20$, $d = 10$ μm).
——— GAS, ——— PARTICLES, ------ FROZEN FLOW.

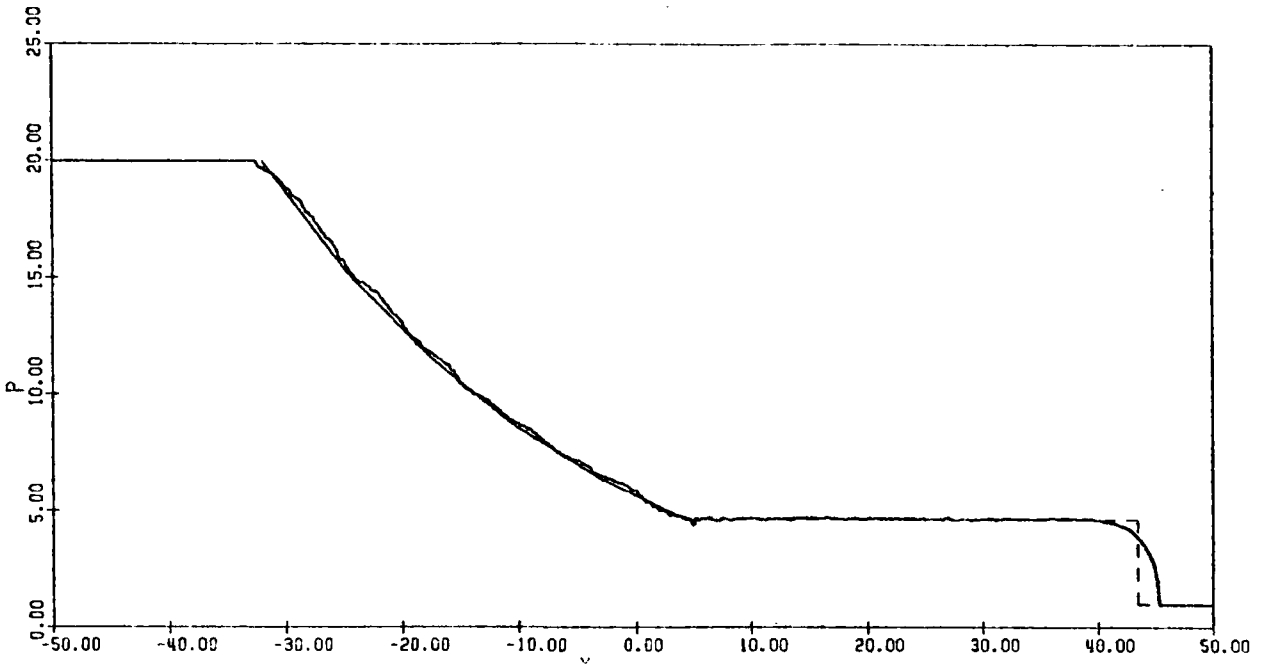

(a) Pressure

(b) Mass Concentration

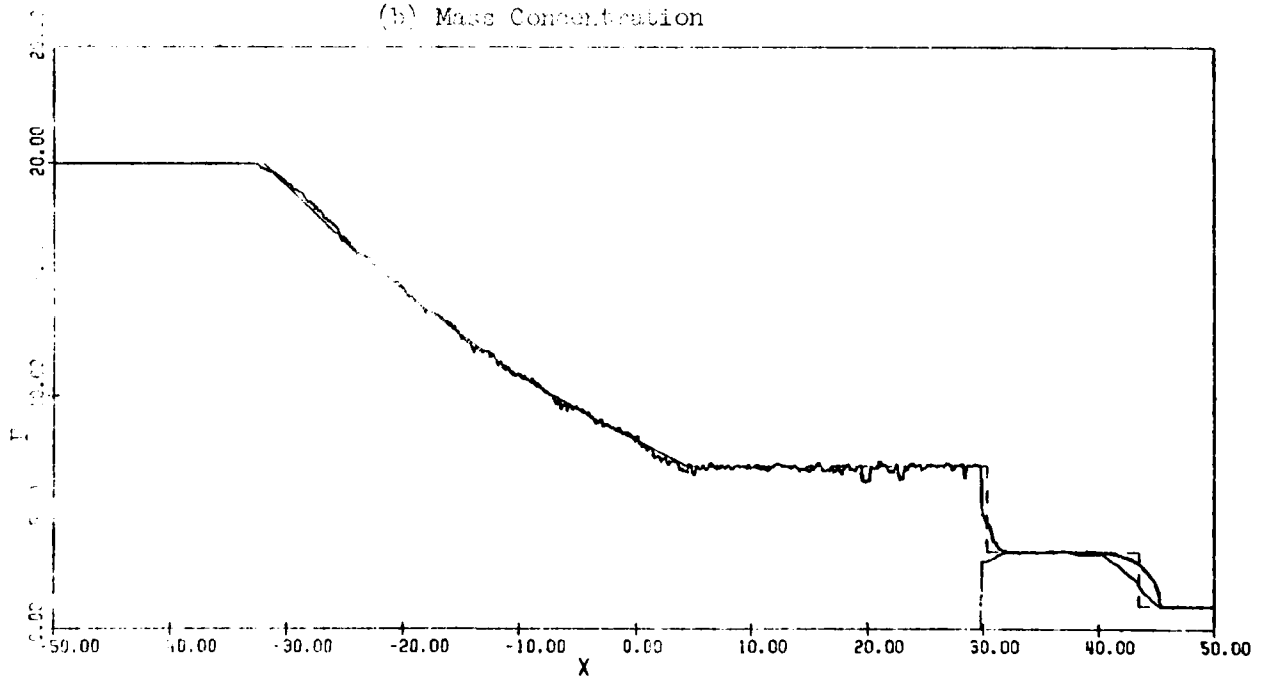

FIG. 26 FLOW QUANTITIES AT $\tau = 32$ ($\alpha = 1$), $P_{41} = 20$, d = 10 μm).
——— GAS, ——— PARTICLES, ------ EQUILIBRIUM FLOW.

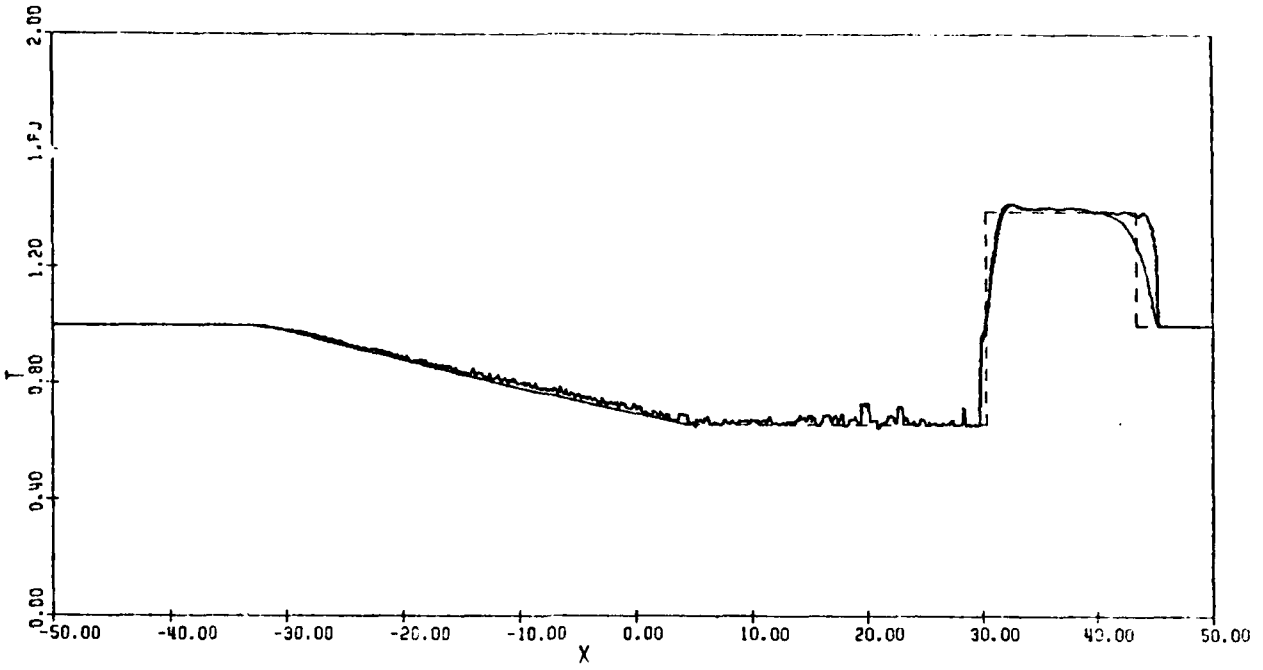

(c) Temperature

(d) Velocity

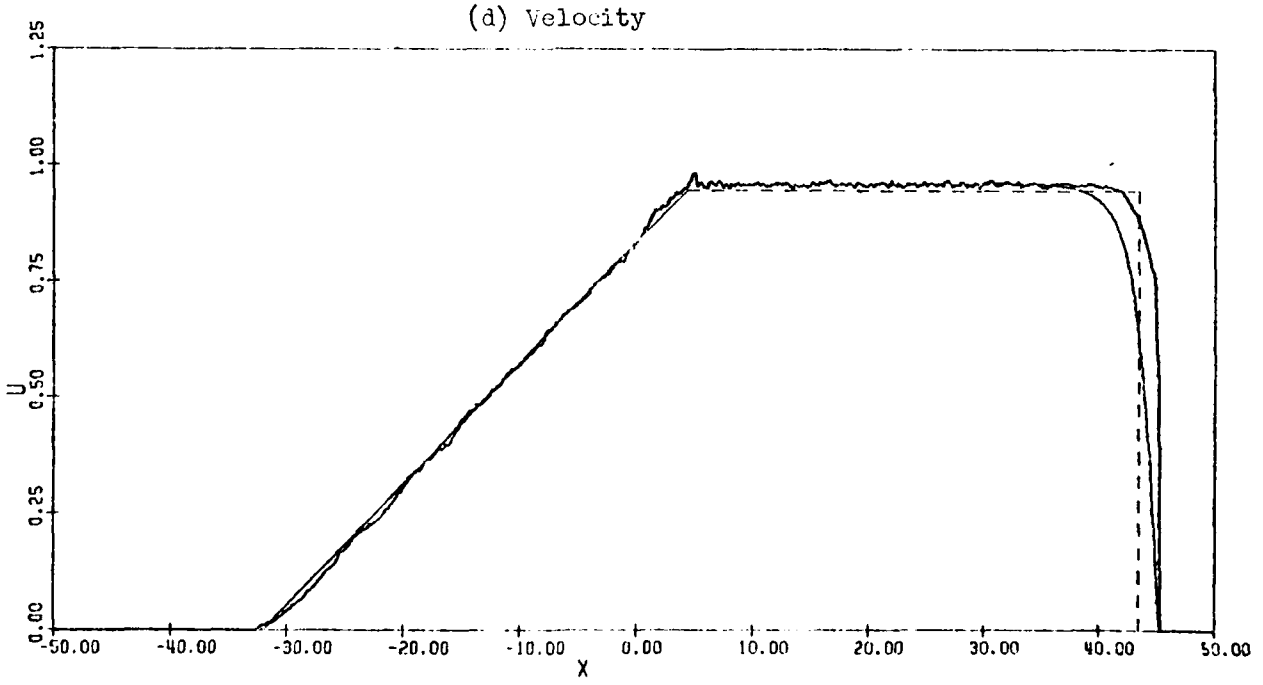

FIG. 26 (CONTINUED) FLOW QUANTITIES AT $\tau = 32$ ($\alpha = 1$, $P_{41} = 20$, $d = 10\ \mu m$).

——— GAS, ——— PARTICLES, ------ EQUILIBRIUM FLOW.

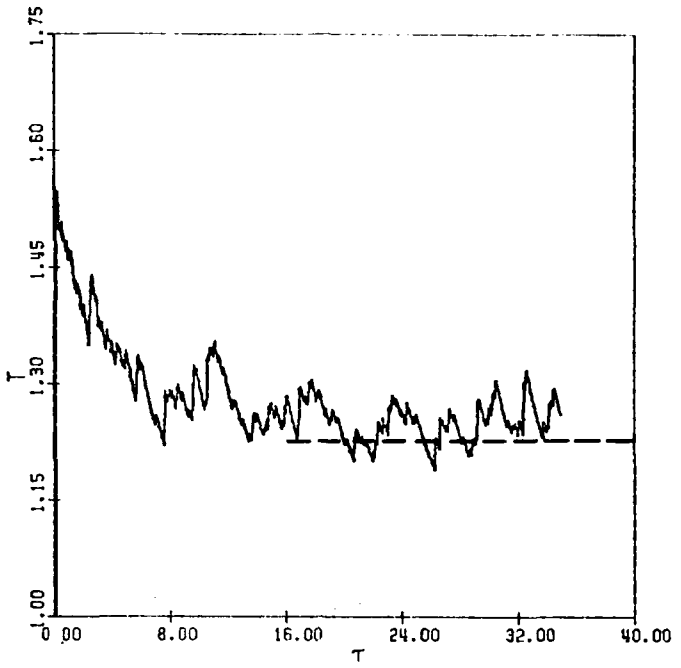

(a) Temperature

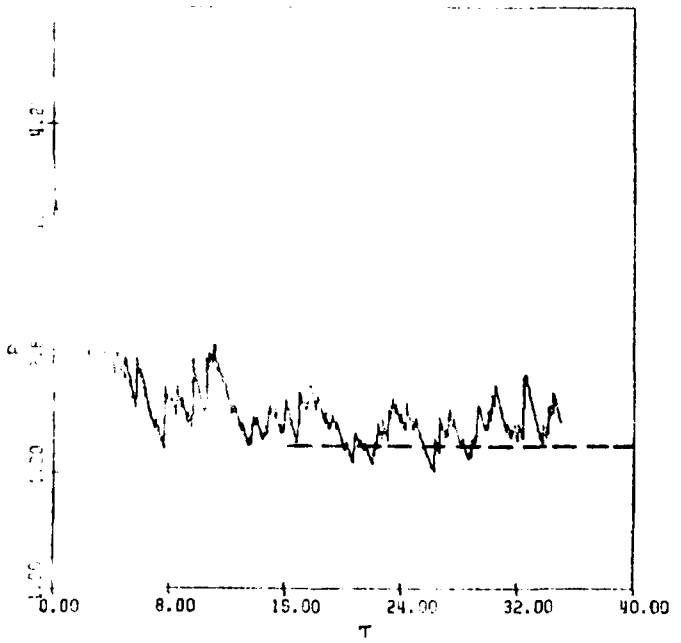

VARIATIONS WITH TIME OF TEMPERATURE AND PRESSURE OF GAS JUST BEHIND DISCONTINUOUS FROZEN SHOCK FRONT ($\alpha = 1$, $P_{41} = 20$, $d = 10\ \mu m$).

------ EXPECTED FINAL VALUE.

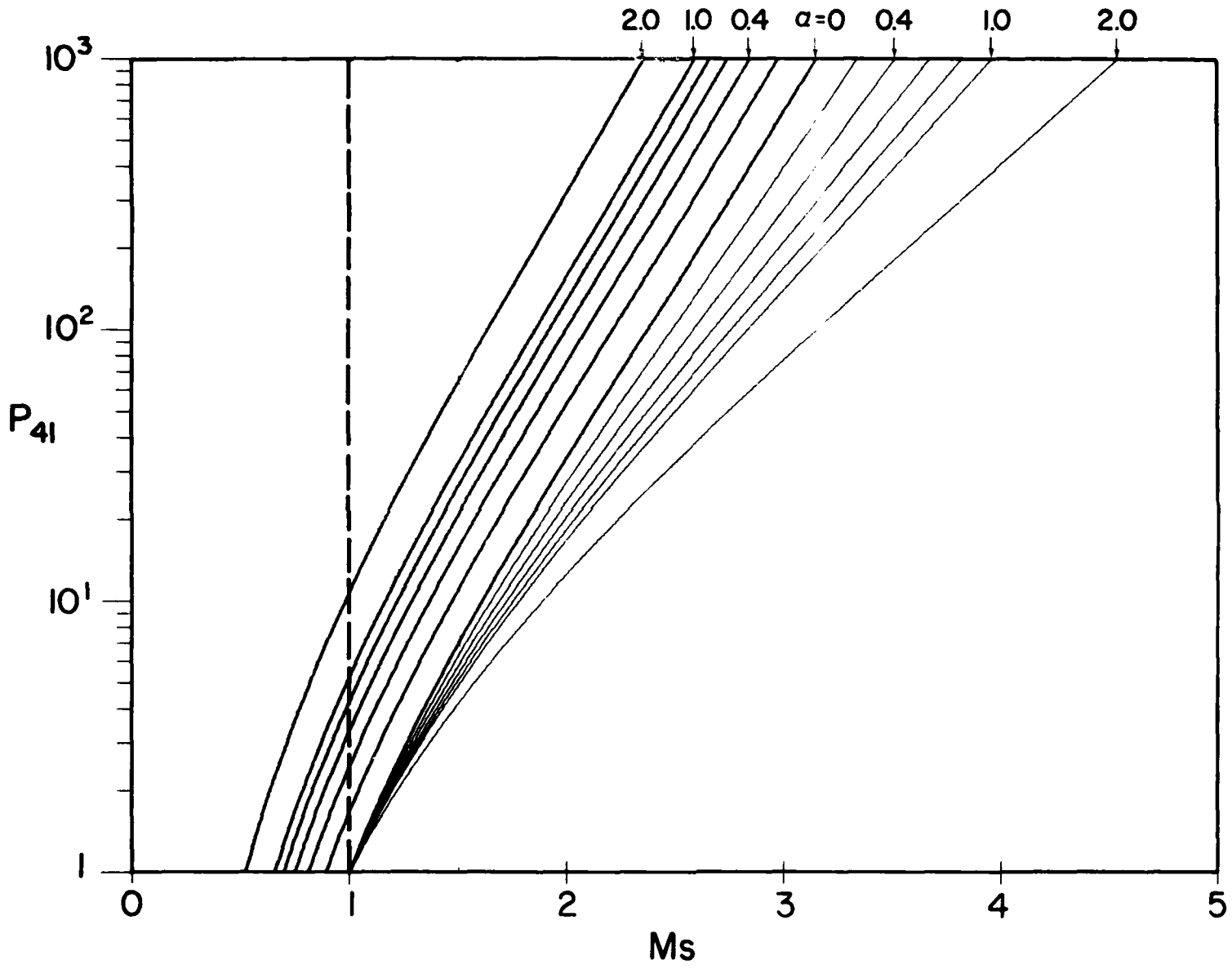

FIG. 28 VARIATION OF SHOCK WAVE MACH NUMBER M_s WITH DIAPHRAGM PRESSURE RATIO P_{41}.
——— M_s BASED ON FROZEN SPEED OF SOUND a_{1_f}, ——— M_s BASED ON EQUILIBRIUM SPEED OF SOUND a_{1_e}.

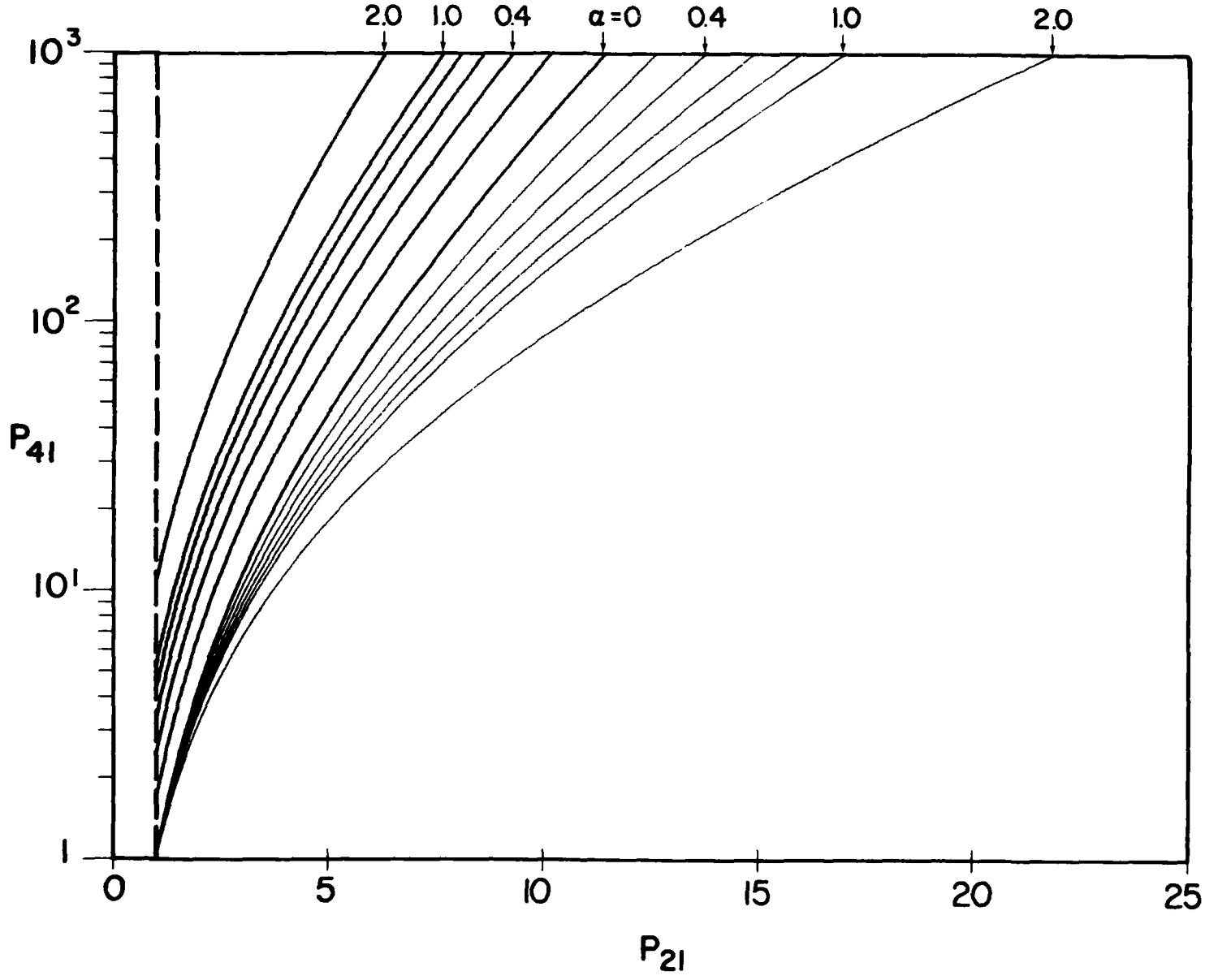

FIG. 29 VARIATION OF SHOCK PRESSURE RATIO P_{21} WITH DIAPHRAGM PRESSURE RATIO P_{41}.
——— FROZEN VALUE, ——— EQUILIBRIUM VALUE.

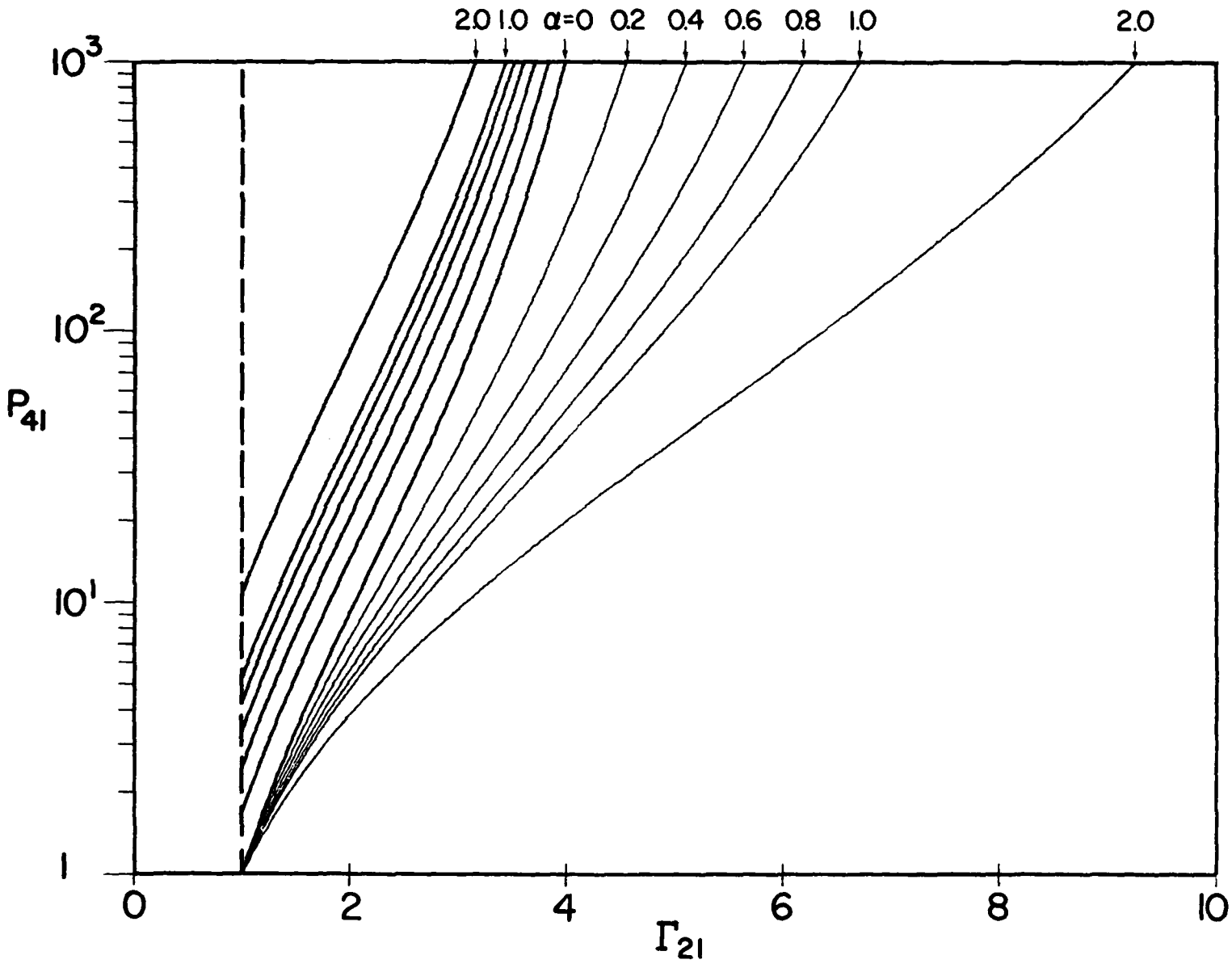

FIG. 30 VARIATION OF DENSITY RATIO Γ_{21} WITH DIAPHRAGM PRESSURE RATIO P_{41}.
——— FROZEN VALUE, ——— EQUILIBRIUM VALUE.

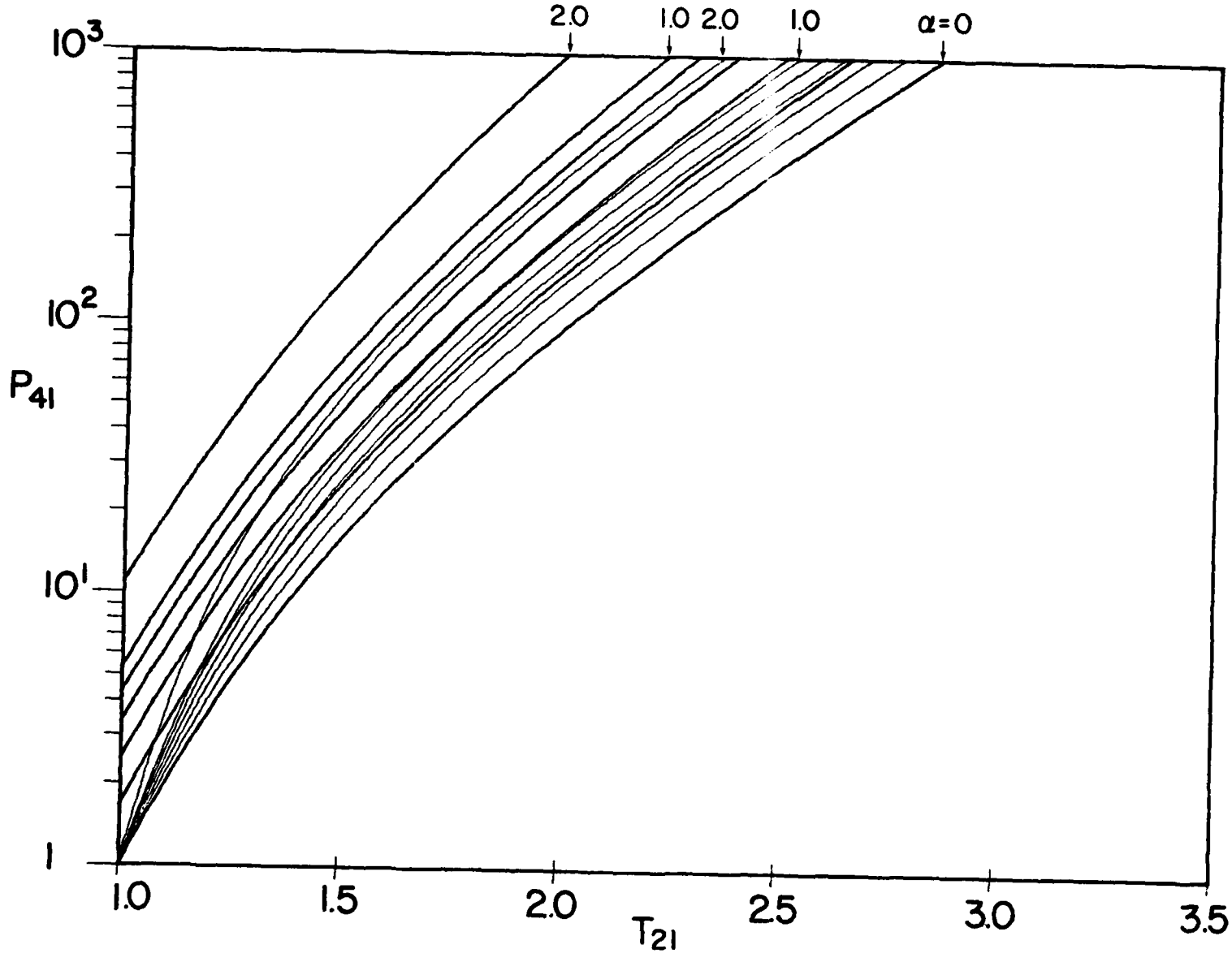

FIG. 31 VARIATION OF TEMPERATURE RATIO T_{21} WITH DIAPHRAGM PRESSURE RATIO P_{41}.
——— FROZEN VALUE, ——— EQUILIBRIUM VALUE.

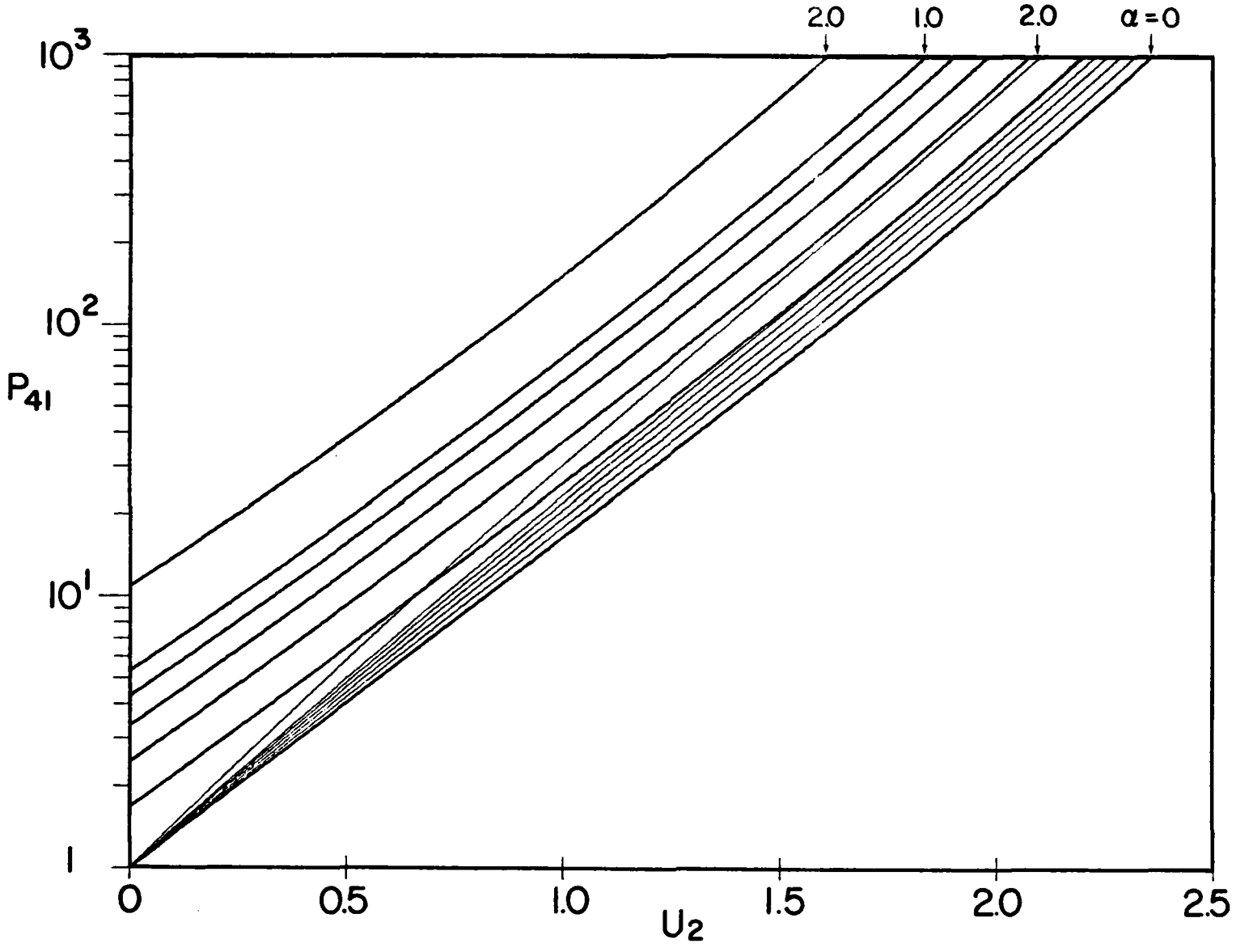

FIG. 32 VARIATION OF VELOCITY U_2 WITH DIAPHRAGM PRESSURE RATIO P_{41}.
——— FROZEN VALUE, ——— EQUILIBRIUM VALUE.

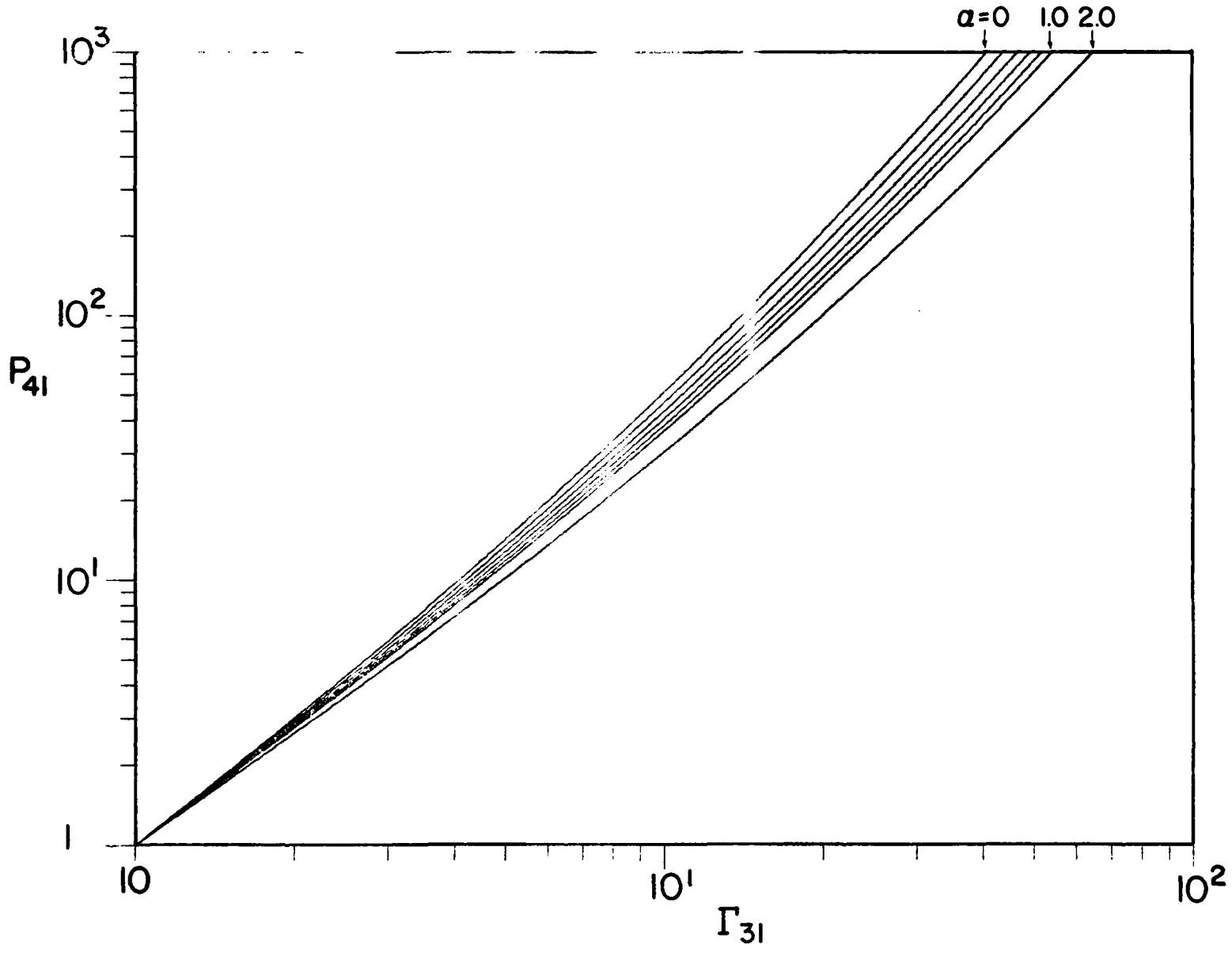

FIG. 33 VARIATION OF DENSITY RATIO Γ_{31} WITH DIAPHRAGM PRESSURE RATIO P_{41}.

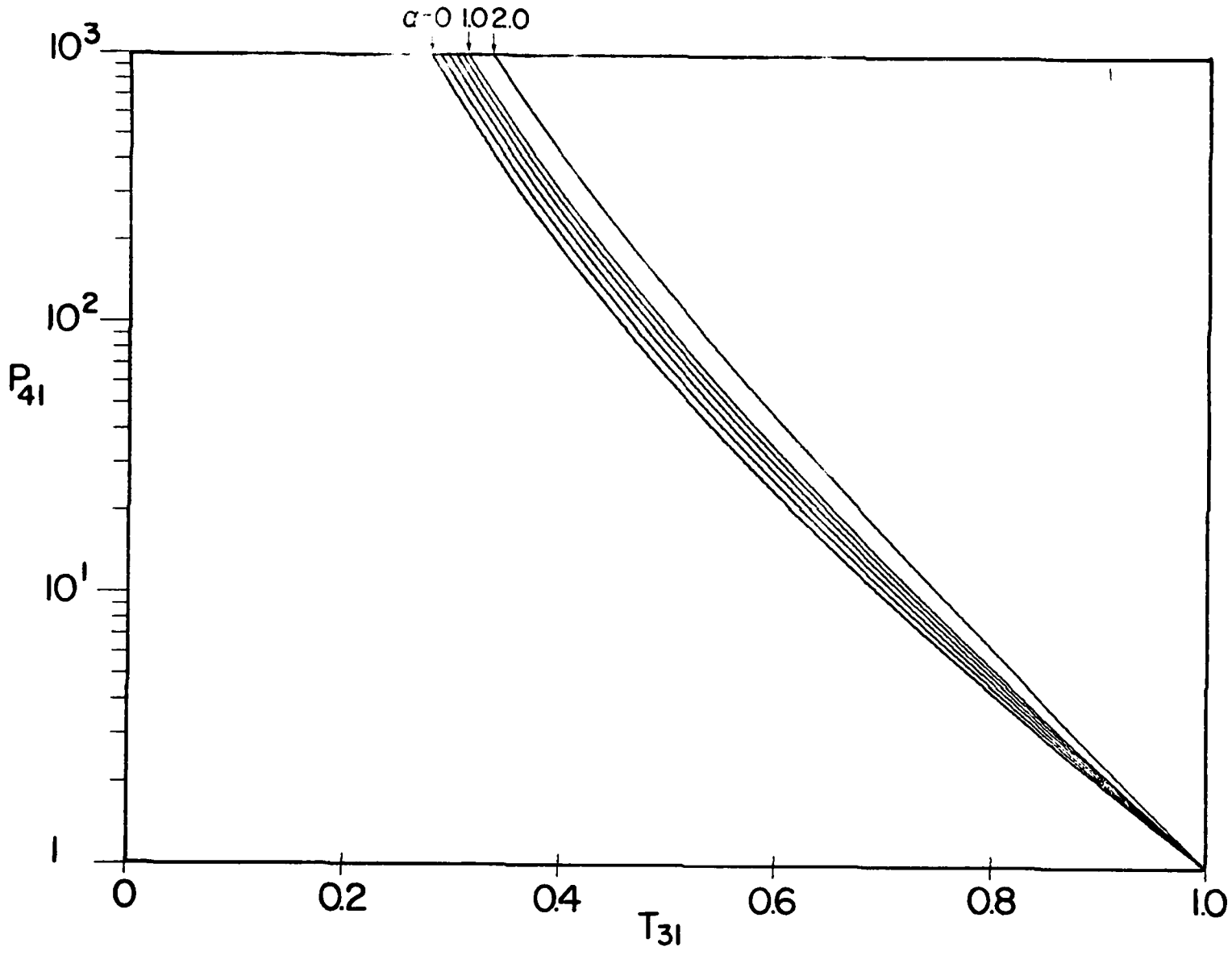

FIG. 34 VARIATION OF TEMPERATURE RATIO T_{31} WITH DIAPHRAGM PRESSURE RATIO P_{41}.

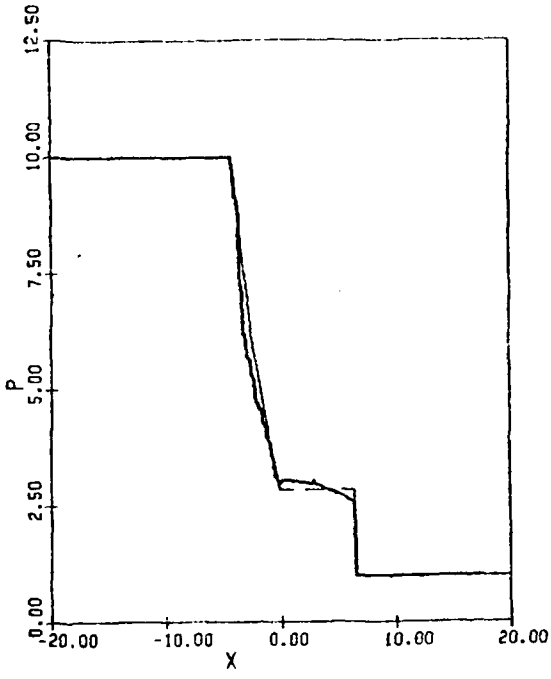

(a) Pressure

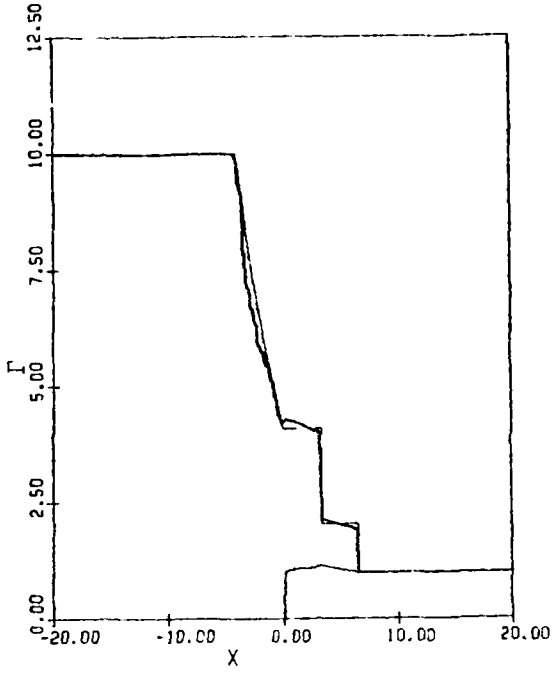

(b) Mass Concentration

(c) Temperature

(d) Velocity

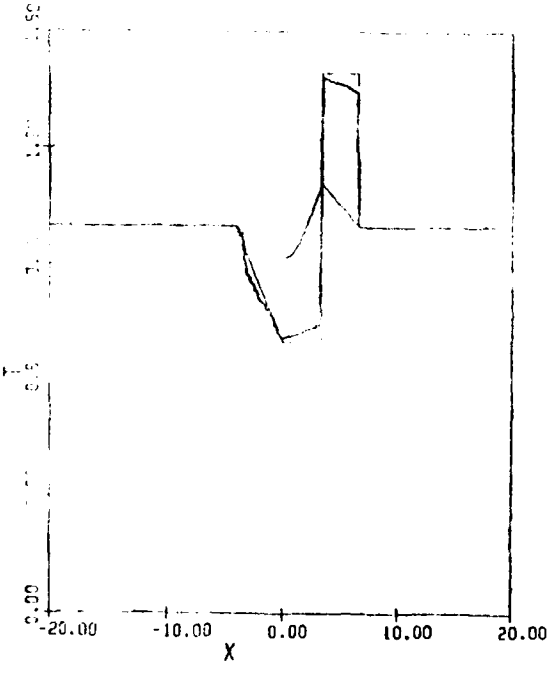

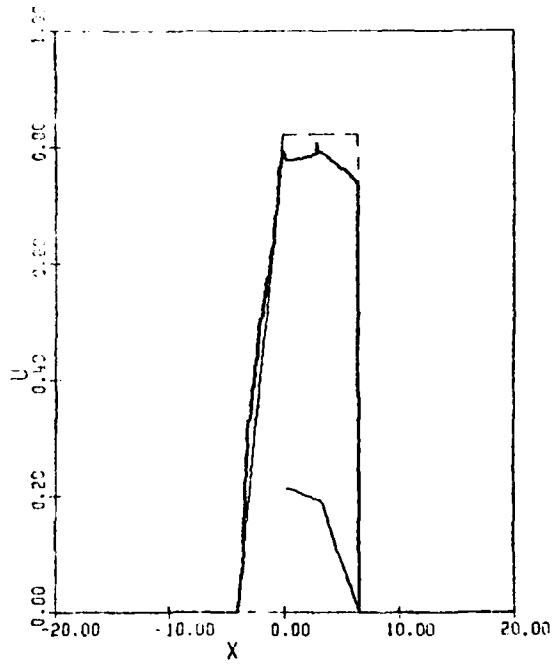

FIG. 35 FLOW QUANTITIES AT $\tau = 4$ ($C_D = 24/Re$, Nu = 2, $\alpha = 1$, $P_{41} = 10$, d = 10 μm).
——— GAS, ——— PARTICLES, ------ FROZEN FLOW.

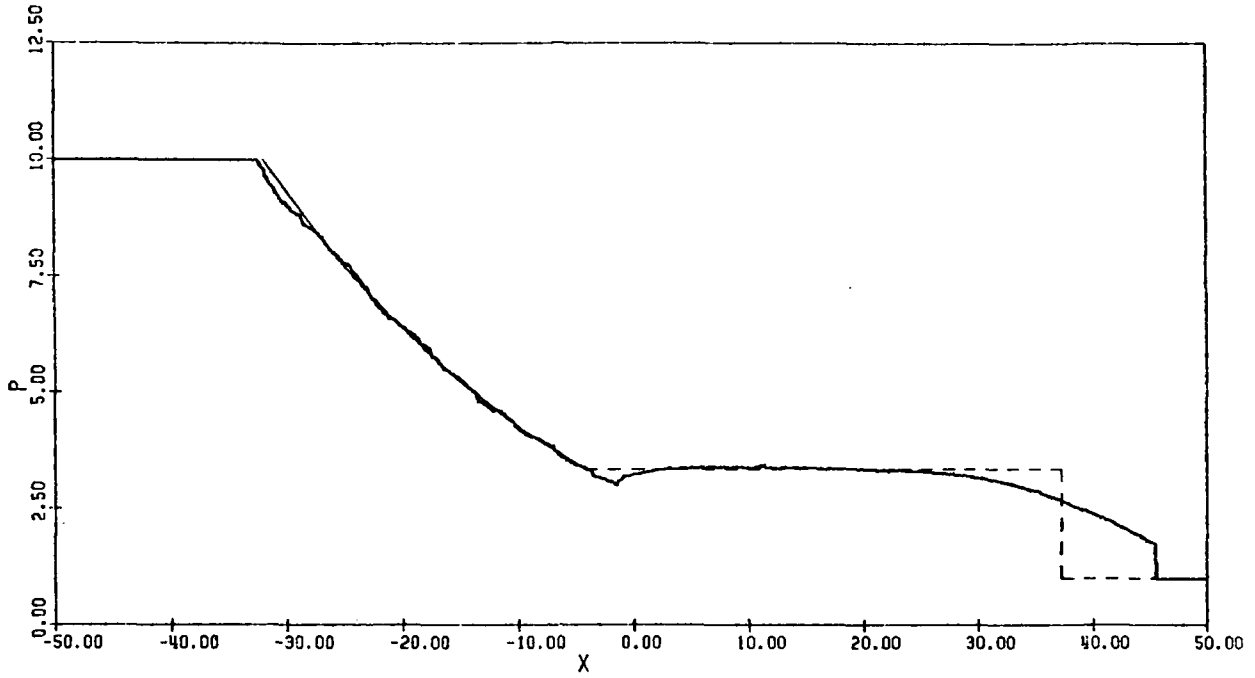

(a) Pressure

(b) Mass Concentration

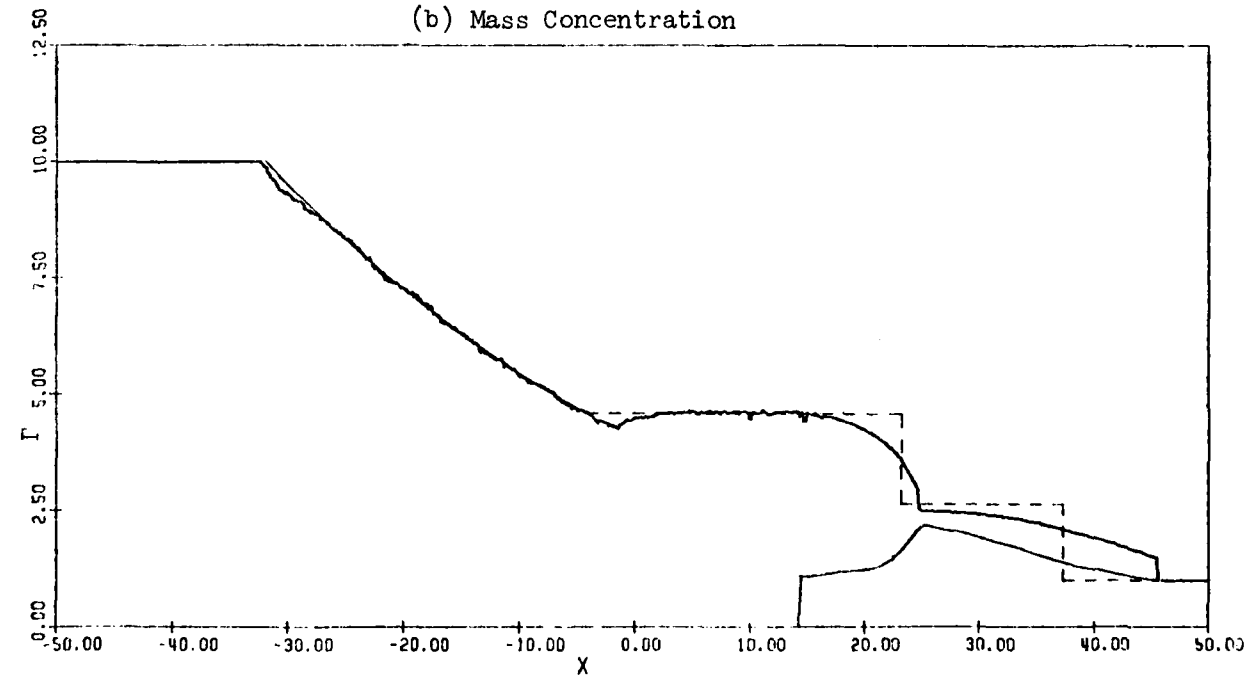

FIG. 36 FLOW QUANTITIES AT $\tau = 32$ ($C_D = 24/Re$, $Nu = 2$, $\alpha = 1$, $P_{41} = 10$, $d = 10$ μm).
——— GAS, ——— PARTICLES, ------ EQUILIBRIUM FLOW.

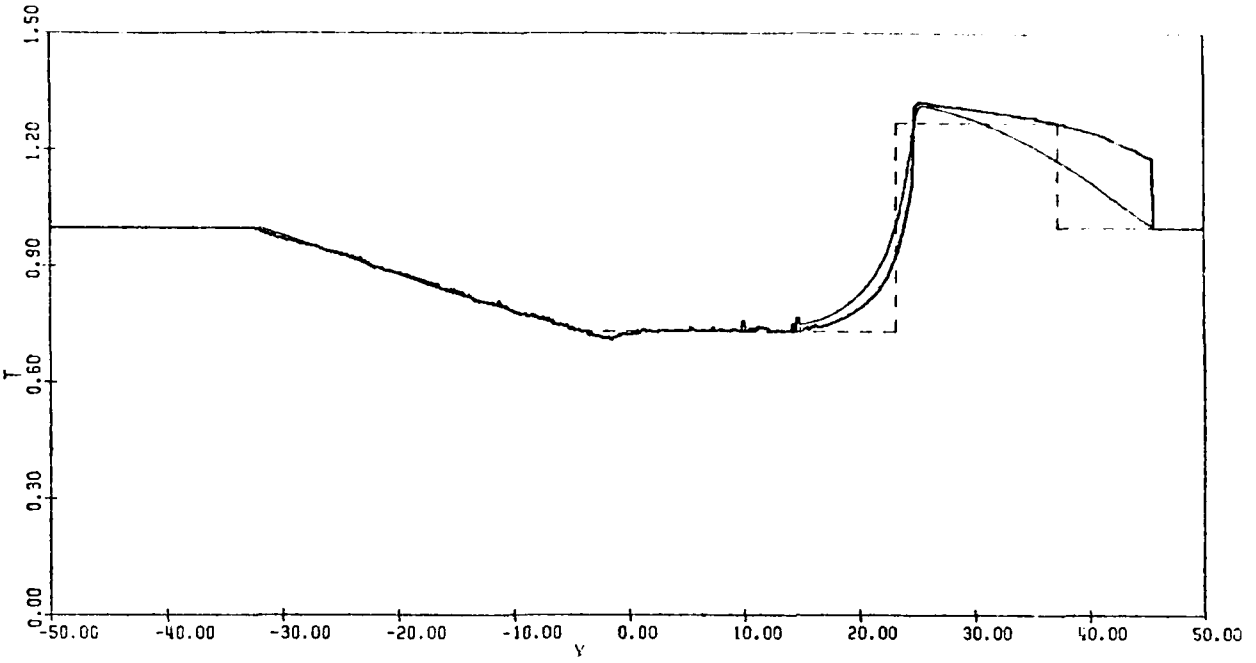

(c) Temperature

(d) Velocity

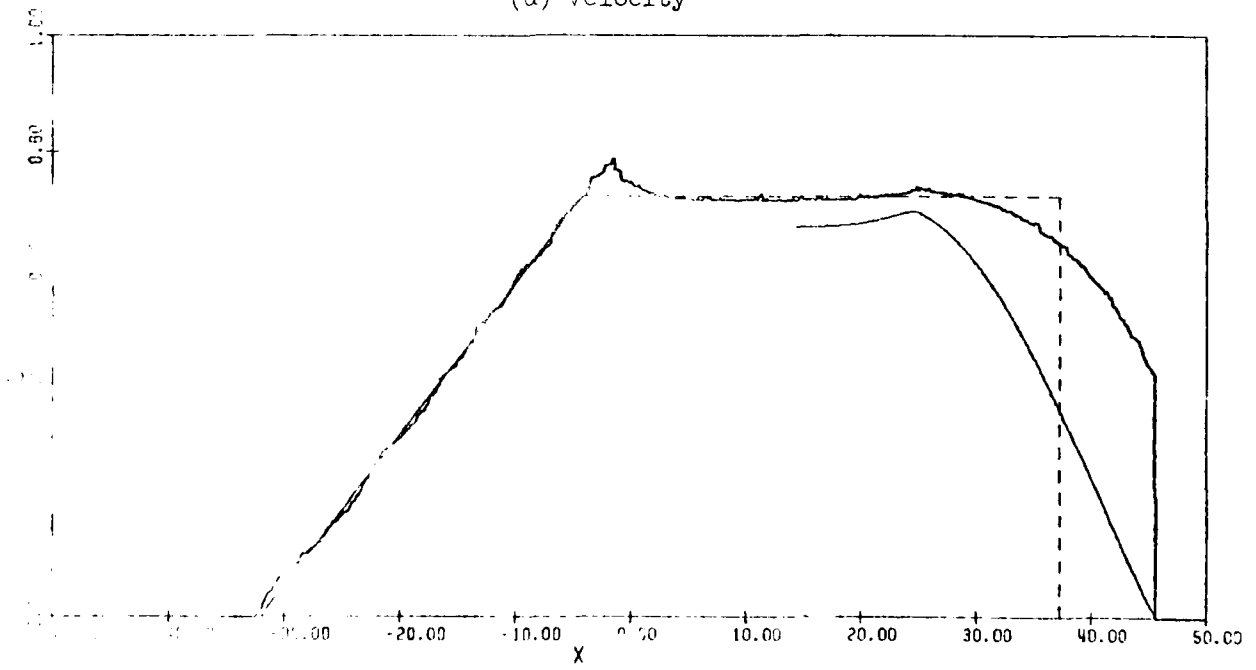

( ) LOW QUANTITIES AT = 32 ($C_D = 24/Re$, Nu = 2, $\alpha = 1$, $P_{41} = 10$, $l = 10$ μm).

——— GAS, ——— PARTICLES. ------ EQUILIBRIUM FLOW.

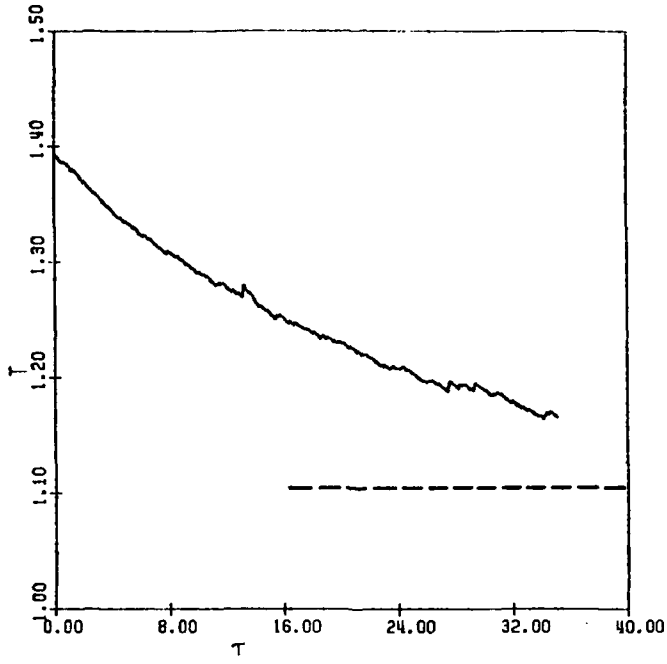

(a) Temperature

(b) Pressure

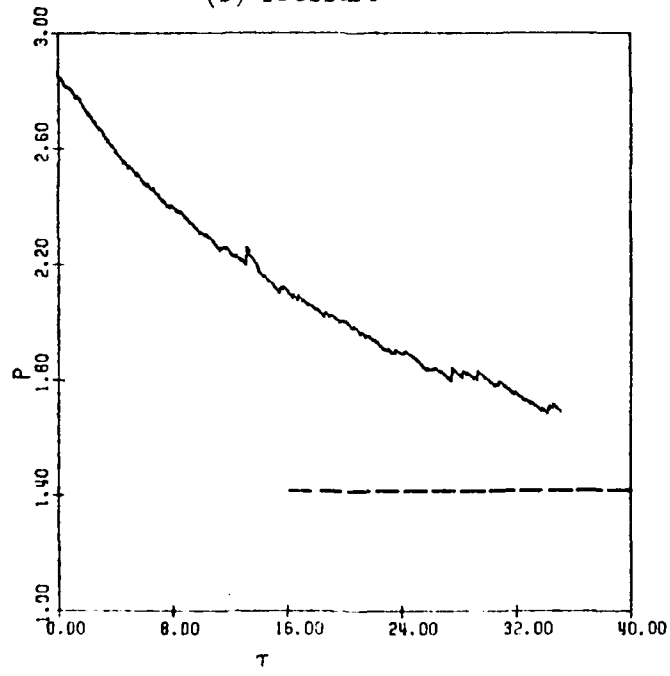

FIG. 37 VARIATIONS WITH TIME OF TEMPERATURE AND PRESSURE OF GAS JUST BEHIND DISCONTINUOUS FROZEN SHOCK FRONT ($C_D = 24/Re$, $Nu = 2$, $\alpha = 1$, $P_{41} = 10$, $d = 10$ μm).

------ EXPECTED FINAL VALUE.

UTIAS Report No. 250

Institute for Aerospace Studies, University of Toronto (UTIAS)
4925 Dufferin Street, Downsview, Ontario, Canada, M3H 5T6

ON A DUSTY-GAS SHOCK TUBE

Miura, H. and Glass, I. I.

1. Dusty-gas shock waves 2. Dusty-gas shock-tube flows 3. Nonequilibrium dusty-gas flows
4. Shock-wave and contact-front transitions

I. Miura, H., Glass, I. I. II. UTIAS Report No. 250

Analytical and numerical methods were used to investigate the flow induced by a shock wave in a shock-tube channel containing air laden with suspended small solid particles. Exact results are given for the frozen and equilibrium shock-wave properties as a function of diaphragm-pressure ratio and shock-wave Mach numbers. The driver contained air at high pressure. A modified random-choice method together with an operator-splitting technique show clearly both the decay of a discontinuous frozen shock wave and a contact discontinuity and the formation of a stationary shock structure and an effective contact front of finite thickness.

The effects of particle diameter, particle-number density and diaphragm-pressure ratio on the transitional behaviour of the flow are investigated in detail. The alteration of the flow properties due to the presence of particles is discussed in detail and compared with classical shock-tube flows.

Available copies of this report are limited. Return this card to UTIAS, if you require a copy.

Available copies of this report are limited. Return this card to UTIAS, if you require a copy.

UTIAS Report No. 250

Institute for Aerospace Studies, University of Toronto (UTIAS)
4925 Dufferin Street, Downsview, Ontario, Canada, M3H 5T6

ON A DUSTY-GAS SHOCK TUBE

Miura, H. and Glass, I. I.

1. Dusty-gas shock waves 2. Dusty-gas shock-tube flows 3. Nonequilibrium dusty-gas flows
4. Shock-wave and contact-front transitions

I. Miura, H., Glass, I. I. II. UTIAS Report No. 250

Analytical and numerical methods were used to investigate the flow induced by a shock wave in a shock-tube channel containing air laden with suspended small solid particles. Exact results are given for the frozen and equilibrium shock-wave properties as a function of diaphragm-pressure ratio and shock-wave Mach numbers. The driver contained air at high pressure. A modified random-choice method together with an operator-splitting technique show clearly both the decay of a discontinuous frozen shock wave and a contact discontinuity and the formation of a stationary shock structure and an effective contact front of finite thickness.

The effects of particle diameter, particle-number density and diaphragm-pressure ratio on the transitional behaviour of the flow are investigated in detail. The alteration of the flow properties due to the presence of particles is discussed in detail and compared with classical shock-tube flows.

Available copies of this report are limited. Return this card to UTIAS, if you require a copy.